

Structure and metamorphism along the Burntside Lake Shear Zone near Ely, MN

A Thesis
SUBMITTED TO THE FACULTY OF
UNIVERSITY OF MINNESOTA
BY

Jennifer Noelle Goldner

IN PARTIAL FULFILLMENT OF THE REQUIREMENTS
FOR THE DEGREE OF
MASTER OF SCIENCE

John Goodge, Vicki Hansen

August 2013

Acknowledgements

First and foremost I want thank my husband. Without his constant support and encouragement, this thesis would never have been completed. I also would like to thank my advisors, John and Vicki without whose knowledge and guidance this thesis would not have been possible. I would also like to thank my field assistant Hillary for all of her enthusiasm, support, especially in the canoe. And I must thank my fellow graduate students, Sally Goodman, Emerald Erikson, and Susie Karberg for their insight, support and assistance on various aspects of this project from helping me with GIS, to working through field problems and for the thought provoking discussions in the grad office.

I would also thank the McKnight Foundation for support of this research granted to V.L. Hansen by the McKnight Presidential Endowment. I would also like to thank the Natural Resources Research Institute for funding field equipment to complete field work; the UMD Department of geological sciences for the graduate assistance-ship. And last but not least Dr. Erich Petersen and the University of Utah Department of geology for the use of their petrographic microscope.

ABSTRACT

Archean granite-greenstone terrains (GGTs) occur in the stable interior cratons of Australia, India, South Africa, and North America. GGTs represent the best remaining evidence of the tectonic regime that reigned in the Archean. For this reason, GGTs continue to be thoroughly studied to better understand the tectonic evolution of Archean cratons. GGTs consist of ovoid granitoid bodies surrounded by deformed, metamorphosed volcanic sequences of intermediate to mafic composition.

There are two principal opposing hypotheses on the genesis of GGTs: 1) sagduction/diapirism, whereby density instabilities lead to the subsiding of greenstone layers, and the rising of granitoid bodies; and 2) modern-style island-arc accretionary tectonics. The island arc-accretion hypothesis requires a rheologically strong, brittle lithosphere in order for subduction to occur. In contrast, the sagduction hypothesis requires a rheologically ductile weak lithosphere to allow for the diapiric mechanism of GGT genesis. It is assumed that the Archean geotherm was much steeper compared to the modern. A higher geotherm would have affected the lithosphere's rheology, making it more ductile than present lithosphere. If this scenario holds true, the ability of the lithosphere to act in a brittle manner, thus allowing subduction, becomes questionable.

Many workers have classically interpreted the Superior Province of northern Minnesota and Canada as the prime example of modern-style accretionary tectonics occurring during the Archean. The northeast-trending Burntside Lake shear zone (BLSZ) lies at the boundary of the Archean Vermilion Granitic Complex and The Newton Lake Formation. The position of the BLSZ between a granitoid body and a greenstone belt allows for the study of the interaction between these two units, offering an opportunity to study how Archean tectonic processes may have occurred. Through examination of tectonic fabrics in the field and microstructures in the lab, this shear zone appears to be a vertical zone of dip-slip deformation. The vertical, dip-slip, north-side-up orientation of this zone is also supported by geothermometric calculations indicating a thermal gradient across the zone of relatively warmer temperatures to the north and cooler conditions to the south of the shear zone.

Foliation throughout the BLSZ strikes generally NE-SW, at an angle slightly oblique to the topographic expression of the zone itself, and has a nearly vertical dip. Lineations, primarily elongation lineations, throughout the area are steep, mostly plunging 80-90°. On the thin section scale, foliations vary from planar to anastomosing. Foliation is defined primarily by the alignment of biotite, chlorite and hornblende, and elongate needles of these minerals define lineations. S-C' fabrics composed of biotite and chlorite were used to determine sense of shear, along with sigma grains when applicable. These microfabrics are poorly preserved and in some thin sections completely ambiguous, resulting in few samples having definitive petrofabrics with which to interpret shear sense. Throughout this paper, confidence in shear sense is assigned a number from one to five, with five being the most confident and one being the least. North-side-up shear sense dominates rocks in the field area with three thin section samples giving evidence with a confidence rating of 5, one at 3, and one at 2. Two samples indicated south-side-up kinematics with a confidence level of 1 and 3.

The evidence from observations in the field (changes in grain size, metamorphic grade) and microstructural analysis supports the idea of a vertical zone of deformation

with dominant sense of north-side-up displacement in addition to local south-side-up displacement. North-side-up displacement is supported by geothermometry completed on garnet-biotite pairs, chlorite compositions, and hornblende-plagioclase pairs from metamorphic rocks. Geothermometry indicates amphibolite-facies metamorphism north of the BLSZ and lower greenschist-facies metamorphism south of the BLSZ.

In the study area, the BLSZ does not show evidence of strike-slip displacement, as predicted by plate tectonic hypotheses. The vertical motion recorded by fabric orientations, fabric kinematics and thermometry along this portion of the BLSZ fits the hypothesis of sagduction/diapirism.

Further study will allow for a greater understanding of the complex history recorded in the rocks defining the Burntside Lake shear zone. Specifically, study could be done to further constrain pressure/temperature conditions, kinematics, and the timing between the conflicting senses of shear apparent in some of the samples utilized in this study. Last, a comparison of the many shear zones in the area will help to better understand timing and kinematic relations between units of the broader Superior Province.

Table of Contents

| | |
|--|----|
| Table of Figures..... | v |
| Table of Tables..... | vi |
| Chapter 1. INTRODUCTION..... | 1 |
| Chapter 2. BACKGROUND..... | 4 |
| 2.1 <i>Archean Tectonics</i> | 4 |
| 2.2 <i>Geology of the study area</i> | 10 |
| 2.3 <i>Previous Studies</i> | 12 |
| Chapter 3. METHODS..... | 16 |
| 3.1 <i>Field Methods</i> | 16 |
| 3.2 <i>Petrography</i> | 17 |
| 3.3 <i>Electron Microprobe Analysis</i> | 18 |
| 3.4 <i>Treatment of Microprobe Data</i> | 19 |
| 3.5 <i>Structural and Microstructural Analysis</i> | 20 |
| Chapter 4. RESULTS..... | 22 |
| 4.1 <i>Field Relationships</i> | 22 |
| 4.2 <i>Petrography</i> | 25 |
| 4.3 <i>Mineral Chemistry and P-T Calculations</i> | 26 |
| Structural Data..... | 43 |
| Microstructural Analysis..... | 47 |
| Chapter 5. DISCUSSION..... | 53 |
| 5.1 <i>Discussion of Petrological and P-T Analysis</i> | 53 |
| 5.2 <i>Discussion of Structural and Microstructural Kinematic Analysis</i> | 61 |
| Chapter 6. SUMMARY AND CONCLUSIONS..... | 64 |
| REFERENCES..... | 65 |
| APPENDIX 2..... | 73 |
| APPENDIX 3..... | 83 |
| APPENDIX 3 cont..... | 85 |
| APPENDIX 3, cont..... | 87 |
| APPENDIX 3 cont..... | 89 |
| APPENDIX 3, cont..... | 91 |

Table of Figures

| | |
|---|-------|
| Figure 1: Sagduction/Diapirism Model..... | 6 |
| Figure 2: Arc Accretion Model..... | 8 |
| Figure 3: Simplified map of the Superior Province..... | 11 |
| Figure 4: Shear Sense Indicators..... | 20 |
| Figure 5: Field Photograph of Metavolcaniclastic Unit..... | 22 |
| Figure 6: Field Photograph of Biotite Schist Unit..... | 23 |
| Figure 7: Map of geothermometry samples..... | 28 |
| Figure 8: BSE Image of Sample 59-11l..... | 33 |
| Figure 9: BSE Image of Sample 137-11l..... | 34 |
| Figure 10: Garnet Map Sample 59-11l..... | 36 |
| Figure 11: Garnet Map Sample 137-11l..... | 37 |
| Figure 12: Geothermometry Plot of 59-11l..... | 38 |
| Figure 13: Geothermometry Plot 137-11l..... | 39 |
| Figure 14: A stereoplot foliation surrounding the BLSZ..... | 43 |
| Figure 15: Foliation Trend Map..... | 45 |
| Figure 16: Photomicrograph of Microstructures in Sample 107-11l..... | 48 |
| Figure 17: Photomicrograph of Microstructures in Sample 157-11l..... | 49 |
| Figure 18: Photomicrograph of Microstructures in Sample 175-all | 50 |
| Figure 19: Photomicrograph of Microstructures in Sample 61-1all | 51 |
| Figure 20: Offset along the BLSZ..... | 54 |
| Figure 21: Formula Proportions Diagrams..... | 56-58 |
| Figure 22: Geothermometry and Deformation Map..... | 59 |

Table of Tables

| | |
|--|----|
| Table 1: Summary of Deformation Events Recognized by Others..... | 8 |
| Table 2: Petrographic Description of Major Metamorphic Rock Types..... | 25 |
| Table 3: Mineral Compositions Determined by Microprobe Analysis..... | 28 |
| Table 4: Garnet-Biotite Thermometry Results..... | 36 |
| Table 5: Hornblende-Plagioclase Thermometry Results..... | 38 |
| Table 6: Chlorite Thermometry Results..... | 38 |

Plate 1: Geologic map of the field area. Geology after Jirsa and Miller 2004. Plotted on the map are foliation orientations gathered in the field supplemented by with data from the Ely and Shagawa quad maps by Green (1982) and Sims (1978). Also shown on the map are stop locations.

1. INTRODUCTION

Granite-greenstone terrains (GGTs) occur uniquely within Archean cratons on many continents, including: the Dharwar craton of India, the Pilbara and Yilgarn cratons of Australia, the Barberton and Kaapvaal cratons of Africa, the Kolar craton of India, and the Superior Province of northern Minnesota and Canada. GGTs represent an important record of tectonic processes occurring in the Archean because of preserved primary igneous terrains related to craton formation (Condie, 1980). For this reason, GGTs are studied in order to gain insight into the tectonic history and origin of these ancient cratons.

GGTs occur as ovoid bodies of tonalite, trondhjemite and granodiorite-granite (TTG) surrounded by anastomosing greenstone-type supracrustal rocks (Bedard et al., 2003). The ovoid TTG bodies generally have a uniform composition, as well as uniform ages across the entire terrain in which the TTGs occur (Bedard et al., 2003), suggesting geologically rapid magma genesis. The anastomosing greenstone bodies get their name from the characteristic green color of the rocks, a consequence of low-grade metamorphism of mafic to ultramafic sub-aerial to sub-aqueous volcanic sequences. Also characteristic of the greenstone bodies are their involvement in synclinal keel structures, as opposed to the characteristic domal structures of the TTGs (Collins et al., 1998). As a whole, GGTs are commonly belt-shaped and can extend laterally for hundreds of kilometers.

Workers studying Archean tectonic processes have proposed two principal hypotheses to explain the genesis of Archean GGTs. The first hypothesis, here

designated sagduction/diapirism, explains the genesis of GGTs whereby warm eruptive greenstone units thermally blanket underlying granitic crust, which induces a density instability. Eventually, due to this instability, granite bodies will rise (similar to salt diapirs) while greenstone units sink into inter-granitoid basins (Anhaeusser, 1969; Macgregor, 1951; Rey, 2003). The second hypothesis extrapolates modern-style island-arc accretionary tectonics into early Earth history to explain the formation of GGTs. In this arc-accretion model, greenstone units are thought to represent preserved and folded oceanic-island or back-arc volcanic crust, and granitoid units represent intrusive arc-type igneous activity (Windley, 1984). Both the granitoid and greenstone components are thought to be derived by subduction-related magmatism. Key to understanding GGTs are the structural boundaries juxtaposing granite and greenstone units. Deciphering physical conditions and sense of displacement on such structures can help to distinguish between these hypotheses.

The Superior Province of northern Minnesota and Canada is one of the most intensively studied Archean cratons. Many workers have interpreted the Superior Province as the prime example of modern-style accretionary tectonics occurring during the Archean (Bauer, 1990; Card, 1990; Jirsa, 1992; Tabor, 1991).

The Burntside Lake shear zone (BLSZ) lies at the boundary between the Archean Vermilion Granitic Complex and Newton Lake Formation in the Wawa subprovince of the Superior Province. The Vermilion Granitic Complex consists of granite, tonalite, migmatite, and amphibolite-grade schist and gneiss (Sims and Morey, 1978). The Newton Lake Formation consists dominantly of mafic to ultramafic metabasalt, with a minor component of volcanoclastic units (Peterson and Jirsa, 1999).

The BLSZ is an apparent splay from the Vermilion fault, which extends from the town of Vermilion through northeastern Minnesota and continues northeast into Canada (Wolf, 2006). The trace of the BLSZ is approximately NE-SW and its linear trace suggests the zone has a near-vertical orientation.

BLSZ's position between a gneiss body and associated schist units and a greenstone belt allows for the study of the interaction between these two units, offering an opportunity to study a key aspect of Archean tectonic processes. I conducted fieldwork along an 8-km portion of the BLSZ near Ely, Minnesota in summer 2007 to map geologic units, collect structural data from planar and linear fabrics, and collect samples for petrologic and microstructural examination in the lab.

2. BACKGROUND

2.1 Archean Tectonics

Granite-greenstone terrains are one of the dominant and unique features of Archean crust globally. In an effort to understand Archean craton genesis, two main hypotheses have been proposed to explain the origin of granite and greenstone units: the first, genesis by sagduction/diapirism, and the second, genesis by modern accretionary tectonic processes.

The sagduction/diapirism hypothesis has recently been revived, after being proposed in early literature discussing Archean tectonic processes. (Anhaeusser, 1969; Macgregor, 1951) Anhaeusser (1969), based on review of other studies in Archean cratons, proposed that greenstones were deposited onto a thin granitic crust, with subsequent granitoid bodies rising and causing the greenstones to 'slump' between the rising granite bodies. However, some literature cites evidence from the Superior Province as well in support of the sagduction/diapirism hypothesis (Macgregor, 1951; Collins et al., 1998; Bedard et al., 2003; Rey et al., 2003; Van Kranendonk et al., 2004; Lin, 2005; Rey and Houseman, 2006). A major tenet of the sagduction/diapirism model is that higher geothermal gradients prevailed in the Archean, as did an overall warmer Earth as compared to conditions today (Abbott, 1994; Campbell, 1992, 1989; Nisbet, 1993). This concept is not considered in the modern accretionary tectonics hypothesis. Warmer conditions during the Archean would allow for the rheologically ductile process of sagduction/diapirism to take place due to the reduced strength of underlying crust, allowing isostatic buoyancy forces to induce the sinking of the greenstones and the rising of the granites (Rey and Houseman, 2006). In sagduction/diapirism, granitoid bodies are

emplaced into an overlying blanket of extrusive igneous rocks (Collins et al., 1998; Fig. 2). The relatively low rheological contrast and the strong density contrast between the granitoid and greenstone bodies leads to a greenstone down and granitoid up scenario (Lin, 2005).

The sagduction/diapirism model accounts for the trends in age and lithology observed in GGTs, as well as orientation of fabric elements, defined by the following:

- 1) the inconsistency of fabric elements such as foliations and lineations (Bedard, 2003);
- 2) the rather uniform age of TTG bodies throughout GGTs; and 3) the similarity of greenstone bodies throughout GGTs, as well as the relative similarity between TTGs.

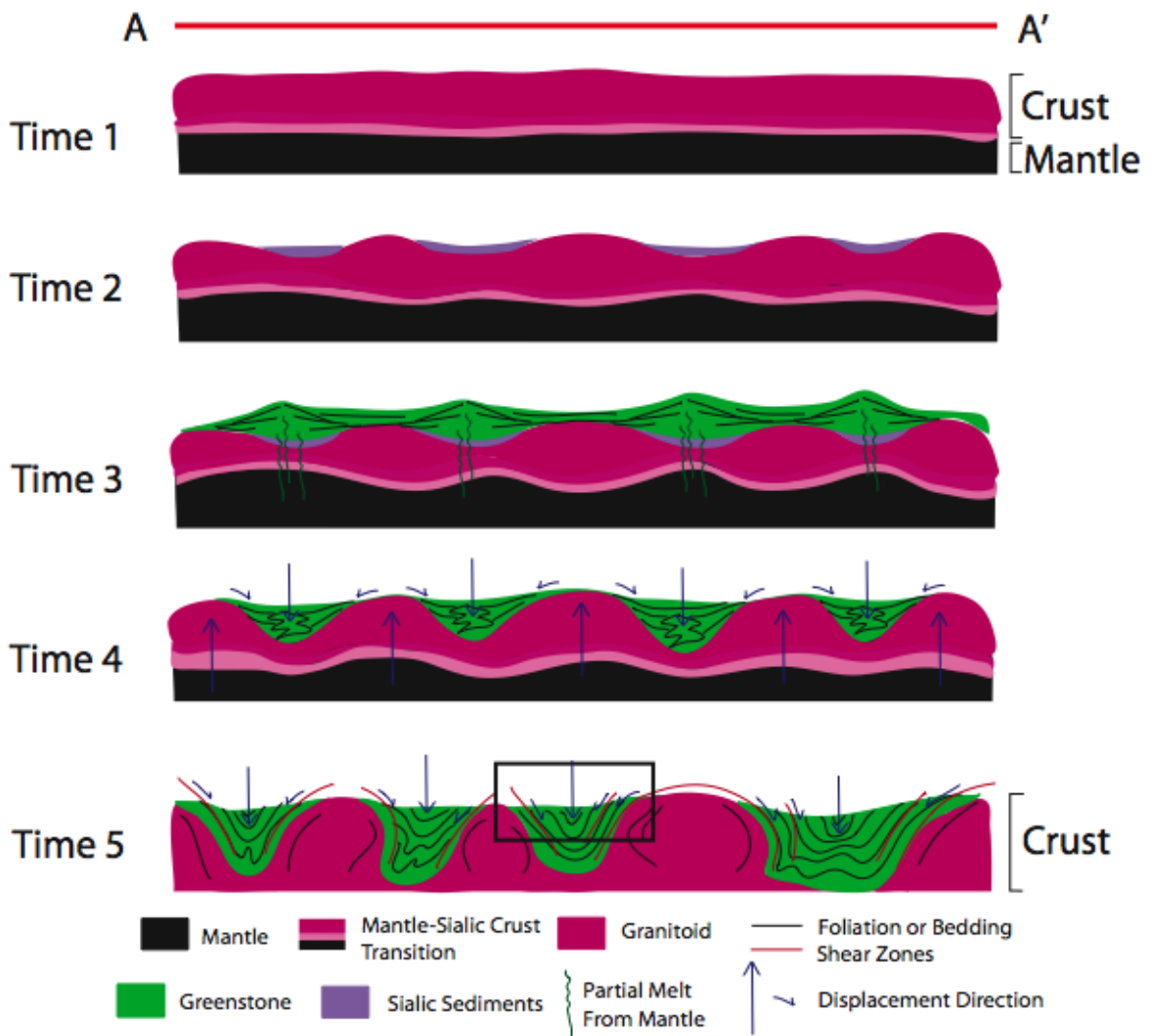


Figure 1. Cartoon model of sagduction/diapirism process after Anheusser, 1969; Windley, 1984; Rey et al., 2003; Van Kranendonk et al., 2004. Time 1 = original differentiation of Earth's sialic crust, thickness variations possible. Time 2 = erosion and deposition of sediments from sialic crust. Time 3 = volcanism from the mantle in thin areas of the crust. Time 4 = initiation of density-driven sagging of volcanic-sedimentary basins and diapiric rise of granitoids. Time 5 = conclusion of density reorganization of

the upper crust and final stage of crustal assembly. Line A to A' represents an entire granite-greenstone terrain. Box in Time 5 = hypothetical Vermilion District setting

The Superior Province is also commonly cited as the type location of modern accretionary tectonics occurring in the Archean (Hudleston et al., 1988; Card, 1990; Bauer and Bidwell, 1990; Jirsa et al., 1991; Tabor and Hudleston, 1991; Bauer et al., 1992; de Witt, 1998; Cawood et al. 2006; Fig. 3). Of the arguments made in these previous studies, a model invoking transpression is most commonly cited. Transpression is thought to have occurred by north-south shortening accompanied by a dextral strike-slip component of displacement, which has been attributed to oblique accretion of new crust (Hudleston et al., 1987; Hudleston et al., 1988; Tabor and Hudleston, 1990).

Lastly, others draw on both hypotheses to describe the geology of the Superior Province. Bedard, 2003 and Lin, 2005 both invoke the vertical displacement highlighted in the sagduction/diapirism hypothesis as well as the horizontal displacement dominant in the accretionary tectonics model. Such hybrid models should also be carefully considered in analysis of Superior Province geology.

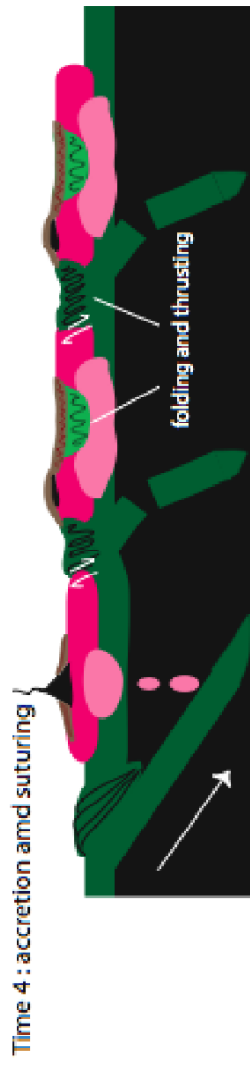
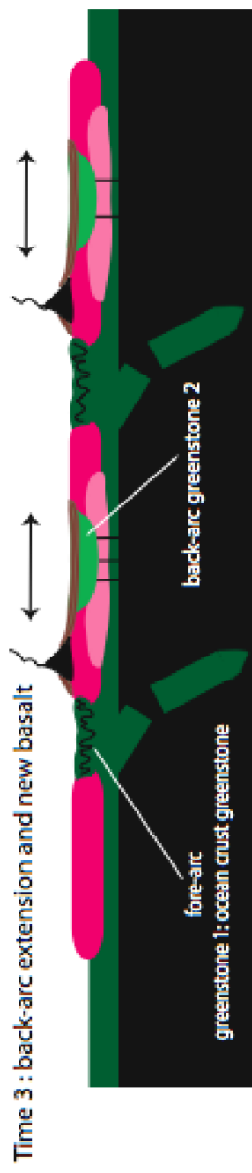
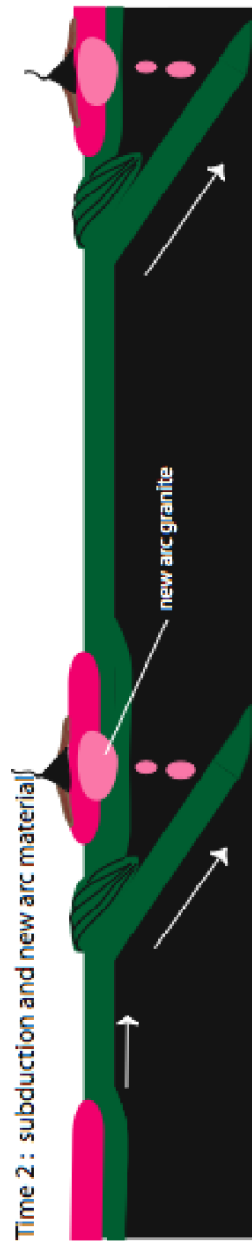


Figure 2: Cartoon of arc accretion model. Time 1=Remnant arc terrains separated by oceanic crust. Time 2= Subduction occurs creating new igneous material. Time 3= Back-arc extension occurs creating basaltic material. Time 4= Final accretion and terrane suturing. Time 5= The resultant terrane with a general granite-greenstone organization.

2.2 Geology of the study area

The BLSZ is located in the southern Superior Province near the boundary of the Quetico and Wawa subprovinces (Figure 3) and stretches 50 km from the Vermilion fault in Minnesota northeastward to Ontario. The BLSZ separates the Vermilion Granitic Complex to the northwest from the Newton Lake Formation southeast of the fault (Plate 1).

The Newton Lake Formation consists of pillowed basalts, subaqueous mafic lavas, gabbros, diabases, and mafic to ultra-mafic sills, as well as bimodal volcanic units, with felsic volcanics rocks chiefly to the east and mafic volcanics rocks to the west (Bauer, 1990; Sims, 1976). The Newton Lake Formation has undergone regional metamorphism as strong as greenschist facies early after its formation (Green and Schultz, 1982).

The Vermilion Granitic Complex is generally divided into two dominant components: 1) a migmatite composed dominantly of granitic rocks found in the western part of the complex; and 2) the Lac La Croix Granite, the younger of the two (Bauer, 1986), which dominates the eastern region (Bauer, 1985). Additionally, the Vermilion Granitic Complex is surrounded by a margin of biotite schist (Bauer et al., 1992). The migmatites in the western portion of the complex have a schist-rich component in which the schistose rocks are as much as 25% of the total proportion (Bauer, 1985). These schist-rich migmatites are mainly in the southern part of the complex where veins of trondhjemite intrude them, creating locally complex intrusive migmatites (Bauer, 1990). The Lac La Croix Granite (Bauer, 1985) is a medium-grained grayish-pink biotite granite

(Bauer et al., 1992). The southern most extent of the Vermilion Granitic Complex is dominated by an amphibolite grade biotite schist which becomes increasingly migmatitic towards the center of the complex, north of the Vermilion fault (Bauer, 1986). This biotite schist has two foliations, S_1 and S_2 . S_1 is thought to parallel bedding, thus representing primary layering except in the rare instance of small-scale folds of bedding where S_1 is axial planar. The S_2 foliation is an axial planar foliation. S_1 and S_2 form an intersection lineation (Bauer, 1986).

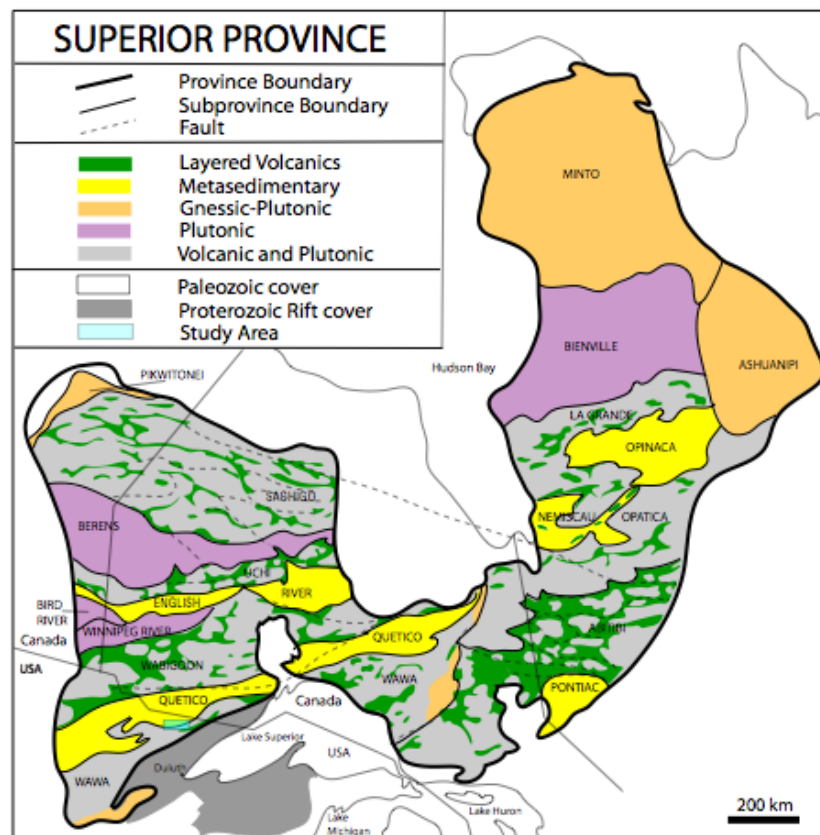


Figure 3: Simplified geologic map of the Superior Province of Canada and northern Minnesota with subprovince boundaries and the study area designated by the small blue rectangle in the south-west part of the map area after Card, 1990.

2.3 Previous Studies

Previous workers have proposed as many as seven separate deformation events in the area of the southern Superior Province of Minnesota, all of which are thought to support the hypothesis of Phanerozoic-style island-arc accretionary tectonics operating in the Archean (Table 1). These deformation events are summarized as:

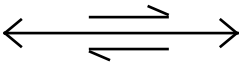
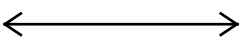
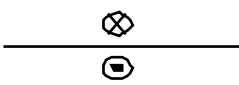
1. Nappe-forming event with weak fabric evidence
2. East-west folding accompanied by dextral shear and north-south shortening
3. West-trending open folding (Jenny, I am not sure what is meant by this?)
4. North-trending kink folding (again, north-trending folding doesn't make sense)
5. North-side-up displacement along the BLSZ and Haley fault
6. Sinistral displacement on the North Arm fault
7. Dextral displacement along the Vermilion, Wolf Lake and Shagawa faults.

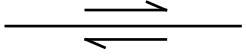
Studies focused on the BLSZ are limited. Students in a Keck Symposium project studied rock units and relative age relationships between units (intrusions, dikes and sills) along a trace of the BLSZ surrounding Basswood Lake in northeastern Minnesota. In this study, mapping of deformation features found faults/shear zones in what was termed the Burntside Lake fault zone (due to the evidence of brittle faulting) and small splays from the shear zone (namely the Pipestone Trace) (Woodard and Weaver, 1994). Structural analyses as well as mineralogical analyses were performed to understand offset

and strain across the zone. Structural studies performed on the splays indicated both sinistral and dextral offset, with slightly more evidence indicating dextral offset. One study performed by Font (1994) concluded that there was an early ductile event followed by a brittle event. Johnson (1994) proposed vertical displacement evidenced by an increase in metamorphic grade, in which the vertical displacement was accommodated by a single oblique offset event or multiple motions through time with different orientations. Yet another student concluded that faulting occurred between 2.6 and 1.2 Ga (Woodward, 1994).

More recently, Wolf (2006) studied the Canadian extent of the BLSZ in Quetico Provincial Park of Ontario, Canada. The study included structural, geochemical and geochronological work to understand the timing and type of deformation that occurred along the Burntside Lake and Shagawa/Knife Lake shear zones. In his study area, strain was recorded by formation of stretching lineations, rotated porphyroblasts, C-S fabrics, and folded veins, which indicated that deformation occurred by dextral and thrust motion along the BLZS. Wolf also noted some retrograde metamorphism from amphibolite to greenschist facies, as indicated by the retrogression of amphibole to chlorite. Geochronology indicated an average age of the host units between 2740 to 2686 Ma (Wolf, 2006).

Table 1: Summary of deformation events recognized by others.

| Deformation Event | Features | Fabric associated with this deformation | Map View |
|-------------------|---|--|---|
| D ₁ | A nappe-forming event (Bauer, 1985, 1986, 1990; Hooper, 1971; Hudleston, 1988). | Little fabric evidence (weak S ₁) | |
| D ₂ | East-west, upright folds (F ₂) that plunge east or west (Bauer, 1985; Hooper, 1971); (Hudleston, 1988) (Bauer, 1990; Tabor, 1991). Accompanied by dextral shear and north-south shortening (Hudleston, 1988). | S ₂ (axial planar cleavage, Jirsa et al., 1992) and L ₂ . F ₂ folds vary from isoclinal to open (Jirsa et al., 1992). |  |
| D ₃ | West-trending non-cylindrical folds in the Vermilion granitic complex (southern VGC, Bauer and Bidwell, 1990). West-trending cylindrical folds (F ₃) (northern VGC, Bauer et al., 1992) | S ₃ and L ₃ S ₃ is a crenulation cleavage (Bauer, 1988). |  |
| D ₄ | North-trending, steeply plunging kink-fold axes (Hooper and Ojakangas, 1971; Hudleston et al, 1988; Bauer and Bidwell, 1990; Tabor and Hudleston, 1991) | | |
| D ₅ | North-side-up, dip-slip displacement along the Haley and Burntside lake faults (Bauer and | |  |

| | | | |
|----------------|--|--|---|
| | Bidwell, 1990) | | |
| D ₆ | Sinistral shear on the northeast-striking North Arm fault (Bauer and Bidwell, 1990) | |  |
| D ₇ | Dextral shear along the east-west striking Vermilion, Wolf Lake and Shagawa Faults (Bauer and Bidwell, 1990; Wolf, 2006) | |  |

3. METHODS

3.1 Field Methods

Before beginning fieldwork, topographic and bedrock geologic maps were studied to identify areas and method of study of the BLSZ. Existing geologic maps (Green, 1982; Sims, 1978) show geologic units, structures and outcrop areas which were invaluable during fieldwork to identify specific areas for detailed study. Fieldwork was carried out in the summer of 2007; the bulk of the work was completed on foot, although lakeshore exposures were accessed by canoe. Fieldwork consisted of geologic mapping, observation of geologic relationships, collection of structural data, and collection of rock samples (some oriented) for petrographic and microstructural study. In total, 106 rock samples were collected throughout the field area in order to provide a complete representation of the rock types present. Oriented rock samples were mapped to study petrologic, microstructural, and kinematic displacement. Samples without orientation were collected for lithology identification. Due to the very fine-grained nature of the rocks in the field area in addition glacial rounding of low, flat outcrops, kinematic analysis was not possible in the field. The majority of rock samples are of two types: greenstones and biotite schists. Other rock types collected include granite, gabbro, tonalite, garnet-biotite schist, amphibolite, greenstone, and biotite-hornblende schist.

In addition to sample collection, foliation and lineation orientation were recorded where observed. Because of the steep down-dip nature of lineations, lineation pitch was measured in addition to trend and plunge in order to confirm the orientation and to evaluate variation in lineation across the field area. Foliation and lineation

orientations were used along with added marks to orient samples for later sample preparation following the methods of Hansen, 1990.

Sample locations and orientation data were plotted on topographic base maps. A geologic map showing geologic units, geologic structures and sample locations is included with this work (Plate 1). Figures depicting measured structural data are included in section 4.4 Structural and Microstructural Analysis of this work.

3.2 Petrography

Detailed optical petrography allows for rock identification and the assignment of a comprehensive rock name, particularly useful for fine-grained lithologies.

Metamorphic mineral assemblages, textures, and fabrics were used to determine general metamorphic facies as well as relative sequence of mineral growth and deformation.

Metamorphic textures and mineral assemblages also allow for the interpretation of likely protolith. Detailed petrography is necessary to select appropriate samples for quantitative mineral analysis and geothermobarometry.

In addition to documenting mineral assemblages, the description of textures is important in this study to help identify prograde versus retrograde mineral phases, timing of mineral growth (syn-, post-, or pre-kinematic), and to identify relict protolith textures.

Fabrics in L-S tectonites were studied with a large-format polarizing microscope.

Samples containing fabrics that might indicate a sense of motion were examined using methods outlined by Passchier and Trouw (2005).

Of the 106 samples collected, 19 were selected for petrographic analysis.

Samples with readily identifiable foliations and lineations were chosen for thin section

study, as well as any with distinctive mineralogy. Attention was also paid to the spatial distribution of samples to ensure a geographically representative suite of thin sections.

3.3 Electron Microprobe Analysis

Determination of mineral compositions is helpful to identify minerals not easily resolved by optical methods, to evaluate compositions of solid-solution phases, and to determine P-T conditions of crystallization with thermobarometric methods (e.g., Spear, 1993).

Element mapping and quantitative mineral analysis were completed on a JEOL JXA-8900 electron probe microanalyzer (EPMA) in the Department of Earth Sciences at the University of Minnesota-Twin Cities, with assistance of the laboratory technician Ellery Frahm.

Prior to mineral analysis by EPMA, samples were chosen and prepared as polished sections based on mineral assemblages appropriate for use in geothermobarometric calculations. In addition, photomicrographs were taken of all sections to be analyzed; this allowed for the identification of specific targets as well as preparation of image maps to guide analysis during use of the electron microprobe. EPMA spot analyses were collected by using a focused electron beam with an accelerating voltage of 15 kV and a current of 22.5 nA. During sample analysis energy-dispersive spectrometry was used for quickly identifying unknown mineral phases, while wavelength-dispersive spectrometry was used to quantitatively measure mineral compositions. For each mineral grain analyzed, 5-20 'spots' were chosen, depending on the size of the grain being analyzed.

For two of the three samples containing garnet, additional garnet element maps and quantitative analyses of garnet-biotite pairs were obtained. Quantitative analyses of chlorite, hornblende, plagioclase and epidote were obtained where possible. Data from the 8 samples analyzed are listed in Appendix 2.

3.4 Treatment of Microprobe Data

Mineral element data collected from the microprobe are given in weight percent of the oxides. In order to determine mineral formulae and to use these data for geothermometry calculations, they must be recalculated in cation proportions with correct stoichiometry. To do this, standard methods were followed from papers that established the geothermometers used in this study. For cation recalculations, iron is problematic due to the fact that the microprobe does not differentiate between ferric and ferrous valence state of iron. For biotite analyses, 12% of the total iron present was assumed to be ferric, based on Mossbauer spectroscopy presented by Guidotti and Dyar (1991). Additionally, they recommend that of the total Fe^{3+} , only 8% is partitioned into the tetrahedral site and the remaining 4% into the octahedral site (Guidotti and Dyar, 1991). For chlorite formula recalculations, the tetrahedral site (filled with Al and Si) was assumed to equal 4 cations, and any remaining Al was assigned to the octahedral site, based on data from Caritat et al (1993).

For epidote calculations iron is assumed to be all ferric, and for garnet all ferrous. For recalculating hornblende formulas, the method employed by Laird and Albee (1981) was applied to account not only for ferric and ferrous iron, but also to balance alkalis and overall site assignments. This approach was confirmed with limitations set forth by Holland and Blundy (1994) for calculating ferric iron in amphibole.

3.5 Structural and Microstructural Analysis

To understand the kinematic history of the BLSZ, foliation and lineation orientations were measured in the field. These data were plotted on stereographic projections to gain insight into the orientation of the foliations across the zone and additionally the relationship between the foliations and lineations.

To analyze and interpret microstructural textures, the methods of Passchier and Trouw (2005) were followed. All thin sections displaying fabric asymmetries were carefully observed and interpreted. The dominant feature used to determine shear sense was shear band cleavage (Fig. 4), along with mantled porphyroclasts.

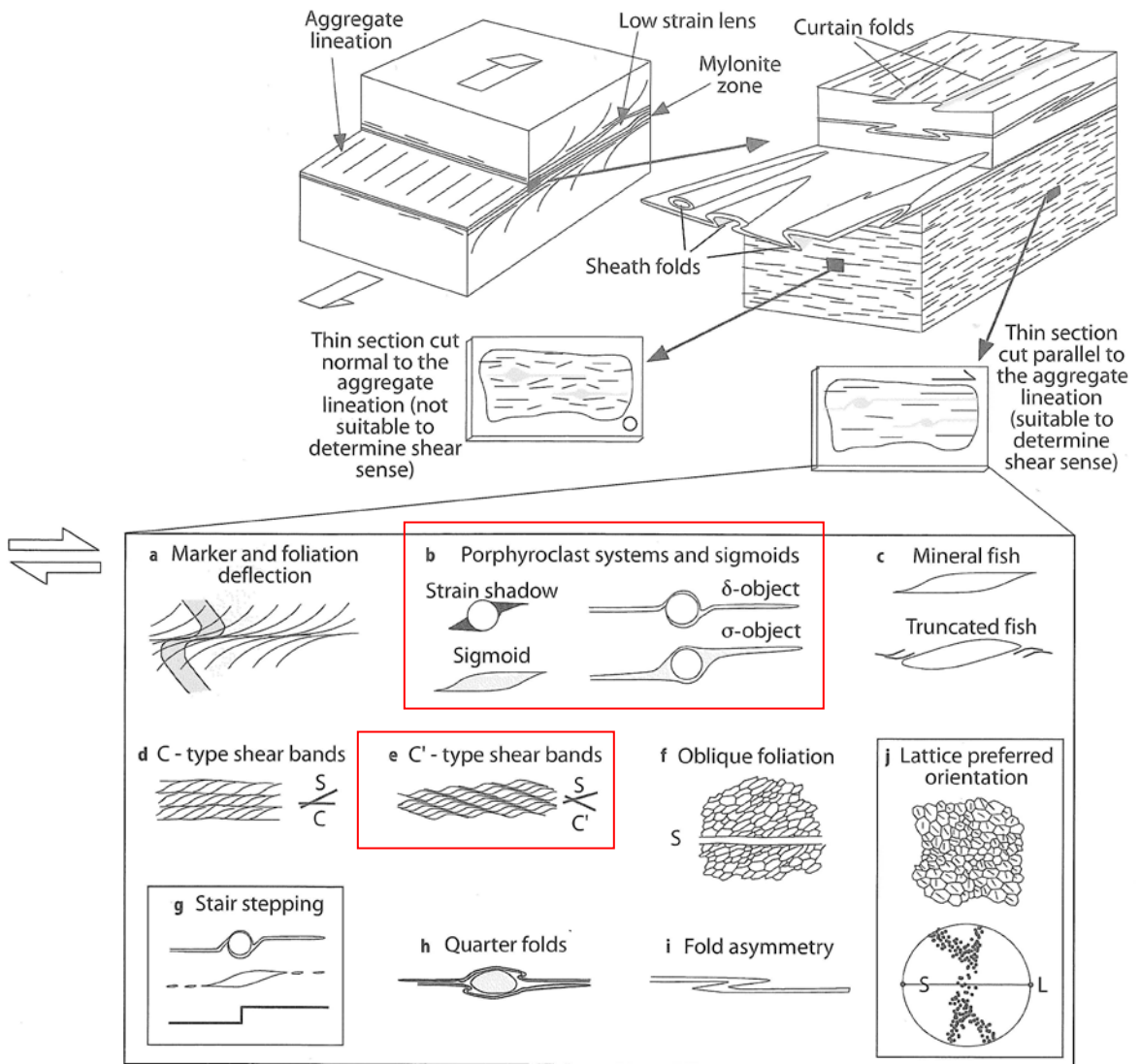


Figure 4: Shear sense indicators in a shear zone. The two types of indicators used in this study are noted by a red box. Modified from Passchier and Trouw (2005).

4. RESULTS

4.1 Field Relationships

Two rock types dominate in this area of the BLSZ where it affects the Wawa and Quetico subprovinces of the Superior province (Figure 3). The first rock unit, found to the south of the BLSZ, is a very fine-grained green-colored unit designated ‘metavolcaniclastic’ greenstone in the field (the term ‘metavolcaniclastics’ was used in the field to describe the very fine-grained, green colored rocks that contained small specks). This ‘metavolcaniclastic’ unit in most places looks massive, but upon closer inspection along broken outcrop edges a very fine foliation is discernable. A mineral lineation, also very difficult to discern in hand sample, exists in these ‘metavolcaniclastics’.

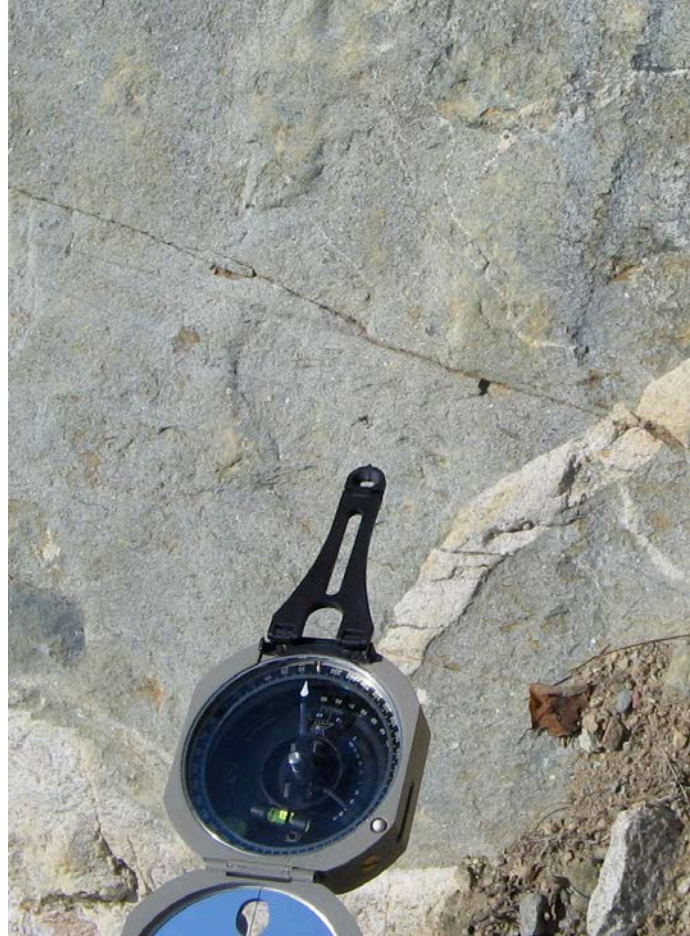


Figure 5: Field photograph showing the fine-grained nature of the ‘metavolcaniclastic’ unit, with Brunton compass for scale and north indicator.

The second rock type, found to the north of the BLSZ, is a fine- to medium-grained biotite schist. The schist unit contains a more easily seen foliation and lineation than that observed in the ‘metavolcaniclastic’ unit. In general, the regional foliation strikes east-west and is sub-vertical. Mineral elongation lineations, where visible, are near vertical. The biotite schist unit appears to accommodate most of the deformation of the BLSZ based on the more pronounced foliation, as well as the observation that the orientation of the fabric in this unit most closely aligns with the topographic expression of the shear zone, as discussed further in the structure portion of this work.

This two-fold field classification worked well in the field to differentiate the ubiquitous very fine-grained rocks; however, these two units were later divided into subtypes based on petrographic analysis (Section 4.2).



Figure 6: Field photograph showing the appearance of the biotite schist. Note the photo is taken from plan view, not the motion plane. Brunton compass for scale and north indicator.

Field relationships between these two units was hard to determine in the field due to the low-lying, topographically depressed nature of the shear zone. Most, if not all, direct contact relationships between the two units (green, metavolcaniclastic rock and schist) were unobservable due to the presence of bog areas and lakes. Therefore, the displacement analysis was restricted to thin section study.

General metamorphic grade based on grain size in the field indicates that rocks to the north of the BLSZ preserve a higher metamorphic grade than rocks to the south. In

addition, deformation is apparently localized in two broad zones in the study area, one in the northeast and one in the southwest, though this apparent pattern may be induced by the location of the lakes and low-lying swampy regions in the field area.

Mapping of the islands of Burntside Lake revealed locations, previously denoted biotite schist (Green and Schultz, 1982; Peterson, 2002), that are thoroughly intruded by granitic and granodioritic bodies as vein-like structures centimeters to tens of centimeters wide. Some of these intrusive ‘veins’ were undeformed whereas others appear to have experienced similar deformation as the intruded schist. On many islands on Burntside Lake, the degree of intrusion, coupled with the pavement-type outcrops, prevented the measurement of foliation due to lack of confidence in consistency of these planes. Additionally, due to the pavement nature of these outcrops, the above description of outcrops and fabric is not based on the motion plane identified later by petrographic analysis.

4.2 Petrography

Petrographic study was utilized to fully describe rock units observed in the field, to determine general metamorphic grade, and to ascertain samples appropriate for microprobe work. Table 2 summarizes the dominant rock types determined by optical petrography. Note the ‘metavolcaniclastic’ unit is here divided into two units; amphibolite and chloritic greenstone, and the schist unit divided into two different units, biotite schist and garnet-biotite schist.

Table 2: Petrographic description of major metamorphic rock types

| Unit Name | Description |
|-----------|-------------|
|-----------|-------------|

| | |
|-----------------------|--|
| Amphibolite | (70% Hbl+Chl, 20% Qtz, 10% Cal, trace opaques) Green, fine-grained (<1mm) rocks with both a foliation and an elongation lineation. The amphibolite contains hornblende or actinolite, quartz, calcite, with accessory opaque phases. Microtextures include undulose anhedral quartz grains and aggregates, subhedral grains of hornblende (dominant) and actinolite (described in only one thin section), and coarse-grained vein-fill calcite. The foliation and lineation are defined by hornblende and actinolite GSPO. One sample contains garnet. |
| Chloritic Greenstone | (65% Chl, 15% Ep, 10% Cal, 7% Qtz, 3% opaques) Green, fine-grained (<1 mm) rock, with a weakly defined foliation and elongation lineation. This greenstone contains chlorite, epidote, calcite, and quartz, with accessory opaque. Microtextures consist of anhedral undulose quartz grains, euhedral to subhedral chlorite grains and euhedral to subhedral opaque phases +/-subhedral epidote porphyroblasts . |
| Biotite Schist | (65% Qtz, 25% Bt, 10% Pl, trace opaques) Dark grey, fine-grained (<1mm) rocks containing both a foliation and an elongation lineation. The biotite schist contains biotite, quartz, and feldspar. Microtextures include anhedral, undulose quartz grains, anhedral plagioclase grains containing tapering albite twins and subhedral to anhedral biotite grains. The way to discontinuous foliation is defined by a biotite GSPO. This sample contains biotite-rich and quartz-rich layers that alternate, indicating possible original bedding, now parallel to foliation. The biotite grains in the foliation also define a weak S-C fabric. |
| Garnet-Biotite Schist | (30% Qtz, 30% Pl, 25% Bt, 10% Chl, 5% Grt) Dark grey, fine-grained (<1mm) rock with a weak foliation and elongation lineation. The schist contains quartz, plagioclase feldspar, biotite, chlorite and garnet, with accessory opaque. Microtextures include euhedral to subhedral equant garnet porphyroblasts; quartz and plagioclase grains are anhedral and undulose, and some samples display minor chlorite replacement of biotite. Biotite defines the foliation. |

4.3 Mineral Chemistry and P-T Calculations

Six samples from the field area were chosen for use in determining mineral chemistry and geothermometry calculations. Figure 14 shows the locations of the samples used to complete the temperature calculations.

Below are brief descriptions of the samples.

159-1: *Chloritic greenstone* (65% Chl, 15% Ep, 10% Cac, 7% Qtz, 3% opaques) is a green, fine-grained (<1 mm) rock, with a weakly defined foliation and elongation lineation. This greenstone contains chlorite, epidote, calcite, and quartz, with accessory opaque phases. This sample was taken south of the BLSZ.

139-1: *Biotite-hornblende schist* (60% Qtz, 15% Bt, 15% Hbl, 5% Pl, 5% Cc, trace opaques) is a dark grey, fine-grained rock with a weak foliation and elongation lineation. The schist contains quartz, biotite, hornblende, plagioclase feldspar, and calcite, with accessory opaque. This sample was taken north of the BLSZ.

59-1: *Garnet-biotite schist* (30% Qtz, 30% Pl, 25% Bt, 10% Chl, 5% Grt) is a dark grey, fine-grained (<1mm) rock with a weak foliation and elongation lineation. The schist contains quartz, plagioclase feldspar, biotite, chlorite and garnet, with accessory opaque. This sample was taken north of the BLSZ.

61-1: *Chloritic greenstone* (40% Cc, 25% Chl, 20% Qtz, 10% feldspar, 5% opaques) is a dark green, fine-grained (<1mm) rock with a foliation and elongation lineation. The greenstone contains calcite, quartz, chlorite

and plagioclase feldspar, with accessory opaque. This sample was taken south of the BLSZ.

137-1: *Garnet-biotite schist* (30% Qtz, 25% Bt, 15% Grt, 15% Pl, 10% Chl, 5% opaques) is a grey, fine-grained (<1mm) rock with a foliation and elongation lineation. The schist contains quartz, biotite, plagioclase, garnet, and chlorite, with accessory opaque. Microtextures include euhedral to subhedral equant garnet porphyroblasts; quartz and plagioclase grains are anhedral and undulose, and chlorite replaces biotite. The foliation and lineation are defined by a GSPO of biotite. The foliation is planar except where it wraps around garnet porphyroblasts, and is interrupted by small quartz grains. This sample was taken north of the BLSZ.

255-1: *Garnet-bearing amphibolite* (60% Hbl, 15% Qtz, 10% Ep, 5% Grt, 5% Cc, 5% Pl) is a dark green, fine-grained (<1mm) rock with a foliation and elongation lineation. The amphibolite contains hornblende, quartz, epidote, plagioclase feldspar, garnet, actinolite and calcite, with accessory opaque. Microtextures include porphyroblastic, equant but broken garnet, quartz and plagioclase occurring as anhedral undulose grains, and euhedral hornblende 'needles' that define the foliation and lineation in this sample. The foliation in the sample is planar and uniform, except where it wraps around garnet/epidote aggregates. The epidote occurs as a replacement of garnet. This sample was taken south of the BLSZ.

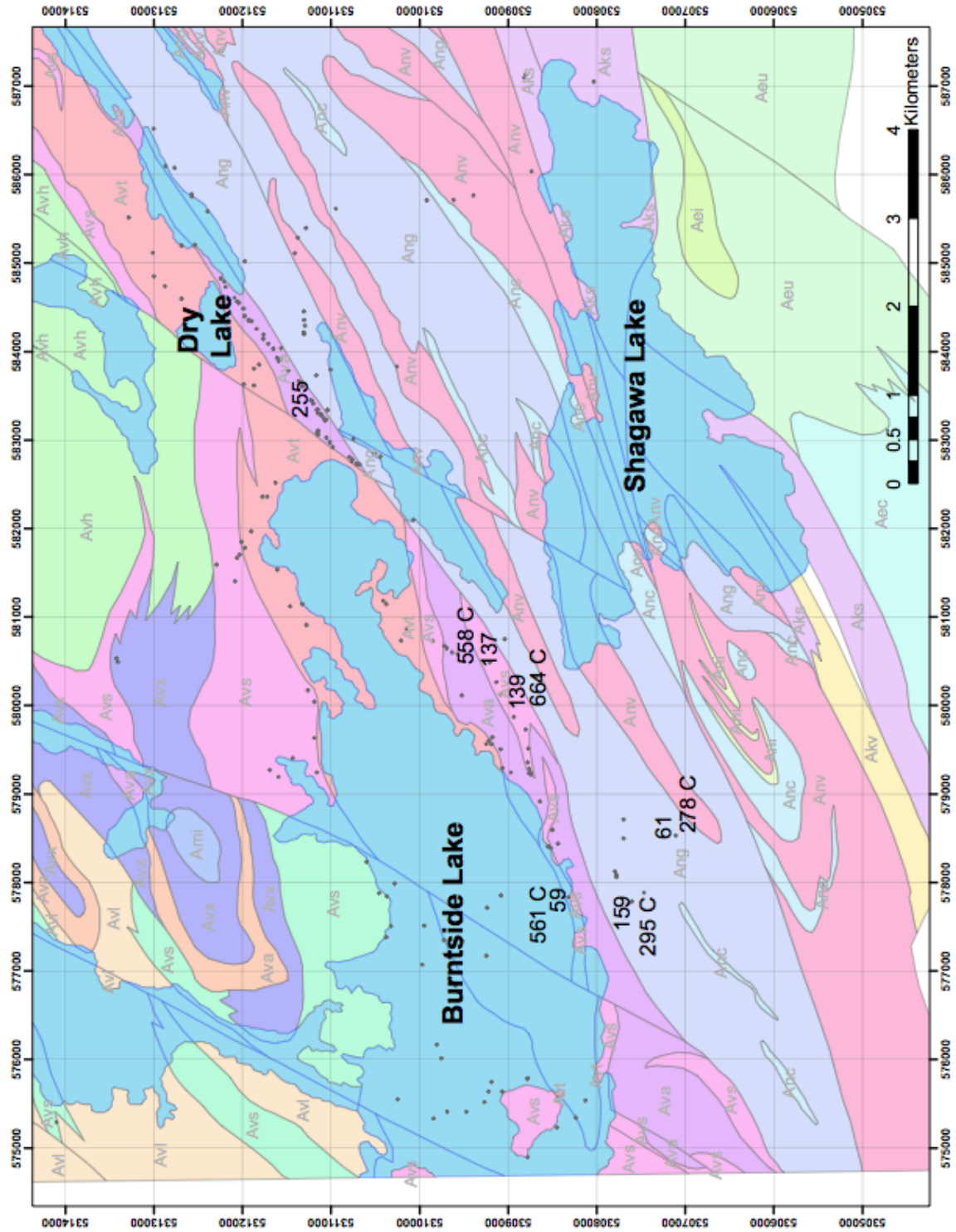


Figure 7: Geologic map from plate 1 showing locations and temperatures yielded from the samples utilized for geothermometry work.

Mineral compositions determined by electron microprobe analysis are listed in Table 3 below. These average mineral compositions were used to calculate pressure and temperature conditions of metamorphism.

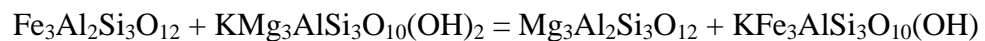
Table 3: Mineral Compositions Determined by Electron Microprobe Analysis

| Sample | 137 Garnet | 59 Garnet | 137 Biotite | 59 Biotite | 255 Hornblende | 139 Hornblende | 255 Plagioclase | 139 Plagioclase | 61 Chlorite | 159 Chlorite |
|--------------------------------|---------------|--------------|----------------|---------------|-------------------|-------------------|--------------------|--------------------|----------------|-----------------|
| SiO ₂ | 37.10 | 36.92 | 35.41 | 36.76 | 44.14 | 43.39 | 56.72 | 62.18 | 25.85 | 25.34 |
| Al ₂ O ₃ | 21.46 | 21.41 | 18.22 | 19.65 | 10.76 | 10.51 | 27.44 | 24.07 | 19.08 | 19.63 |
| TiO ₂ | 0.05 | 0.05 | 2.05 | 0.89 | 0.60 | 0.48 | 0.00 | 0.01 | 0.07 | 0.05 |
| Cr ₂ O ₃ | 0.05 | 0.02 | 0.10 | 0.07 | 0.02 | 0.05 | -0.02 | 0.00 | 0.03 | 0.00 |
| FeO | 26.85 | 29.52 | 17.86 | 21.92 | 19.38 | 17.28 | 0.37 | 0.12 | 31.79 | 30.09 |
| MgO | 2.81 | 3.49 | 11.81 | 8.42 | 9.20 | 10.46 | -0.01 | 0.01 | 10.96 | 12.75 |
| MnO | 8.38 | 5.97 | 0.46 | 2.73 | 0.37 | 0.48 | -0.02 | 0.01 | 0.18 | 0.53 |
| CaO | 4.02 | 2.66 | 0.22 | 1.37 | 12.22 | 11.39 | 9.85 | 5.43 | 0.12 | 0.05 |
| Na ₂ O | 0.02 | 0.01 | 0.18 | 0.62 | 1.17 | 1.14 | 5.84 | 8.36 | 0.39 | 0.03 |
| K ₂ O | 0.05 | 0.28 | 8.40 | 3.74 | 0.31 | 0.92 | 0.07 | 0.20 | 0.03 | 0.03 |
| Total | 100.79 | 100.34 | 94.72 | 96.17 | 98.19 | 96.10 | 100.23 | 100.38 | 88.51 | 88.49 |
| Cations | (12 oxygens) | (12 oxygens) | (22 oxygens) | (22 oxygens) | (23 oxygens) | (23 oxygens) | (8 oxygens) | (8 oxygens) | (14 oxygens) | (14 oxygens) |
| Si | 2.962 | 2.957 | 5.367 | 5.417 | 6.675 | 6.669 | 2.541 | 2.747 | 2.798 | 2.725 |
| Al (IV) | 2.018 | 2.021 | 3.264 | 3.459 | 1.919 | 1.903 | 1.452 | 1.253 | 1.202 | 1.275 |
| Al (VI) | | | | | | | | | 1.237 | 1.213 |
| Ti | 0.003 | 0.003 | 0.233 | 0.105 | 0.068 | 0.055 | 0.000 | 0.001 | 0.006 | 0.004 |
| Cr | 0.003 | 0.001 | 0.012 | 0.008 | 0.003 | 0.006 | 0.014 | 0.000 | 0.003 | 0.000 |
| Fe | 1.792 | 1.978 | 2.275 | 2.803 | 2.451 | 2.395 | 0.000 | 0.006 | 2.885 | 2.707 |
| Mg | 0.335 | 0.423 | 2.680 | 1.978 | 2.075 | 2.395 | -0.001 | 0.000 | 1.773 | 2.043 |
| MN | 0.567 | 0.404 | 0.060 | 0.328 | 0.047 | 0.063 | -0.001 | 0.000 | 0.017 | 0.049 |
| Ca | 0.344 | 0.228 | 0.036 | 0.207 | 1.980 | 1.874 | 0.475 | 0.316 | 0.014 | 0.006 |
| Na | 0.003 | 0.002 | 0.026 | 0.075 | 0.344 | 0.339 | 0.506 | 0.672 | 0.079 | 0.006 |
| K | 0.005 | 0.031 | 1.615 | 0.725 | 0.061 | 0.181 | 0.004 | 0.006 | 0.004 | 0.004 |
| Total | 8.032 | 8.048 | 15.569 | 15.106 | 15.624 | 15.706 | 4.989 | 4.998 | 10.017 | 10.032 |

In general the plagioclase grains measured from the BLSZ are albite rich. The range of plagioclase grains analyzed is between An_{23.3} to An_{34.4}. The garnets from the BLSZ are enriched in almandine, however they range in composition from: Ca_{0.344}Mg_{0.335}Mn_{0.567}Fe_{1.792} to Ca_{0.228}Mg_{0.423}Mn_{0.404}Fe_{1.978} (these are the average garnet composition of both thin sections utilized for mineral chemistry analysis, 137 and 59, respectively). Hornblende from the BLSZ is rich in tschermakite with Na substituting in the M4 site. Chlorite from the zone is rich in chamosite, dominated by Fe substitution (2.707-2.885 Fe, 1.77-2.04_{Mg}).

To calculate temperatures of equilibrium from mineral compositions, I used Frank Spear's GTB program for garnet-biotite based on numerous calibrations (e.g., Ferry and Spear, 1978; Hodges and Spear, 1982; Ganguly and Saxena, 1984; Perchuk and Lavrent'eva, 1984; Indares and Martignole, 1985; Ferry and Spear, 1990; Patino Douce et al., 1993; Holdaway et al., 1997; Gessmann et al., 1997; Kleemann and Reinhardt, 1994) and hornblende-plagioclase pairs using the calibration of Holland and Blundy (1994).

The garnet-biotite thermometer utilizes the exchange of iron and magnesium between garnet and biotite in equilibrium in a sample. The reaction can be written as follows:



In using the garnet-biotite thermometer one must be wary of samples containing high levels of manganese as this can imply non-ideal mixing. One must also be wary of utilizing the garnet biotite thermometer in a system that contains higher levels of Ti, Al, and Ca (in addition to the afore mentioned Mn) because these components of the system

are not generally accounted for in the thermometer. Both samples utilized for the garnet-biotite thermometry are garnet biotite schists with the following assemblages:

Sample 137: 30% Qtz, 25% Bt, 15% Grt, 15% Pl, 10% Chl (retrograde),
5% opaques

Sample 59: 30% Qtz, 30% Pl, 25% Bt, 10% Chl (retrograde), 5% Grt

4.3.1 Garnet Biotite Thermometry

Two thin sections (59-111 and 137-111) contained almandine garnet/biotite pairs. The GTB program contains 11 calibrations for calculating temperature from garnet-biotite exchange reactions. All calibrations were run on garnet-biotite pairs from samples 59 and 137 using the mineral pair in each that displays textures indicative of chemical equilibrium (see Figure 8 and 9 below) to determine which calibrations were the most appropriate for the data collected; this was supplemented by reviewing the literature on these calibrations to understand the theory and metamorphic environments used to generate and quantify the calibrations. From these sections, garnet core and rim compositions were averaged. Biotite analyses were averaged for each section, in an effort to minimize error in analyses.

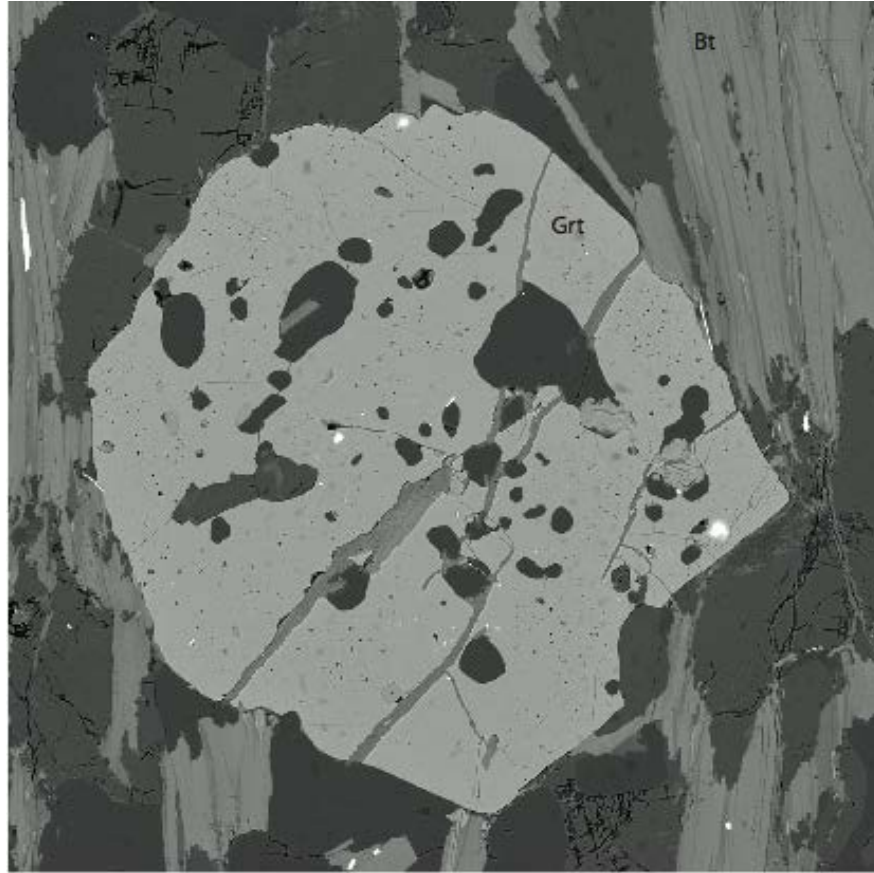


Figure 8: BSE image of garnet porphyroblast in thin section 59-111 utilized for garnet-biotite thermometry. The composition of the labeled biotite grain was used in the temperature determination. Notice the large size and uninterrupted grain boundaries, indicating chemical equilibrium. Grt, garnet; Bt, biotite; field of view is 1.23 mm.

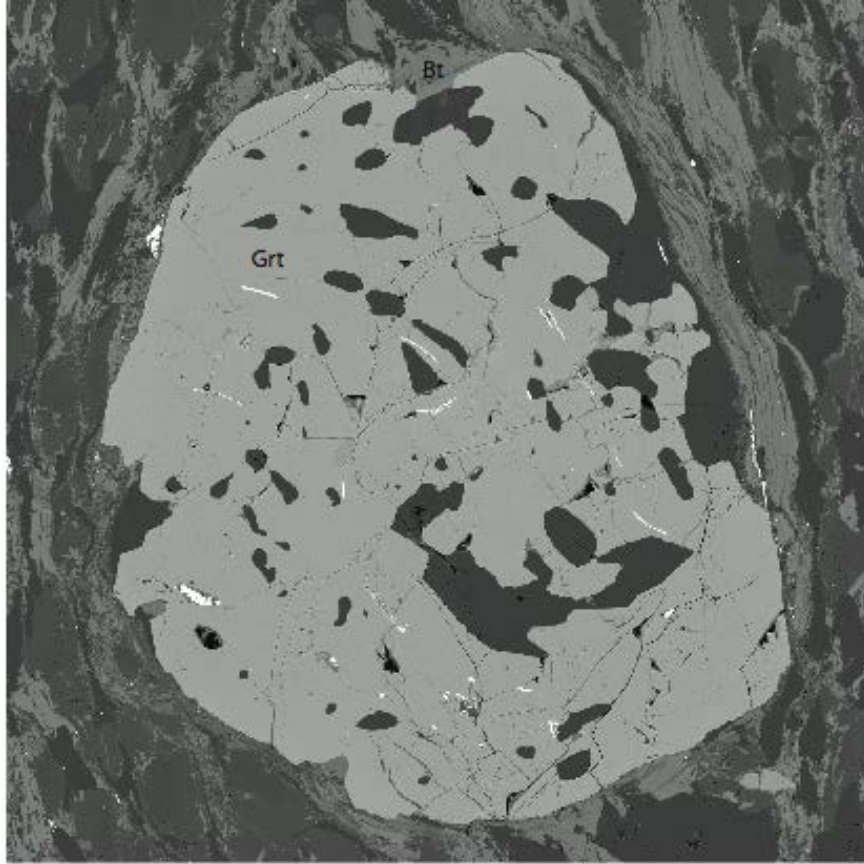
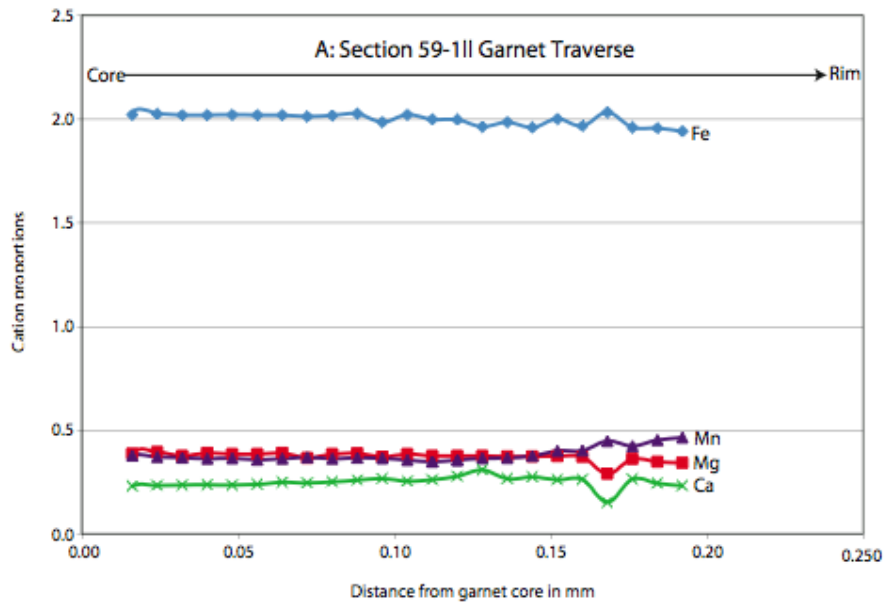


Figure 9: BSE image of garnet porphyroblast on thin section 137-111 utilized for garnet-biotite thermometry. The composition of the labeled biotite grain was used in the temperature determination, based on proximity to the garnet grain as well as by comparisons to other biotite grains in the section near the garnet. Notice the large size and continuous grain boundaries, indicating chemical equilibrium. Grt, garnet; Bt, Biotite; field of view 1.23 mm.

Element maps of garnet porphyroblasts as well as core-to-rim traverses were completed in each section to examine the compositional zoning present in the garnets (Figures 10 and 11). These methods demonstrate that the garnets are only weakly zoned, with Mn content increasing toward the rim of one garnet analyzed. This was taken into

consideration when averaging garnet rim compositions, because elevated Mn content is a sign of non-ideal mixing that may depart from ideal solid solution between Fe and Mg and can lead to errors in temperature estimates. The garnets analyzed are dominated by almandine component ($X_{\text{Fe}} = 0.592\text{-}0.653$), within the range of compositions of $\text{Ca}_{0.344}\text{Mg}_{0.335}\text{Mn}_{0.567}\text{Fe}_{1.792}$ to $\text{Ca}_{0.228}\text{Mg}_{0.423}\text{Mn}_{0.404}\text{Fe}_{1.978}$.



B: Element maps of a garnet from sample 59-111.

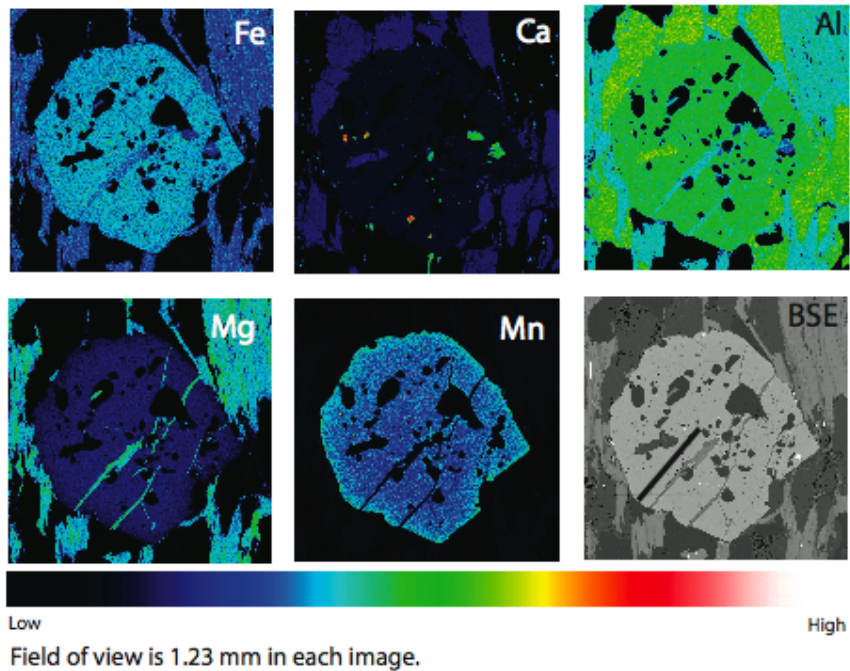
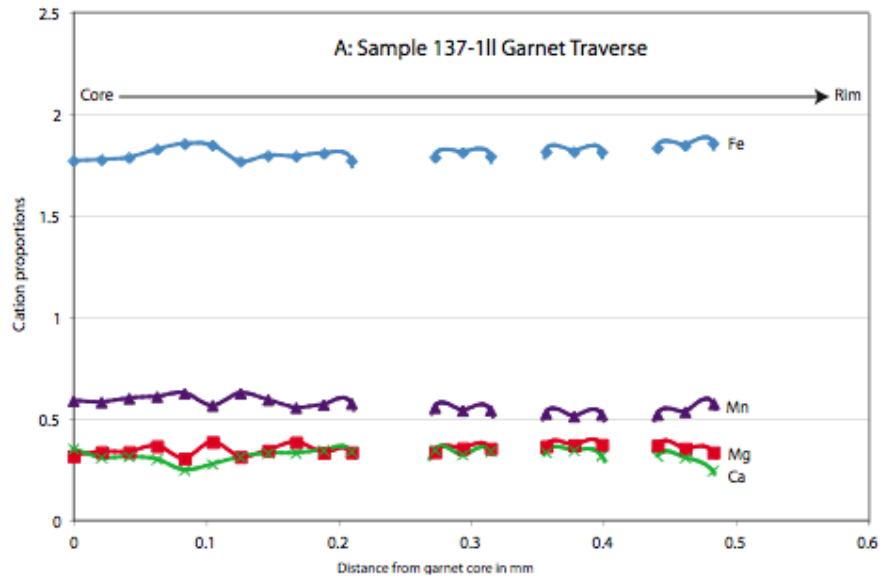


Figure 10: A) Graph of cation proportions vs. distance in garnet to illustrate the homogeneous composition. B) Element maps imaged by EPMA to illustrate the homogeneous composition of the garnet analyzed (BSE=back-scattered electron image).



B: Element maps of a garnet from sample 137-1ll

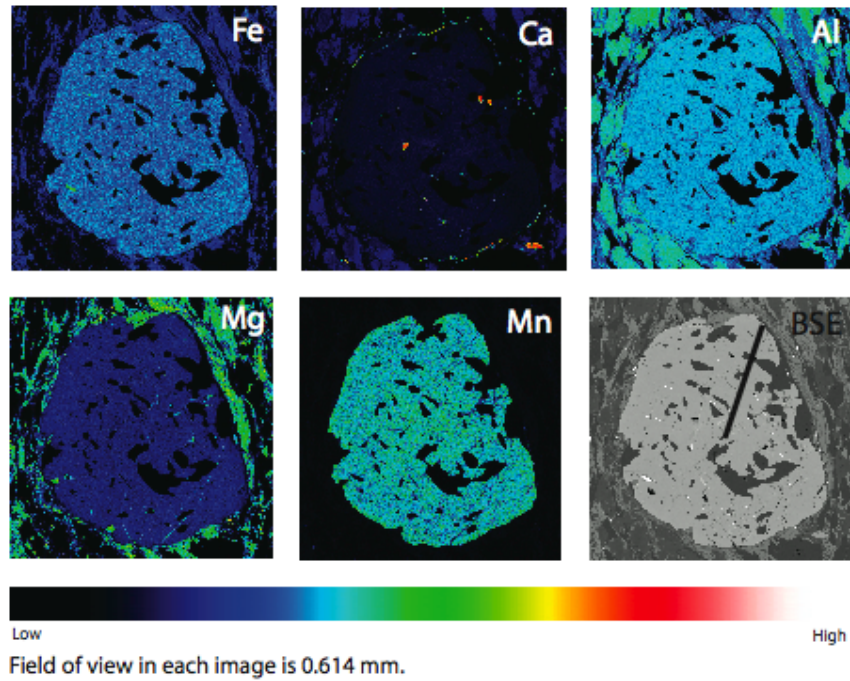


Figure 11: A) Graph of cation proportions vs. distance in garnet to illustrate the homogeneous composition. B) Element maps imaged by EPMA to illustrate the homogeneous composition of the garnet analyzed.

Figures 12 and 13 illustrate the resulting temperatures from entering the average mineral compositions in the GTB program and using the Grt-Bt exchange thermometers.

Tables 4 and 5 summarize the temperatures determined by the approach described.

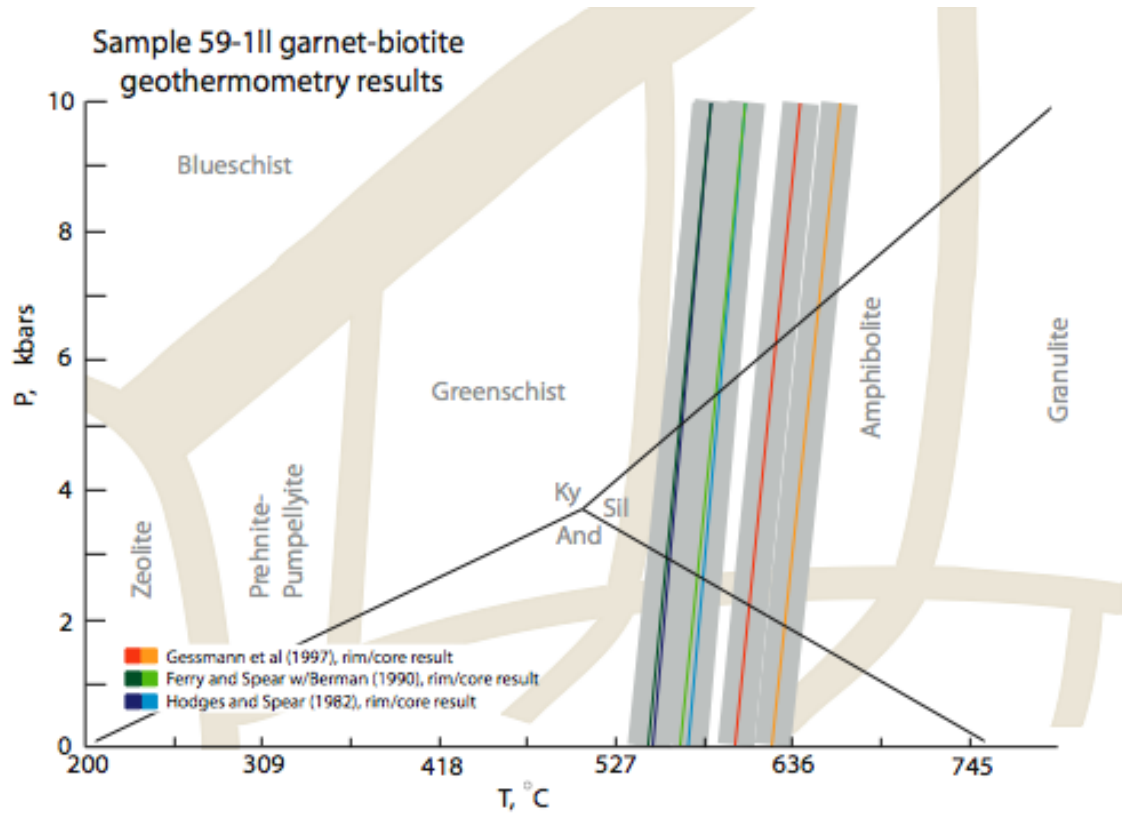


Figure 12: Graph depicting the resulting temperatures from mineral compositions determined in sample 59-111, as calculated using the GTB program. Note the darker colors represent rim results, whereas the lighter colors represent core results. The grey shading represents the error within the thermometer.

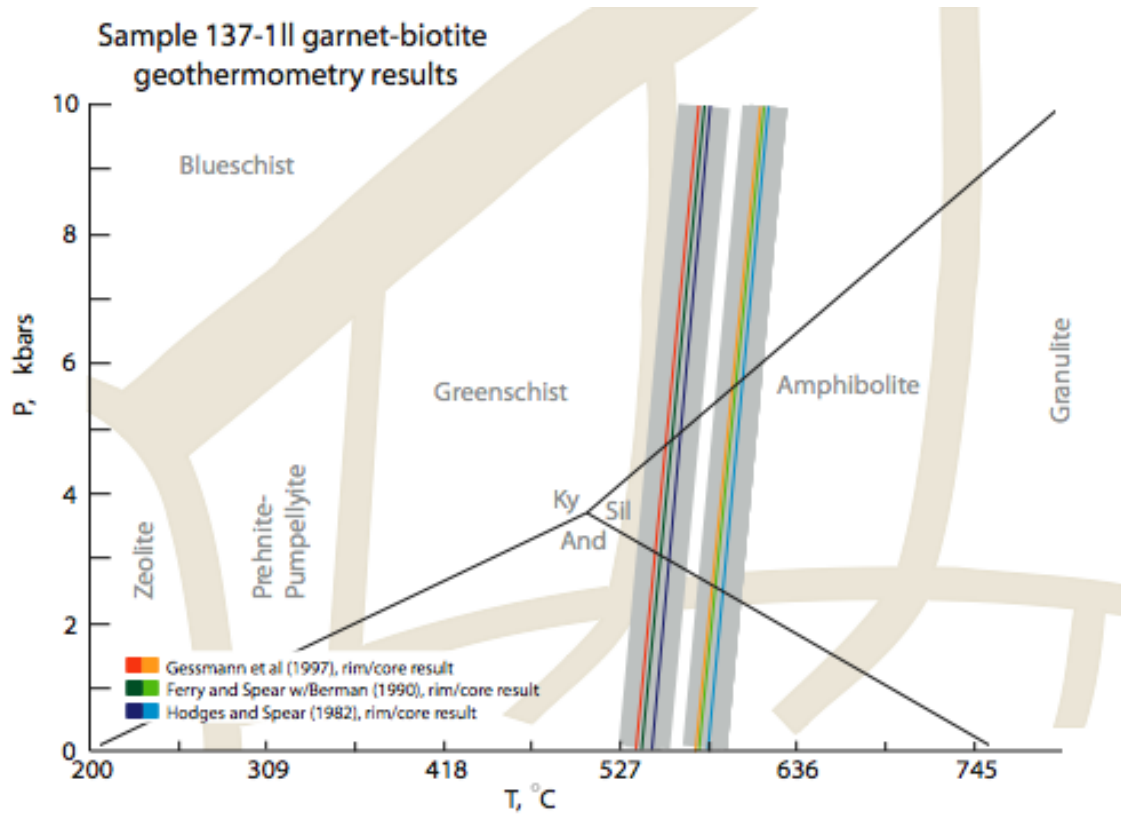


Figure 13: Graph depicting the resulting temperatures from mineral compositions determined in sample 137-111, as calculated using the GTB program. Note the darker colors represent rim results, whereas the lighter colors represent core results. Grey bar represents the general +/- 25 °C error of the thermometer.

Table 4: Garnet-Biotite Thermometry Results (at 3kbar)

| Calibration | Sample 137 | Sample 59 |
|---|------------|-----------|
| Gessmann et al (1997) | 556°C | 613°C |
| Ferry and Spear (1978) w/ Berman (1990) | 558°C | 557°C |
| Hodges and Spear (1982) | 564°C | 561°C |

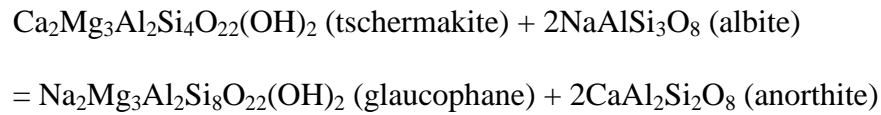
*3 kbar chosen as a reasonable medium-low pressure given the mineral assemblage

The Gessman et al (1997), Ferry and Spear (1978) with Berman (1990) garnet model, and Hodges and Spear (1982) calibrations were chosen because these calibrations are the most utilized calibrations and most suited for the garnet-biotite pairs analyzed in

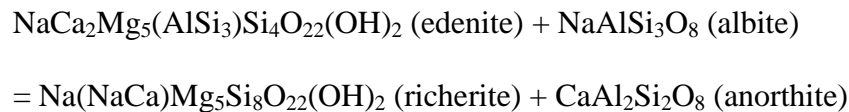
this study. The samples give an average temperature of ~560 °C +/- 25 °C if the temperature from sample 59 by Gessman et al 1997 calibration is left out from the calculation.

4.3.2 Hornblende-Plagioclase Thermometry

The hornblende-plagioclase thermometer used in this study is based on the exchange of (NaSi) for (CaAl)₋₁ between hornblende and plagioclase. The reaction can be written (Holland, 1994):



or



For the hornblende-plagioclase pair in sample 139, the thermometer calibration of Holland and Blundy (1994) was used. Temperature results are limited to an uncertainty of +/- 40°C within the range of 400-1000°C (Holland and Blundy, 1994). This calibration is not suitable for barometry. Few geobarometers utilizing amphibole group minerals have been proposed in the scientific literature due to their compositional complexity (Blundy, 1990). The table below summarizes the resulting temperatures utilizing the Holland and Blundy calibration on sample 139:

Table 5: Hornblende-Plagioclase Thermometry Results

| <u>Author/Calibration</u> | <u>Sample 139</u> |
|---------------------------|-------------------|
| Holland and Blundy (1994) | 664°C |

4.3.3 Chlorite Thermometry

The general formula for chlorite is as follows: $(R^{2+}_u R^{3+}_y \square_z)^{VI} (Si_{4-x} Al_x)^{IV} O_{10+w} (OH)_{8-w}$. In this formula: R^{2+} is usually Mg^{2+} or Fe^{2+} , R^{3+} is usually Fe^{3+} or Al^{3+} , and \square represents a structural vacancy. The chlorite thermometer is based on Al substitution in the tetrahedral site for Si. Along with this Al-Si substitution, octahedral Fe content increases and octahedral vacancies decrease (Frimmel, 1997).

Samples 61 and 159, both identified as chloritic greenstones, were utilized for the temperature calculations. The chlorite temperature calculations are based on a trioctahedral chlorite (Frimmel, 1997). Therefore, one must know that one's samples contain trioctahedral chlorite, not dioctahedral chlorite. The calculations would be false if used with dioctahedral chlorite. Xie et al. (1997) showed there is a correlation between the presence of other aluminous phases and an increase of Al_2O_3 in chlorite. In fact, as the subsisting aluminous phases become enriched in Al_2O_3 so the Al_2O_3 content in the associated chlorite increases as well, so the presence of additional aluminous phases must be taken into consideration when using the chlorite thermometer. For temperatures based on chlorite compositions I used the following calibrations:

$$T = -61.92 + 321.98(Al) \text{ (Cathlineau, 1988)}$$

$$T = 106 Al + 18$$

$$\text{where } Al = Al + 0.7 (Fe/[Fe+Mg]) \text{ (Kranidiotis, 1987)}$$

$$T = 17.5 + 106.2 [2^{IV}Al - 0.88 (X_{Fe} - 0.34)] \text{ (Frimmel, 1997)}$$

The table below summarizes the resulting temperatures obtained from chlorite thermometry:

Table 6: Chlorite Thermometry Results

| <u>Calibration</u> | <u>Sample 61</u> | <u>Sample 159</u> |
|-------------------------------|------------------|-------------------|
| Cathlineau (1988) | 191°C | 195°C |
| Frimmel (1997) | 278°C | 295°C |
| Kranidotis and Maclean (1987) | 325°C | 349°C |

The differences in resulting temperatures in chlorite are not negligible. However chlorite thermometry on its own should be taken with care and generally not as a stand-alone indicator of temperature because some studies have found the Al-in-chlorite thermometry to show large discrepancies between the calibrations (De Caritat, 1993; Frimmel, 1997). However, the two samples give similar temperatures for any one calibration.

In summary, results of garnet-biotite and hornblende-plagioclase thermometry performed in rocks north of the BLSZ gave higher temperature results than the chlorite thermometry performed on greenstones south of the BLSZ. This information indicates that the rocks north of the BLSZ experienced higher-grade metamorphism.

4.4 Structural and Microstructural Analysis

Structural Data

Foliation and lineation measurements collected in the field were supplemented with measurements compiled from the Shagawa and Ely geologic quadrangle maps (Green, 1982; Sims, 1978). Throughout the field area, average foliation is oriented N82E,63SE; however, in some areas of the zone the foliation steepens to nearly vertical. The stereonet shown in Figure 14 summarizes the orientation of foliation.

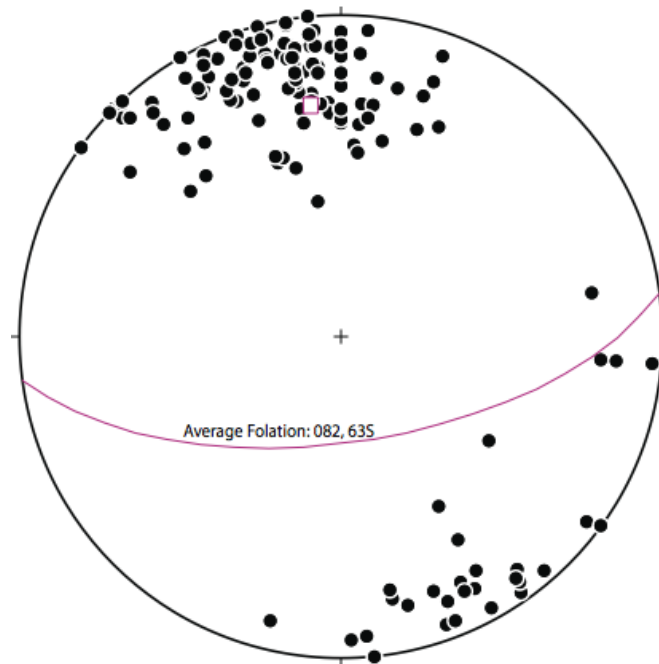


Figure 45: A stereonet plot of poles to foliation measured in the field and supplemented by data from the Shagawa and Ely quadrangle maps. Average foliation is shown by the pink girdle, generated by using the plot mean vector function in Stereonet (Allmendinger 2006.)

An elongation lineation (Le) observed in the study area is defined by elongate biotite, actinolite, and chlorite within the foliation plane. Taking into account the nearly vertical orientation of the BLSZ, Le is easier to visualize using pitch. In the field area, Le consistently has a pitch between 80-90°.

Plotting and extrapolating foliation trajectories highlights an interesting relationship with the previously mapped and topographic expression of the BLSZ, as shown in the foliation trend map (Fig 15). Foliations are closely parallel to the south of the zone, however to the north of the BLSZ the foliation trend and from nearly parallel to oblique, and in some cases nearly perpendicular, to the main trend of the BLSZ. This

would indicate the possibility of another influence on the foliation orientation to the north of the BLSZ.

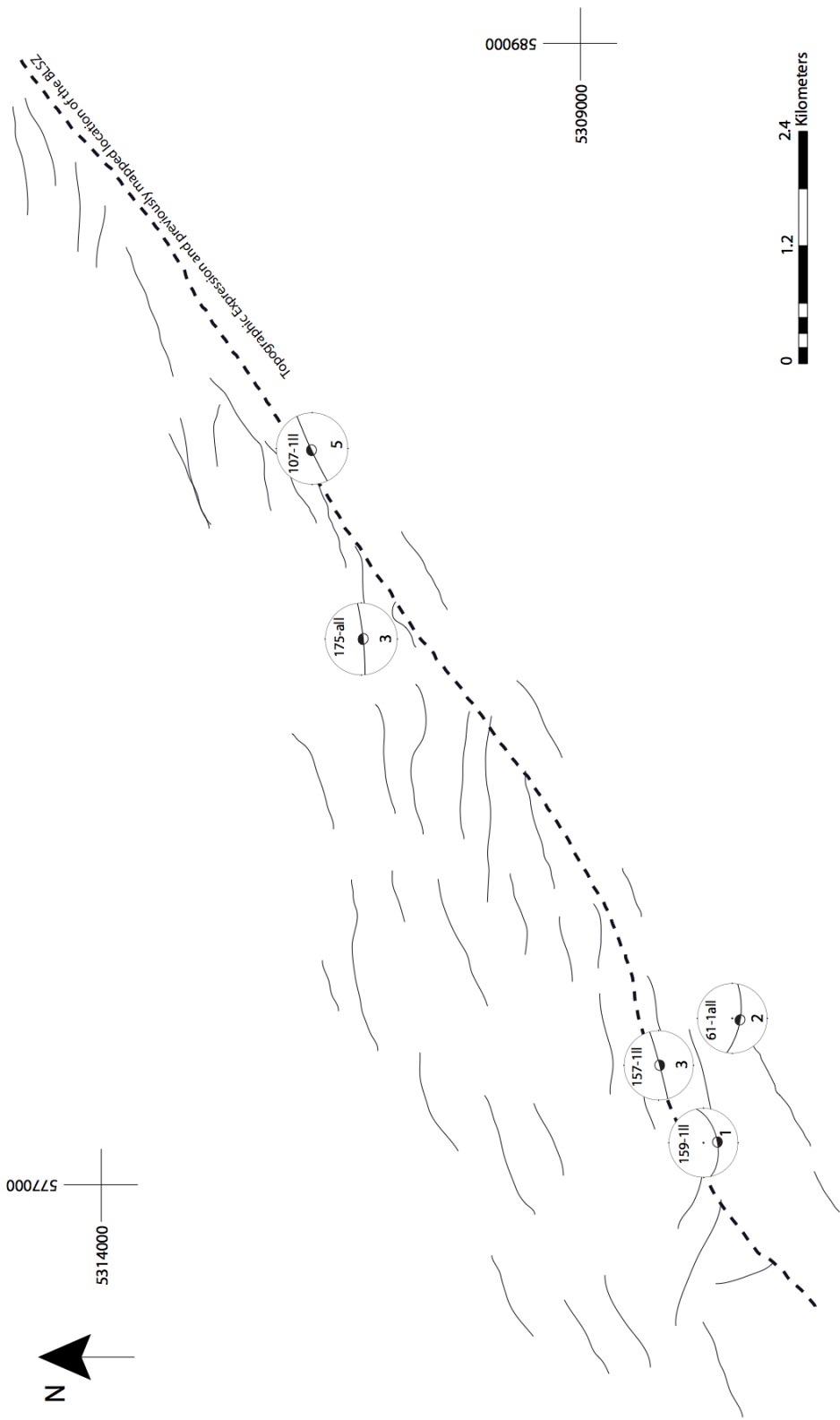


Figure 15: Foliation trend map illustrating the broad orientation of foliation (thin black lines) relative to the Burntside Lake Shear zone (thick dashed line), as well as average lineation. The synoptic stereoplots display average foliation orientation and up/down direction (illustrated by a half-filled circle in the center of the stereoplot, in which the black half of the circle represents upward displacement), the numbers on the stereonet represent confidence in the up/down direction, with 5 being most confident and 1 being the least confident.

Microstructural Analysis

Five samples, out of 21, were chosen for microstructural analysis based on the presence of visible textures and location with respect to the BLSZ to ensure adequate geographic coverage. The rock samples chosen are chloritic greenstones, amphibolite, and biotite schist whose foliation and lineations are defined by grain-shape preferred orientation and mineral elongation. Overall, the samples are very fine-grained, making field observation of microfabrics and interpreting displacement directions difficult. The most commonly observed structure was S-C tectonite fabric, along with some grain-shape preferred orientation and apparent deformation of thin, fine-grained veins. The photomicrographs in figures 16-19 illustrate the types of fabrics present in the samples and interpreted displacement directions. In each, I describe shear sense and give a confidence rating for the shear-sense indicator(s). The confidence level is based on a qualitative scale from 1-5, with 5 having the most confidence and 1 having the least confidence.

Sample 107 is a greenstone containing quartz, biotite, plagioclase and epidote, with trace amounts of apatite and opaque mineral phases. The interpreted protolith is a volcanoclastic rock. This sample contains a C-C' fabric (Fig 17).

The C planes are wavy and closely spaced, intersected by more widely-spaced C' planes. The C-C' planes indicate north-side-up displacement parallel to a steeply-plunging Le (Fig 16). Two additional samples, 61-1all and 175-all, also support the north-side-up displacement, however the confidence level on these samples is much lower than 107, at 2 and 3 respectively.

Sample 157 is a chloritic greenstone containing actinolite, chlorite, calcite and epidote, with trace amounts of opaque mineral phases. The sample contains S-C fabric defined broadly by large chlorite mats, as well as the occurrence of opaque phases that show increased population density along the S and C planes. The S-C asymmetry indicates south-side-up displacement (Fig 17).

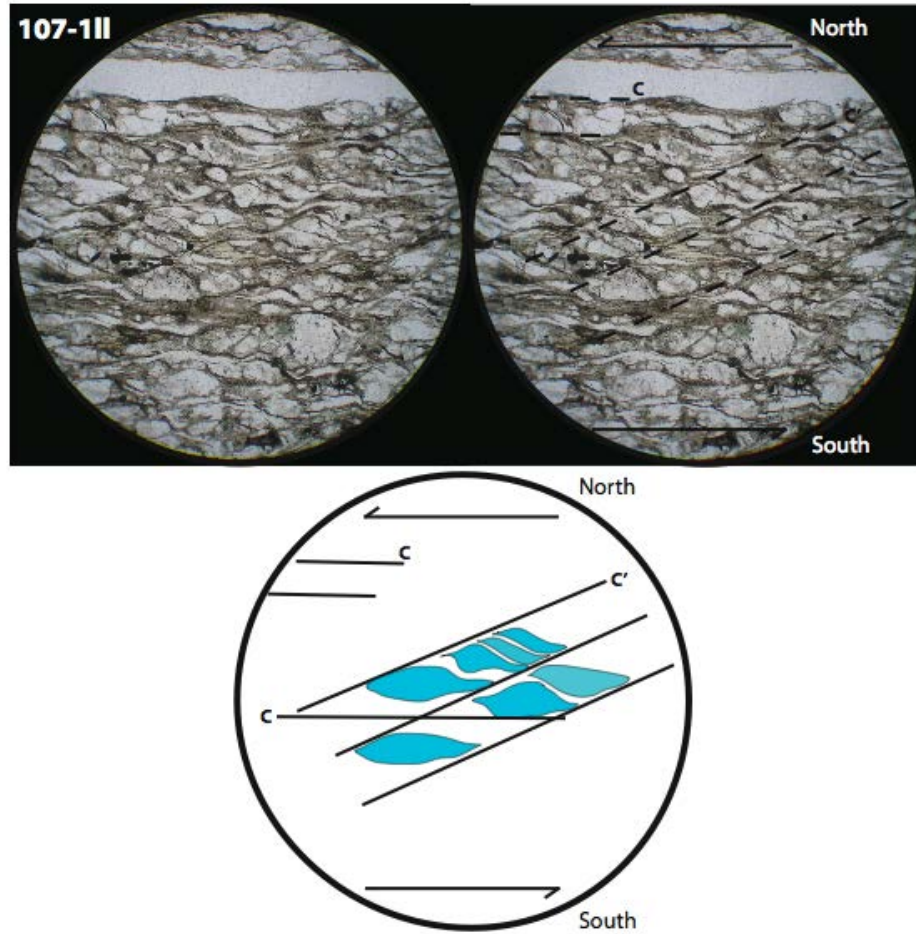


Figure 16: Photomicrograph of sample 107-11l containing C-C' fabrics which indicate north-side-up shear sense. Photomicrograph taken at 100x, field of view is 500 μ m. View is a motion plane view, normal to schistosity and parallel to L_e . Confidence level: 5.

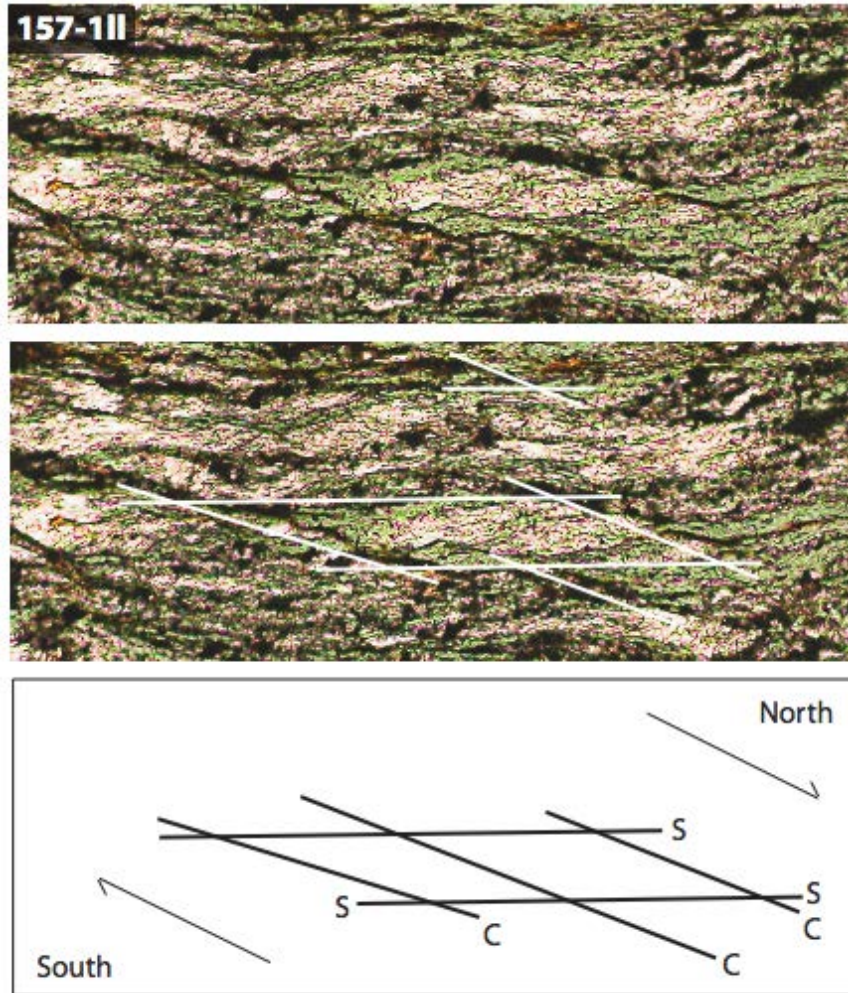


Figure 17: Photomicrograph and annotation illustrating the S-C fabrics recorded in sample 157-1ll. Photomicrograph taken at 100x, field of view is 1800 μm . The S-C fabrics record right-lateral displacement that when placed in geographical context, indicate south-side-up kinematics. Confidence level: 3.

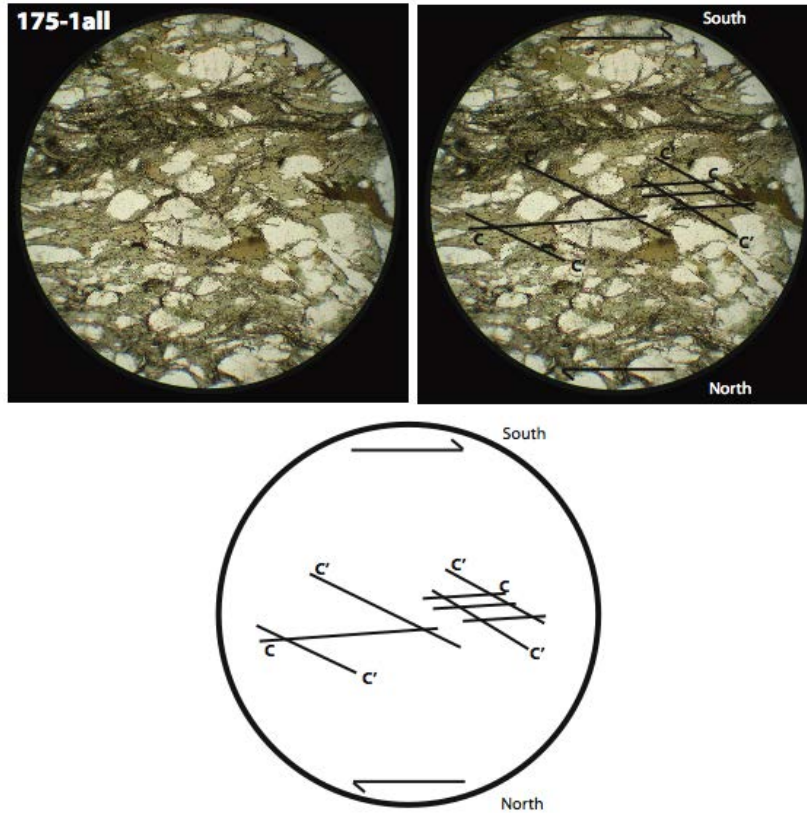


Figure 18: Photomicrograph and annotation illustrating the C-C' fabrics recorded in samples 175-11l. The C-C' fabrics record apparent right-lateral displacement that when placed in geographical context, indicate north-side-up kinematics. Confidence level: 3.

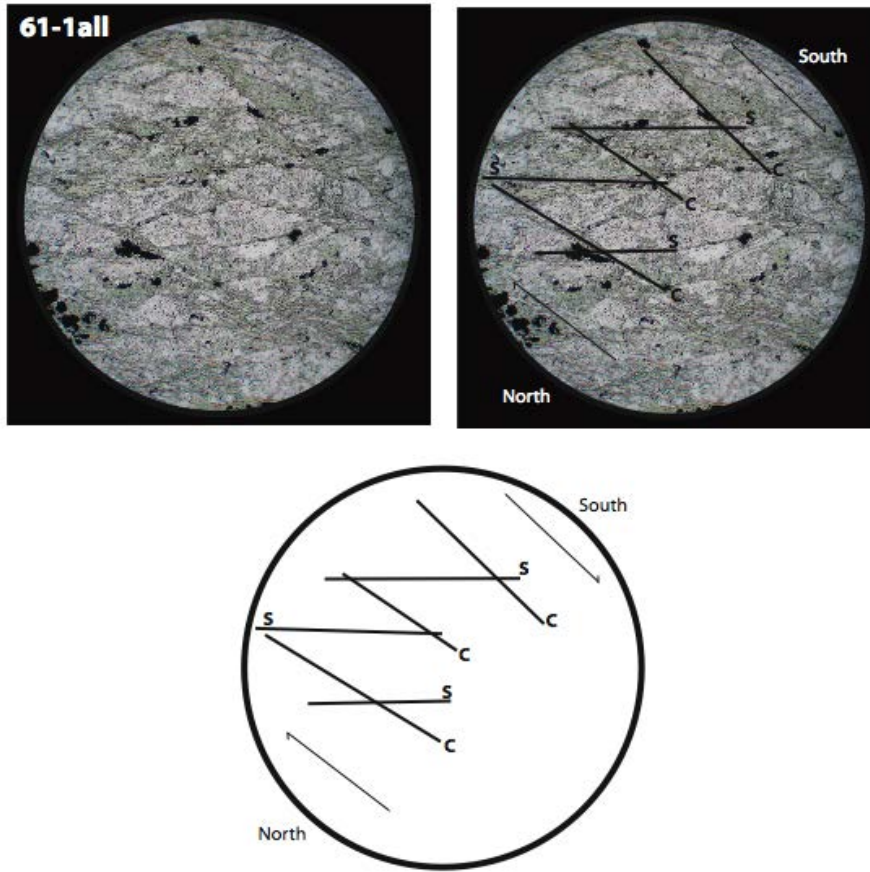


Figure 19: Photomicrograph and annotation illustrating the S-C fabrics recorded in samples 61-1all. The S-C fabrics record apparent right-lateral displacement that when placed in geographical context, indicate north-side-up kinematics. Confidence level: 2.

5. DISCUSSION

5.1 Discussion of Petrological and P-T Analysis

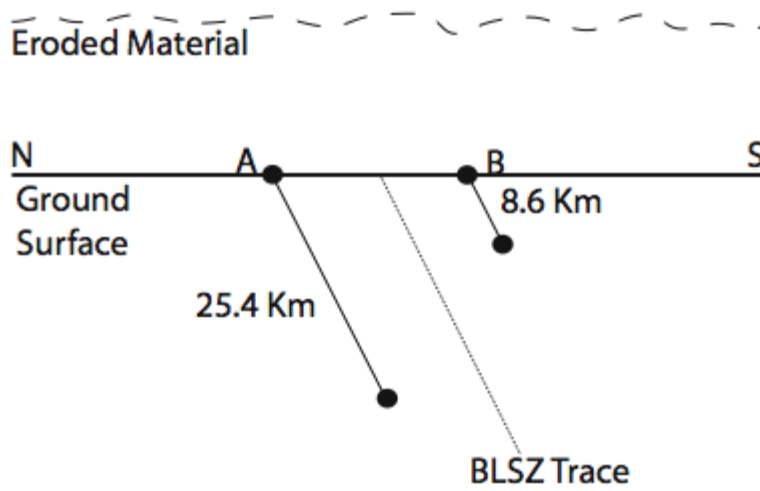
Analysis of mineral compositions in rocks from the BLSZ area leads to a broad conclusion that the rocks to the north of the shear zone experienced higher-grade metamorphism than rocks to the south. The general mineral assemblage of quartzofeldspathic rocks to the north of the BLSZ is garnet + biotite + quartz + plagioclase +/- hornblende. The garnet-biotite thermometry results indicate an average temperature of ~560 °C, with higher temperatures recorded by compositions in the core of the garnets and lower temperatures recorded by the rims. The general mineral assemblage of the metavolcaniclastic rocks to the south of the BLSZ is plagioclase + chlorite + calcite + epidote +/- amphibole, but it should be emphasized that in addition to a metamorphic discontinuity across the shear zone that there is also a change in rock bulk composition. Also found to the north of the BLSZ is a biotite-hornblende schist in which one hornblende-plagioclase pair yielded a temperature of 664 °C. The apparent difference in metamorphic temperatures recorded by rocks to the north of the BLSZ (560 °C by garnet-biotite and 664 °C by hornblende-plagioclase) could be a result of uncertainties associated with application of the different thermometers, or they could be real differences reflecting spatial variation between samples. The uncertainty in the garnet-biotite thermometer is +/- 25 °C and the hornblende-plagioclase thermometer can have an uncertainty up to +/- 75 °C. Combined, the uncertainties in the thermometers alone would account for the difference between resulting temperatures. Additionally, the samples are separated by ~6 km/m in the field area, perhaps indicating non-uniform

offset along the zone in which some rocks were displaced upward from deeper conditions, suggesting that the temperature difference could be real and reflect a true difference in metamorphic temperature along the zone. Chlorite thermometry in samples south of the BLSZ show an average temperature of ~ 190 °C (using the method of Cathlineau, 1988), and ~ 340 °C (using the method of Kranidotis and Maclean, 1987). Combined, the geothermometric data indicate that the rocks to the north of the BLSZ record a higher temperature metamorphism than rocks to the south, consistent with north-side-up displacement along the zone (see figure 21 for a summary map). This interpretation is predicted on the field and microstructural interpretation that displacement on the BLSZ is entirely dip-slip displacement, with no evidence for strike-slip displacement. Thus, the difference in metamorphic conditions is not a result of strike-slip juxtaposition of dissimilar metamorphic rocks, but rather is due to vertical relative displacement.

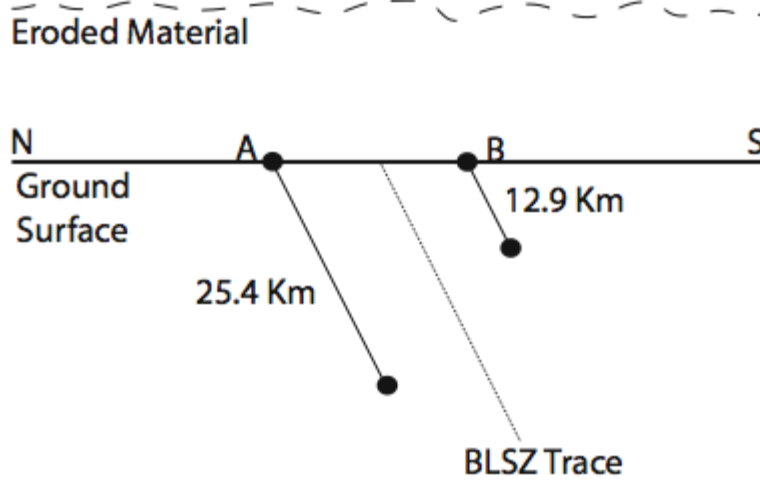
We can also use metamorphic temperatures to approximate the vertical offset along the BLSZ. To estimate the magnitude of vertical displacement, I assume the following: all movement along the zone is dip-slip, an average dip on the BLSZ of 63° , the rocks experienced a geotherm of 25 °C/km during displacement (a standard crustal geotherm), the geothermometry results are accurate, and that a temperature difference is recorded by the average temperature resulting from garnet-biotite thermometry to the north of the zone and chlorite temperatures from the south of the zone. A schematic cartoon showing the geometry used to estimate displacement is shown in Figure 20. The average garnet-biotite temperature of 560 °C was chosen because overall this thermometer is generally less fraught with error and has a smaller uncertainty than

hornblende-plagioclase thermometry. Using these assumptions, three estimates of vertical displacement (one for each chlorite temperature calibration) of X, Y and Z km are shown in Figure 20) Using metamorphic temperature as a proxy of offset along the zone result in an offset of 25.4 Km to the north of the zone and to the south a maximum offset of 15.1 Km and a minimum offset of 8.6 Km.

Scenario A (193 °C, Chl)



Scenario B (278 °C, Chl)



Scenario C (337 °C, Chl)

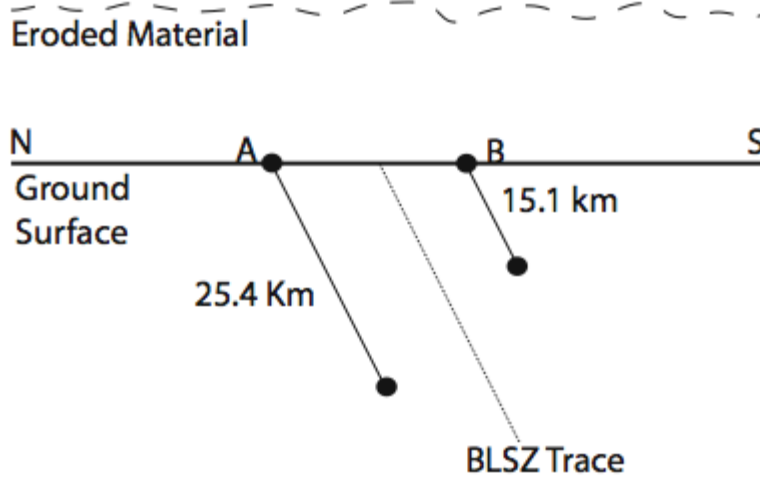
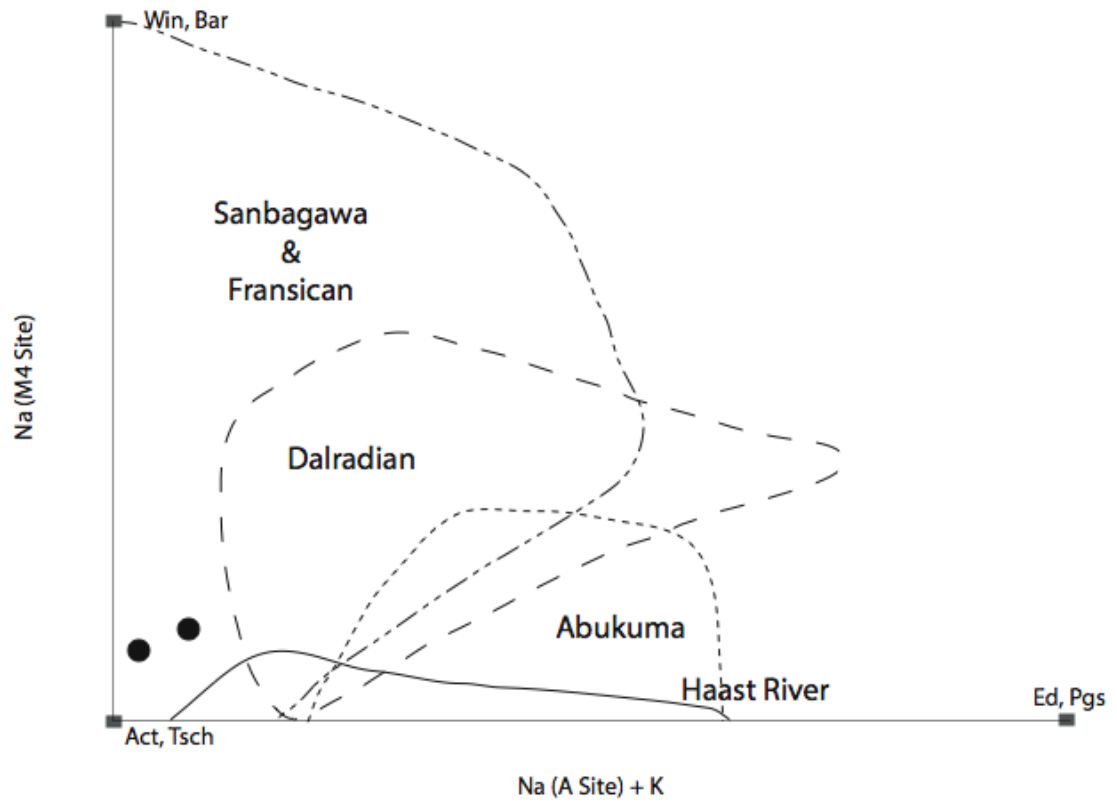


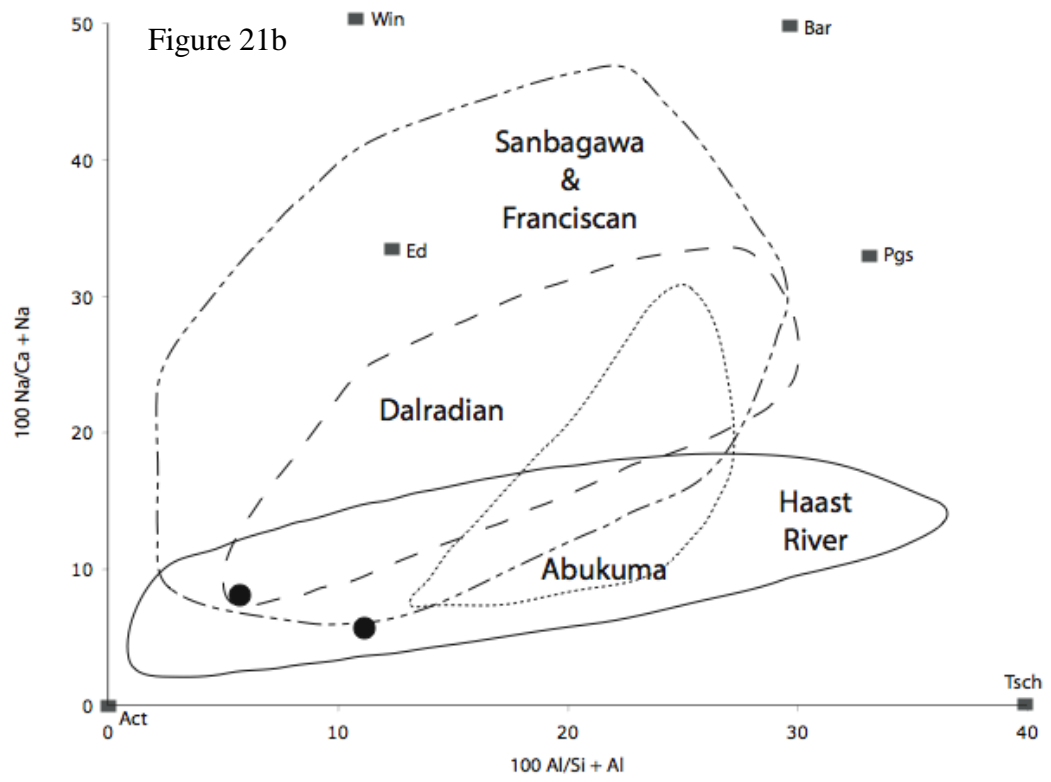
Figure 20: The cartoon above depicts three offset scenarios along the BLSZ as calculated using the average garnet-biotite temperature to the north and chlorite temperatures to the south. The scenarios utilize the following temperatures: all utilize the average garnet-biotite temperature of 560 °C to the north of the zone; scenario 1: average chlorite temperature of 193 °C; scenario 2: average chlorite temperature of 287 °C; scenario 3: average chlorite temperature of 337 °C. Total displacement along the BLSZ is estimated to be 9-15 km.

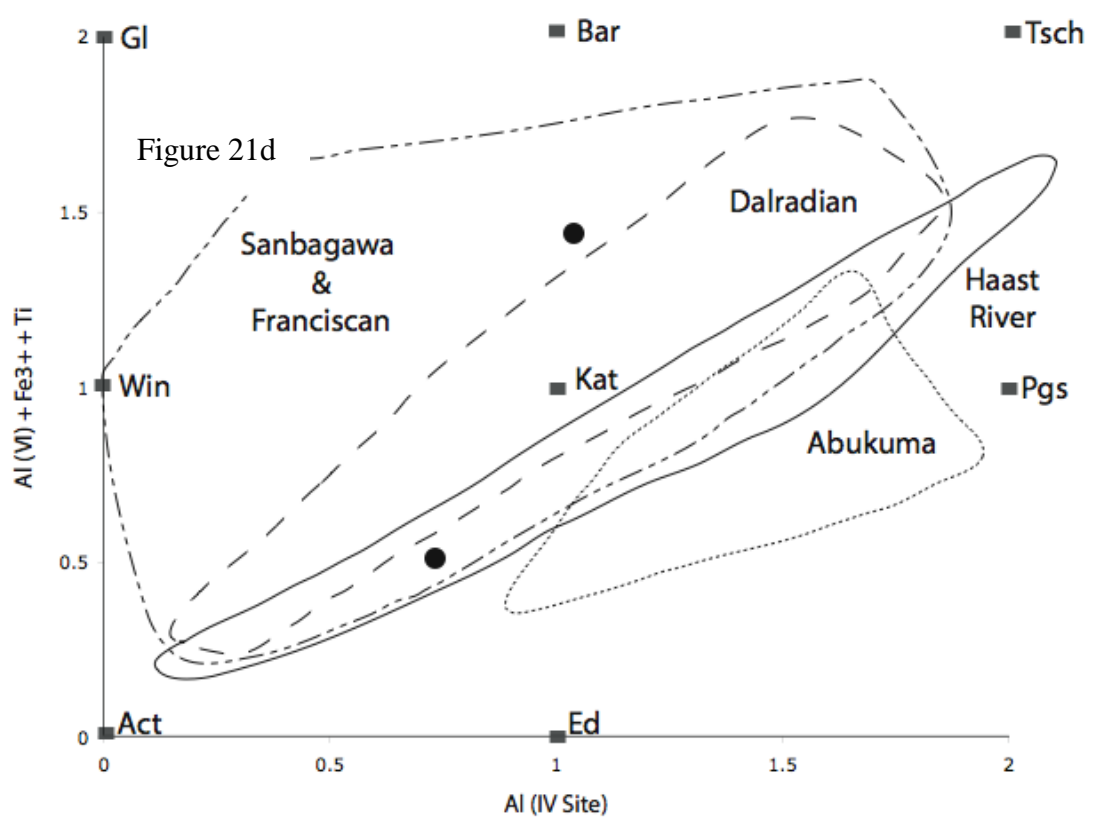
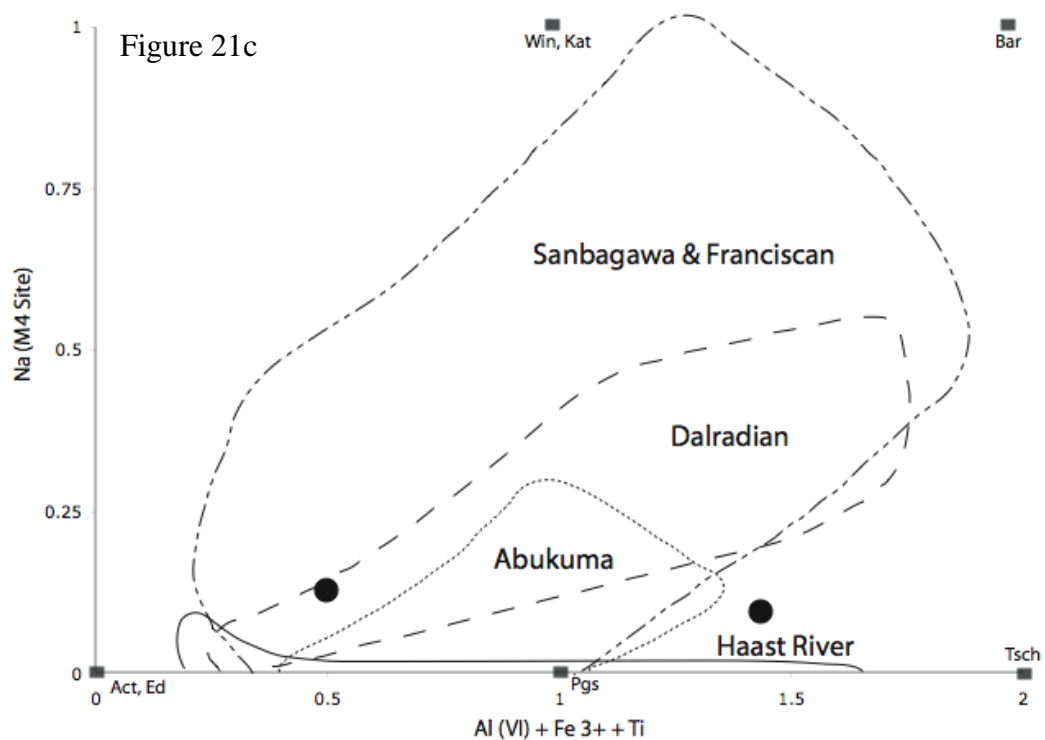
To verify the apparent metamorphic pressure differential across the BLSZ, I analyzed the compositions of Ca-amphiboles to determine their metamorphic geotherm association. Figure 21 shows formula proportion diagrams for amphiboles present south of the BLSZ. Fields on the diagrams outline the compositional ranges of calcic and sodic-calcic amphiboles in mafic schists from different tectonic settings world-wide (Laird and Albee, 1981). The Abukuma belt of Japan is a low-pressure metamorphic terrain; the Haast River Schist group of New Zealand represents a medium-pressure terrain; the Dalradian terrane of southwest Scotland is also a medium-pressure terrain; the Sanbagawa terrain in Japan represents high-pressure facies similar to the Franciscan Complex in California, also a high-pressure terrain.

Figure 21: Formula proportion diagrams of amphibole mineral chemistry (Laird and Albee, 1981). Diamonds indicate the compositions of amphiboles analyzed from one sample in this study. The envelopes on the plots show the compositional ranges of amphiboles occurring in mafic schist in different tectonic settings.

Figure 21a







Amphiboles in sample 160-1 from the BLSZ area generally plot in strongly overlapping fields of the various formula proportion diagrams. Based on the plots and the small dataset, this sample likely indicates a moderate pressure environment south of the BLSZ. This implies that displacement to juxtapose metamorphic rocks on either side of the BLSZ occurred under moderate pressure, shallow to moderate-depth conditions.

5.2 Discussion of Structural and Microstructural Kinematic Analysis

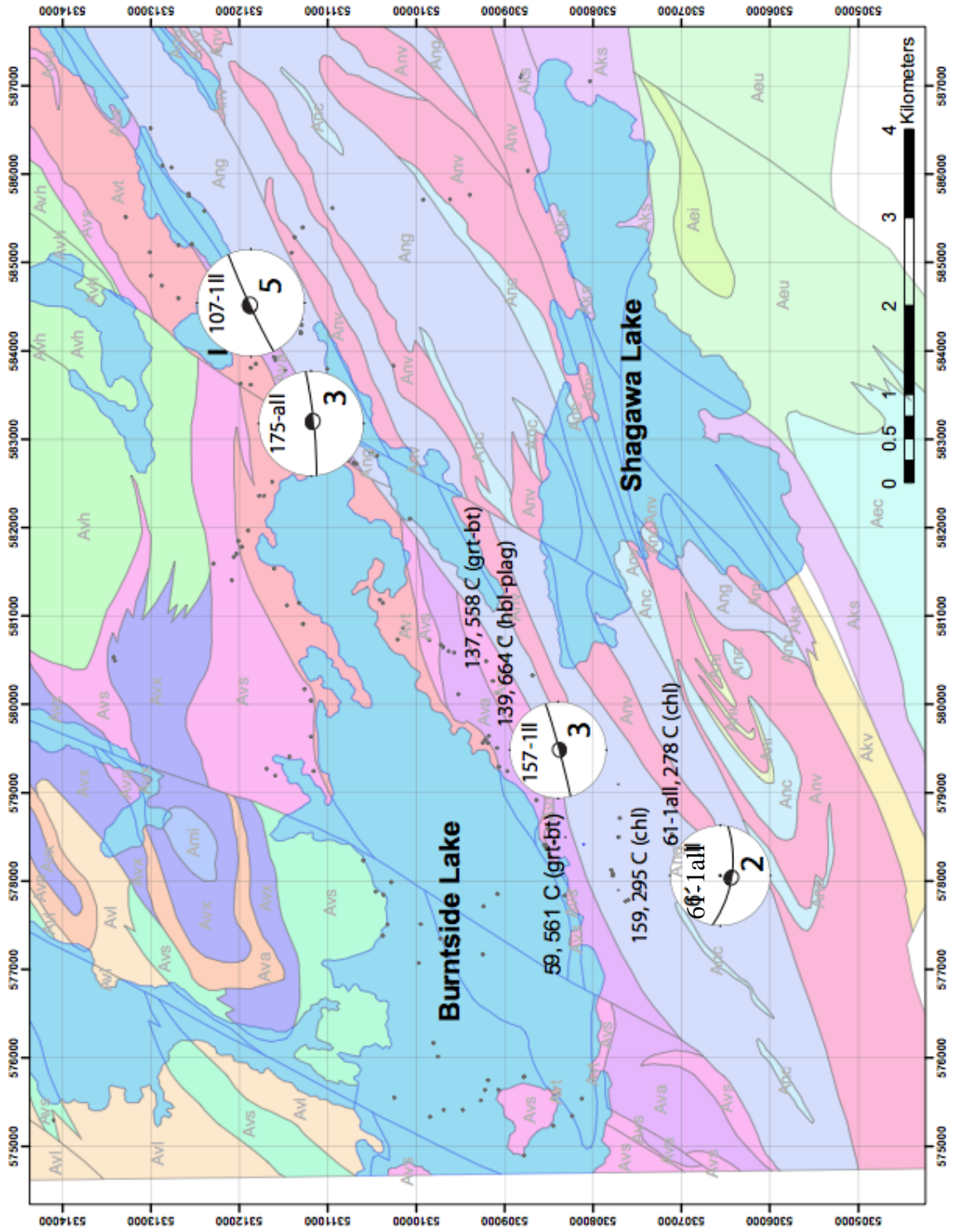
The BLSZ is broadly contained in formations that strike southwest to northeast, and dip steeply southeast. Analysis of structures and kinematics in the field was limited due to the fine-grained nature of the rocks. However, it is clear that the BLSZ contains rocks that can be described as L-S tectonites, and that the observed lineations uniformly plunge steeply in a steeply-dipping foliation. Microstructural analysis of kinematic indicators demonstrates that displacement along the shear zone was mainly by dip-slip. An overall sense of displacement on this shear zone, although constrained to be of dip-slip geometry, is somewhat ambiguous because the fabrics observed support both a north-side-up and south-side-up displacement in different samples. No overprinting of fabrics were observed, so relative timing of north-side-up versus south-side-up was not determined (see figure 22 for a summary map). With no overprinting fabrics to discern relative timing, the following alternate scenarios are possible:

1. The BLSZ could have accommodated different periods of displacement in such a way that the tectonic fabrics in individual rock units were not overprinted

2. Different planes of the zone might have been active at different times, with different displacement, such that individual samples show distinctive asymmetries. Rather than be contradictory, these variations may reflect the complexities of flow within a shear zone that is active over a period of time.

Combining the evidence of predominant north-side-up shear, juxtaposition of higher temperature rock assemblages to the north, and shallow crustal conditions indicated by low metamorphic pressures in the higher-grade rocks to the north, I interpret the BLSZ as having formed principally as a shallow-crustal, normal-sense shear zone at modest crustal levels. More complex movements are likely locally, as indicated in the second scenario above.

Figure 22: A geologic map of the project area with both structural and geothermometric results plotted.



6. SUMMARY AND CONCLUSIONS

This study combines metamorphic petrology with structural geology to reconstruct the conditions and movement history of the Burntside Lake Shear Zone. By understanding shear zones like the BLSZ, we can better understand the mode of Archean craton development represented by granite-greenstone terrains. The results of the study indicate that for the part of the BLSZ studied here, dip-slip motion with north-side-up displacement is indicated both by geothermometry and kinematic indicators recorded in the rock units defining the zone. North-side-up displacement is indicated by contrasts in metamorphic grade, and by microstructural kinematic analysis. Compositions of amphiboles in the field area south of the BLSZ indicate a moderate-pressure environment during displacement. However, moderate-pressure conditions could exist during both sagduction/diapirism as well as during arc accretion, so this finding is not diagnostic of crustal setting.

Further study of the BLSZ, as well as a craton-wide examination of kinematic and metamorphic environments, would benefit our understanding of Archean craton development in the Superior Province. Additionally, there is potential in utilizing the composition of amphiboles in mafic schists to the south of the BLSZ that may provide insight into its pressure-depth setting. One approach would be to collect samples along traverses normal to the shear zone at regular intervals approaching the shear zone to see if there is any change in amphibole composition.

REFERENCES

- Abbott, D.H., Burgess, L., Longhi, J., and Smith, W.H.F., 1994, An empirical thermal history of the Earth's upper mantle: *Journal of Geophysical Research*, v. 99, p. 835-850.
- Anhaeusser, C.R., Mason, R., Viljoen, M.J., Viljoen, R.P., 1969, A Reappraisal of some aspects of Precambrian Shield Geology: *Geological Society of American Bulletin*, v. 80, p. 2175-2200.
- Bauer, R.L., 1985, Correlation of early recumbant and younger upright folding across the boundary between an Archean gneiss belt and greenstone terrane, northeastern Minnesota, *Geology*, Volume 13, p. 657-660.
- , 1986, Multiple folding and pluton emplacement in Archean migmatites of the southern Vermilion granitic complex, northeastern Minnesota: *Canadian Journal of Earth Science*, v. 23, p. 1753-1764.
- Bauer, R.L., Bidwell, M.E., 1990, Contrasts in the response to dextral transpression across the Quetico-Wawa subprovince boundary in northeastern Minnesota: *Canadian Journal of Earth Science*, v. 27, p. 1521-1535.
- Bedard, J.H., Brouillette, P., Madore, L., Berclaz, A., 2003, Archaean cratonization and deformation in the northern Superior Province, Canada: an evaluation of plate tectonic versus vertical tectonic models: *Precambrian Research*, v. 127, p. 61-87.
- Blundy, J.D., Holland, T.J.B., 1990, Calcic amphibole equilibria and a new amphibole-palgioclase geothermometer: *Contributions to mineralogy and petrology*, v. 104, p. 208-224.
- Campbell, I.H., and Griffiths, R.W., 1992, The changing nature of mantle hotspots through time: implications for the chemical evolution of the mantle: *Journal of Geology*, v. 92, p. 497-523.
- Campbell, I.H., and Griffiths, R.W. and Hill, R.I., 1989, Melting in an Archean mantle plume: heads it's basalts, tails it's komatiites.: *Nature*, v. 339, p. 697-699.
- Card, K.D., 1990, A review of the superior Province of the Canadian Shield, a product of Archean accretion: *Precambrian Research*, v. 48, p. 99-156.
- Cathlineau, M., 1988, Cation site occupancy in chlorite and illites as a function of temperature: *Clay Minerals*, v. 23, p. 471-485.
- Condie, K.C., 1980, Origin and early development of the Earth's crust: *Precambrian Research*, v. 11, p. 183-197.
- De Caritat, P., Hutcheon, I., Walshe, J.L., 1993, Chlorite geothermometry: A review: *Clays and Clay Minerals*, v. 41, p. 219-239.
- Font, K.R., 1994, The Burntside Lake Fault Zone: a study of two faults in Basswood Lake. In: *The Seventh Keck Symposium in Geology*, Trinity University, p. 156-160.
- Frimmel, H.E., 1997, Chlorite thermometry in the Witwatersrand Basin: Constraints on the Paleoproterozoic geotherm in the Kaapvaal Craton, South Africa: *The Journal of Geology*, v. 105, p. 601-615.

- Green, J.C., Schulz, K.J., 1982, Ely Quarangle, St. Louis and Lake Counties, Minnesota, Miscellaneous Map Series: St. Paul, Minnesota Geological Survey, University of Minnesota.
- Guidotti, C.V., and Dyar, M.D., 1991, Ferric iron in metamorphic biotite and its petrologic and crystallographic implications.: *American Mineralogist*, v. 76, p. 161-175.
- Hansen, V., 1990, Collection and thin section preparation of oriented samples: *Journal of Geological Education*, v. 38, p. 294-297.
- Holland, T., Blundy, J., 1994, Non-ideal interactions in calcic amphiboles and their bearing on amphibole-plagioclase thermometry: *Contributions to mineralogy and petrology*, v. 116, p. 433-447.
- Hooper, P.R., Ojakangas, R.W., 1971, Multiple deformation in Archean rocks of the Vermilion District, northeastern Minnesota: *Canadian Journal of Earth Science*, v. 8.
- Hudleston, P.J., Schultz-Ela, D., Southwick, D.L., 1988, Transpression in an Archean greenstone belt, northern Minnesota: *Canadian Journal of Earth Science*, v. 25, p. 1060-1068.
- Jirsa, M.A., Southwick, D.L., Boerboom, T.J., 1992, Structural evolution of Archean rocks in the western Wawa subprovince, Minnesota: refolding of precleavage nappes during D2 transpression: *Canadian Journal of Earth Science*, v. 29, p. 2146-2155.
- John C. Green, K.J.S., 1982, Geologic Map of the Ely Quadrangle, St. Louis and Lake Counties, Minnesota, Miscellaneous Map Series: St. Paul, Minnesota, University of Minnesota, p. Map M-50.
- Johnson, G.W., 1994, Petrographic and structural interpretation of displacement along the Burntside Lake Fault Zone Basswood Lake area, Northern Minnesota. In: *The Seventh Keck Symposium in Geology*, Trinity University, San Antonio, TX, p. 161-164.
- Kranidiotis, P., MacLean, W.H., 1987, Systematics of chlorite alteration at the Phelps Dodge massive sulfide deposit, Matagami, Quebec: *Economic Geology*, v. 82, p. 1898-1911.
- Laird, J., Albee, A.L., 1981, High pressure metamorphism in mafic schist from northern Vermont: *American Journal of Science*, v. 281, p. 97-126.
- Lin, S., 2005, Synchronous vertical and horizontal tectonism in the Neoproterozoic: Kinematic evidence from a synclinal keel in the northwestern Superior craton, Canada: *Precambrian Research*, v. 139, p. 181-194.
- Macgregor, A.M., 1951, Some milestones in the Precambrian of southern Rhodesia: *Proceedings of the Geological Society of South Africa*, v. 54, p. 27-71.
- Nisbet, E.G., Cheadle, M.J., Arndt, N.T. and Bickle, M.J., 1993, Constraining the potential temperature of the Archean mantle: a review of the evidence from komatiites: *Lithos*, v. 30, p. 291-307.
- Rey, P.F., Philippot, P., Thebaud, N., 2003, Contribution of mantle plumes, crustal thickening and greenstone blanketing to the 2.75-2.65 Ga global crisis: *Precambrian Research*, v. 127, p. 43-60.
- Rey, P.F., Houseman, G., Lithospheric scale gravitational flow: the impact of body forces on orogenic processes from Archean to Phanerozoic. From: Buiter, S.J.H.,

- Schreurs. (eds), 2006: Analogue and Numerical Modeling of Crustal-Scale Processes: Geological Society, London, Special Publications, V. 253, P. 153-167.
- Sims, P.K., 1976, Early Precambrian tectonic-igneous evolution in the Vermilion district, northeastern Minnesota: GSA Bulletin, v. 87, p. 379-389.
- Sims, P.K., Mudrey, M.G., Jr., 1978, Geologic Map of the Shagawa Lake Quadrangle, St. Louis County, Minnesota, Geologic Quadrangle Map, U.S. Geological Survey, p. Map GQ - 1423.
- Tabor, J.R., Hudleston, P.J., 1991, Deformation at an Archean subprovince boundary, northern Minnesota: Canadian Journal of Earth Science, v. 28, p. 292-307.
- Van Kranendonk, M. J., Collins, W. J., Hickman, A., and Pawley, M. J., 2004. Critical tests of vertical vs. horizontal tectonic models for the Archean East Pilbara Granite-Greenstone Terrane, Pilbara Craton, Western Australia. Precambrian Research, v, 131, p. 173-211.
- Windley, B.F., 1984, The Evolving Continents, Chichester-Wiley, London.
- Wolf, D.E., 2006, The Burntside Lake and Shagawa/Knife Lake shear zones: Deformation kinematics, geochemistry and geochronology; Wawa subprovince, Ontario Canada, M.S. Thesis, Washington State University.
- Woodward, H.H., Weaver, S.G., Booth, K., Font, K., Johnson, G.C., Metz, T., Stevens, L., Tremper, C., 1994, Burntside Lake Fault Zone, Minnesota-Canada: The Seventh Keck Symposium in Geology Abstracts Volume.
- Xie, X., Byerly, G.R., Ferrell, R.E., Jr., 1997, Ilb trioctahedral chlorite from the Barberton greenstone belt: crystal structure and rock composition constraints with implications to geothermometry. Contributions to Mineralogy and Petrology, v. 126, p. 275-291.

APPENDIX 1 Sample Descriptions

159-1: *Chloritic greenstone* (65% Chl, 15% Ep, 10% Cac, 7% Qtz, 3% opaques) is a green, fine-grained (<1 mm) rock, with a weakly defined foliation and elongation lineation. This greenstone contains chlorite, epidote, calcite, and quartz, with accessory opaque phases. Coarser-grained chlorite has a grain-shape preferred orientation (GSPO) that defines the planar to wavy foliation and an S-C fabric. Microtextures consist of subhedral epidote porphyroblasts, anhedral undulose quartz grains, euhedral to subhedral chlorite grains and euhedral to subhedral opaque phases. In some cases, chlorite wraps around or replaces epidote porphyroblasts. The opaque phases have fringes of quartz. Calcite is a secondary phase appearing only in veins throughout the sample.

107-1: Greenstone (40% Bt, 35% Qtz, 10% Pl, 10% opaques, 5% Ep, trace apatite) is a dark green, fine-grained (<1mm) rock. The greenstone contains quartz, biotite, epidote, and plagioclase feldspar, with accessory apatite and opaque phases. Microtextures consist of undulose quartz ribbons, along with euhedral to subhedral biotite grains. The foliation, defined by a GSPO of biotite, is wavy to discontinuous. The biotite present in the sample defines an S-C fabric. Both anhedral plagioclase grains containing tapering albite twins and subhedral epidote occur as porphyroclasts. Quartz and biotite grains define the elongation lineation in this sample. In outcrop this unit is very fine grained; however, it is competent yet a very thin, poorly developed foliation is present suggesting some degree of metamorphism.

139-1: *Biotite-hornblende schist* (60% Qtz, 15% Bt, 15% Hbl, 5% Pl, 5% Cc, trace opaques) is a dark grey, fine-grained rock with a weak foliation and elongation lineation. The schist contains quartz, biotite, hornblende, plagioclase feldspar, and calcite, with accessory opaque. Microtextures consist of anhedral, undulose grains of quartz, and anhedral grains of plagioclase with weakly defined albite twinning. A GSPO of euhedral grains of biotite and hornblende defines the foliation in this rock. The foliation in this sample is planar and uniform, and it is crosscut by quartz and calcite aggregate veins.

255-1: *Garnet-bearing amphibolite* (60% Hbl, 15% Qtz, 10% Ep, 5% Grt, 5% Cc, 5% Pl) is a dark green, fine-grained (<1mm) rock with a foliation and elongation lineation. The amphibolite contains hornblende, quartz, epidote, plagioclase feldspar, garnet, actinolite and calcite, with accessory opaque. Microtextures include porphyroblastic, equant but broken garnet, quartz and plagioclase occurring as anhedral undulose grains, and euhedral hornblende 'needles' that define the foliation and lineation in this sample. The foliation in the sample is planar and uniform, except where it wraps around garnet/epidote aggregates. The epidote occurs as a replacement of garnet.

59-1: *Garnet-biotite schist* (30% Qtz, 30% Pl, 25% Bt, 10% Chl, 5% Grt) is a dark grey, fine-grained (<1mm) rock with a weak foliation and elongation lineation. The schist contains quartz, plagioclase feldspar, biotite, chlorite and garnet, with accessory opaque. Microtextures consist of euhedral, equant garnet porphyroblasts, anhedral undulose grains of quartz, subhedral to anhedral plagioclase grains displaying bent and tapering albite twins, and chlorite replacement of biotite. Euhedral, elongate biotite grains define

the foliation and lineation in this sample. The foliation is wavy, and deflects around quartz veins.

137-1: *Garnet-biotite schist* (30% Qtz, 25% Bt, 15% Grt, 15% Pl, 10% Chl (retrograde), 5% opaques) is a grey, fine-grained (<1mm) rock with a foliation and an elongation lineation. The schist contains quartz, biotite, plagioclase, garnet, and chlorite (retrograde), with accessory opaque. Microtextures include euhedral to subhedral equant garnet porphyroblasts; quartz and plagioclase grains are anhedral and undulose, and chlorite replaces biotite. The foliation and lineation are defined by a GSPO of biotite. The foliation is planar except where it wraps around garnet porphyroblasts, and is interrupted by small quartz grains.

61-1: *Chloritic greenstone* (40% Cc, 25% Chl, 20% Qtz, 10% feldspar, 5% opaques) is a dark green, fine-grained (<1mm) rock with a foliation and an elongation lineation. The greenstone contains calcite, quartz, chlorite and plagioclase feldspar, with accessory opaque. Microtextures consist of anhedral, undulose grains of quartz and plagioclase, and a GSPO in chlorite define the foliation and lineation in this sample. The chlorite foliation is wavy, wrapping around quartz and opaque grains.

68-1: *Amphibolite* (65% Hbl, 25% Qtz, 10% Pl, trace Cc) is a dark green, fine-grained (<1mm), rock with both a foliation and an elongation lineation. The amphibolite contains hornblende, quartz, plagioclase feldspar, and calcite. Microtextures consist of anhedral undulose grains of quartz and plagioclase, the latter showing tapered albite twins.

Coarse-grained euhedral, elongate hornblende grains define the wavy foliation and lineation in this sample.

157-1: *Chloritic greenstone* (35% Qtz, 20% Act, 20% Cc, 15% Chl, 10% Ep, trace opaque phases) is a green, fine-grained (<1mm) rock with both a foliation and an elongation lineation. The greenstone contains quartz, calcite, chlorite, and epidote, with accessory opaque. Microtextures include anhedral, undulose grains of quartz, calcite grains with twinning, and fine-grained chlorite, which defines the wavy foliation in this sample. The foliation wraps around larger quartz aggregates and calcite veining. Some chlorite grows in coarser-grained mats; these mats display an S-C fabric.

160-1: *Chloritic greenstone* (35% Chl, 20% Act, 15% Qtz, 15% Ep, 5% Plag) is a green, fine-grained (<1mm) rock with both a foliation and an elongation lineation. The greenstone contains chlorite, actinolite, quartz, epidote, plagioclase and calcite, with accessory opaque. Microtextures consist of anhedral undulose grains of quartz, anhedral grains and aggregates of calcite, and porphyroclastic equant epidote grains that have small quartz-filled fringes. Straight, uniform foliation is defined by a fine-grained chlorite/actinolite GSPO, and crosscut by veins filled with quartz and calcite. The lineation is defined by chlorite. Some of the chlorite grows in larger mats; these mats display a weak S-C fabric.

60-1/60-2 *Amphibolite* (70% Hbl/Chl, 20% Qtz, 10% Cc, trace opaques) is a green, fine-grained (<1mm) rock with both a foliation and an elongation lineation. The amphibolite

contains hornblende, actinolite, quartz, calcite, with accessory opaque phases.

Microtextures include undulose anhedral quartz grains and aggregates, subhedral grains of hornblende and actinolite, and coarse-grained vein-fill calcite. The foliation and lineation are defined by hornblende and actinolite GSPO. The foliation in this sample is planar and uniform, except where it wraps/deflects around a quartz or calcite vein.

175 *Biotite schist* (65% Qtz, 25% Bt, 10% Pl, trace opaques) is a dark grey, fine-grained (<1mm) rock containing both a foliation and an elongation lineation. The biotite schist contains biotite, quartz, and feldspar. Microtextures include anhedral, undulose quartz grains, anhedral plagioclase grains containing tapering albite twins, and subhedral to anhedral biotite grains. The wavy to discontinuous foliation is defined by a biotite GSPO. This sample contains biotite-rich and quartz-rich layers that alternate, indicating possible original bedding, now parallel to foliation. The biotite grains in the foliation also define a weak S-C fabric.

141-1 *Quartz-rich hornblende-biotite schist* (45% Qtz, 35% Bt, 7% Hbl, 5% Ep, 5% Pl, 3% opaques) is a light grey, fine-grained (<1mm) rock containing both a foliation and a weak lineation. This biotite schist contains quartz, biotite, and hornblende with a trace amount of epidote, and accessory opaque phases. Microtextures include subhedral undulose quartz grains, euhedral elongate biotite grains, and subhedral to anhedral hornblende grains. The planar, uniform foliation and lineation are defined by a biotite GSPO.

APPENDIX 2 Microprobe Data

Analyses with lines through them were not used in geothermal calculations due to poor analyses, perhaps the mineral targeted was missed, an inclusion analyzed or otherwise non-ideal mineral grains.

Hornblende Analyses

| Sample | 255-1II | 255-1II | 255-1II | 255-1II | 255-1II | 139-1II | 139-1II | 139-1II | 139-1II | 139-1II |
|--------------------------------|---------|---------|---------|---------|---------|---------|---------|---------|---------|---------|
| SiO ₂ | 43.57 | 43.88 | 44.18 | 44.34 | 44.71 | 42.91 | 44.19 | 43.51 | 42.97 | 61.55 |
| Al ₂ O ₃ | 10.77 | 10.57 | 11.05 | 10.88 | 10.56 | 10.58 | 10.49 | 10.69 | 10.27 | 24.71 |
| TiO ₂ | 0.57 | 0.59 | 0.6 | 0.67 | 0.58 | 0.44 | 0.45 | 0.60 | 0.41 | -0.06 |
| Cr ₂ O ₃ | 0.0 | 0.04 | 0 | 0.062 | 0.02 | 0.15 | -0.01 | 0.062 | 0.01 | 0.031 |
| FeO | 19.44 | 19.23 | 19.62 | 19.45 | 19.16 | 17.58 | 17.23 | 17.64 | 16.65 | 0.43 |
| MgO | 8.94 | 9.27 | 9.1 | 9.34 | 9.38 | 10.49 | 10.81 | 10.54 | 9.98 | 0.02 |
| MnO | 0.33 | 0.37 | 0.39 | 0.4 | 0.36 | 0.49 | 0.52 | 0.45 | 0.47 | 0.03 |
| CaO | 12.02 | 12.29 | 12.08 | 12.37 | 12.33 | 11.85 | 11.88 | 11.84 | 10.01 | 5.47 |
| Na ₂ O | 1.14 | 1.342 | 1.21 | 1.15 | 1.02 | 1.22 | 1.22 | 1.25 | 0.87 | 8.67 |
| K ₂ O | 0.33 | 0.29 | 0.3 | 0.33 | 0.32 | 1.03 | 1.01 | 0.98 | 0.67 | 0.15 |
| Total | 97.13 | 97.87 | 98.53 | 98.97 | 98.44 | 96.74 | 97.79 | 97.57 | 92.31 | 100.99 |

Plagioclase Analyses

| Comment | 255-1II | 255-1II | 255-1II | 255-1II | 255-1II | 255-1II |
|--------------------------------|-------------------|---------|---------|---------|---------|------------------|
| SiO ₂ | 49.18 | 57.89 | 50.98 | 56.17 | 61.84 | 45.64 |
| Al ₂ O ₃ | 12.56 | 26.91 | 30.53 | 28.05 | 24.29 | 10.55 |
| TiO ₂ | 0.54 | 0 | 0.03 | -0.04 | 0 | 0.42 |
| Cr ₂ O ₃ | 0 | -0.04 | 0 | -0.004 | -0.04 | 0.07 |
| FeO | 17.64 | 0.31 | 0.49 | 0.31 | 0.35 | 19.17 |
| MgO | 7.79 | -0.01 | 0.01 | -0.01 | -0.01 | 9.28 |
| MnO | 0.28 | -0.01 | -0.02 | -0.03 | -0.02 | 0.42 |
| CaO | 11.08 | 8.41 | 13.59 | 10.06 | 7.34 | 12.15 |
| Na ₂ O | 2.34 | 6.56 | 3.74 | 6.02 | 7.03 | 1.28 |
| K ₂ O | 0.25 | 0.06 | 0.04 | 0.09 | 0.08 | 0.28 |
| Total | 101.63 | 100.07 | 99.38 | 100.61 | 100.88 | 99.26 |

Plagioclase Analyses

| 139-1II | 139-1II | 139-1II | 139-1II | 139-1II | 139-1II |
|---------|------------------|---------|---------|---------|------------------|
| 62.96 | 99.06 | 60.89 | 62.75 | 62.13 | 51.67 |
| 23.88 | 0.01 | 24.7 | 23.64 | 24.08 | 20.33 |
| 0.01 | 0.03 | 0.01 | 0.02 | 0.02 | 1.12 |
| 0.02 | 0.04 | 0.03 | -0.02 | -0.05 | 0.17 |
| 0.13 | 0.07 | 0.11 | 0.09 | 0.16 | 7.6 |
| 0.03 | 0 | 0.01 | 0 | 0 | 4.08 |
| -0.02 | 0 | 0.03 | 0.01 | 0.01 | 0.10 |
| 5.1 | 0.03 | 6.17 | 4.91 | 5.53 | 3.04 |

| | | | | | |
|--------|------------------|--------|--------|---------|------------------|
| 8.49 | 0.02 | 8.04 | 8.57 | 8.33 | 5.67 |
| 0.26 | 0 | 0.13 | 0.19 | 0.21 | 3.92 |
| 100.84 | 99.27 | 100.12 | 100.15 | 100.411 | 97.69 |

Plagioclase Analyses

| | | | | | |
|--------|--------|--------|--------|--------|--------|
| 59-1ll | 59-1ll | 59-1ll | 59-1ll | 59-1ll | 59-1ll |
| 60.54 | 59.97 | 60.45 | 59.91 | 60.17 | 60.65 |
| 24.33 | 25.07 | 24.76 | 25.60 | 25.37 | 25.05 |
| 0.06 | 0.01 | 0 | 0.06 | 0.05 | 0.04 |
| 0.02 | 0 | 0.02 | -0.02 | 0.01 | 0.01 |
| 0.32 | 0.17 | 0.21 | 0.09 | 0.04 | 0.11 |
| 0 | 0 | 0.01 | 0 | 0 | 0.02 |
| 0.01 | 0.04 | 0 | 0.01 | 0.01 | -0.02 |
| 6.03 | 6.77 | 6.36 | 7.03 | 7.02 | 6.52 |
| 8.08 | 7.41 | 7.98 | 7.65 | 7.6 | 8.01 |
| 0.11 | 0.13 | 0.1 | 0.10 | 0.07 | 0.11 |
| 99.5 | 99.58 | 99.88 | 100.44 | 100.36 | 100.48 |

Chlorite Analyses

| | | | | |
|--------------------------------|------------------|------------------|-------------------|------------------|
| Sample | 160-1ll | 160-1ll | 160-1ll | 160-1ll |
| SiO ₂ | 41.07 | 53.12 | 69.39 | 33.87 |
| Al ₂ O ₃ | 1.08 | 10.90 | 16.72 | 3.54 |
| TiO ₂ | 0.08 | 6.22 | 2.55 | 28.08 |
| Cr ₂ O ₃ | -0.04 | 0.05 | 0.01 | 0.03 |
| FeO | 1.41 | 8.60 | 1.63 | 4.37 |
| MgO | 5.06 | 0.21 | 0.58 | 0.85 |
| MnO | 0.23 | 0.08 | 0.05 | 0.09 |
| CaO | 54.81 | 15.96 | 2.38 | 25.22 |
| Na ₂ O | 0.03 | 0.01 | 8.60 | 0.22 |
| K ₂ O | 0.04 | 0.02 | 1.06 | 0.04 |
| Total | 73.77 | 95.17 | 102.97 | 96.30 |

Chlorite Analyses

| | | | | | | |
|--------------------------------|---------|-------------------|---------|---------|---------|------------------|
| Sample | 61-1bll | 61-1bll | 61-1bll | 61-1bll | 61-1bll | 61-1bll |
| SiO ₂ | 24.49 | 68.09 | 29.32 | 23.89 | 25.71 | 67.26 |
| Al ₂ O ₃ | 19.24 | 19.68 | 18.63 | 18.72 | 19.72 | 19.65 |
| TiO ₂ | 0.04 | 0.015 | 0.06 | 0.11 | 0.1 | 0.04 |
| Cr ₂ O ₃ | 0.01 | -0.02 | 0.04 | 0.03 | 0.05 | 0 |
| FeO | 32.66 | 0.47 | 29.7 | 32.17 | 32.62 | 0.5 |
| MgO | 11.1 | 0.02 | 10.43 | 11.30 | 11.00 | 0.09 |
| MnO | 0.18 | 0 | 0.14 | 0.23 | 0.19 | -0.03 |
| CaO | 0.01 | 0.28 | 0.43 | 0.04 | 0 | 0.04 |
| Na ₂ O | 0.02 | 11.42 | 1.21 | 0.03 | 0.29 | 11.01 |
| K ₂ O | 0.02 | 0.21 | 0.05 | 0.02 | 0.04 | 0.06 |
| Total | 87.77 | 100.15 | 90.01 | 86.53 | 89.72 | 98.61 |

Chlorite Analyses

| Comment | 159-1II | 159-1II | 159-1II | 159-1II | 159-1II | 159-1II |
|--------------------------------|---------|---------|---------|---------|---------|---------|
| SiO ₂ | 25.392 | 24.789 | 25.797 | 24.61 | 25.966 | 25.474 |
| Al ₂ O ₃ | 19.822 | 19.422 | 19.634 | 18.557 | 20.163 | 20.181 |
| TiO ₂ | 0.014 | -0.013 | 0.078 | 0.014 | 0.092 | 0.099 |
| Cr ₂ O ₃ | -0.013 | -0.032 | 0.003 | 0.034 | 0.055 | -0.026 |
| FeO | 29.785 | 30.488 | 30.746 | 29.649 | 29.654 | 30.215 |
| MgO | 12.888 | 13.031 | 12.885 | 12.06 | 12.89 | 12.719 |
| MnO | 0.541 | 0.588 | 0.503 | 0.477 | 0.523 | 0.565 |
| CaO | 0.031 | 0.032 | 0.051 | 0.163 | 0.007 | 0.016 |
| Na ₂ O | 0.019 | 0.027 | 0.038 | 0.021 | 0.017 | 0.038 |
| K ₂ O | 0.027 | 0.022 | 0.041 | 0.067 | 0.021 | 0.007 |
| Total | 88.506 | 88.354 | 89.776 | 85.652 | 89.388 | 89.288 |

Garnet Analyses

| Sample | 137-1II rim | 137-1II rim | 137-1II rim | 137-1II rim |
|--------------------------------|-------------|-------------|-------------|-------------|-------------|------------------|-------------|-------------|-------------|
| SiO ₂ | 36.79 | 37.05 | 37.04 | 36.86 | 36.84 | 30.55 | 36.88 | 37.06 | 36.85 |
| Al ₂ O ₃ | 21.64 | 21.77 | 21.9 | 21.24 | 21.57 | 18.14 | 21.6 | 21.69 | 21.46 |
| TiO ₂ | -0.04 | 0.04 | 0.04 | 0.01 | 0.14 | 0.49 | 0.02 | -0.03 | 0.04 |
| Cr ₂ O ₃ | 0.02 | 0 | -0.04 | 0.09 | 0.08 | 0.11 | 0.07 | 0.08 | 0.03 |
| FeO | 27.95 | 27.54 | 28.05 | 27.20 | 27.07 | 20.44 | 27.37 | 27.27 | 27.17 |
| MgO | 2.76 | 2.68 | 2.88 | 2.39 | 2.48 | 12.5 | 3.15 | 3.12 | 3.07 |
| MnO | 8.85 | 8.86 | 8.68 | 9.56 | 9.95 | 0.52 | 8.12 | 8.01 | 7.64 |
| CaO | 2.67 | 2.79 | 2.76 | 2.91 | 2.78 | 0.21 | 3.64 | 3.76 | 3.64 |
| Na ₂ O | 0 | 0.01 | 0.02 | 0 | 0.02 | 0.07 | 0.01 | 0.04 | 0.03 |
| K ₂ O | 0.01 | 0.05 | 0.03 | 0.05 | 0.05 | 4.83 | 0.01 | 0.02 | 0.02 |
| Total | 100.66 | 100.78 | 101.35 | 100.33 | 100.97 | 87.82 | 100.87 | 101.03 | 99.93 |

Garnet Analyses

| Sample | 137-1II rim | 137-1II rim | 137-1II rim | 137-1II rim |
|--------------------------------|-------------|-------------|-------------|-------------|-------------|------------------|-------------|-------------|-------------|
| SiO ₂ | 37.42 | 37.32 | 37.12 | 37.24 | 37.35 | 50.2 | 37.07 | 37.10 | 37.23 |
| Al ₂ O ₃ | 21.42 | 21.46 | 21.56 | 21.52 | 21.79 | 16.56 | 21.81 | 21.72 | 21.60 |
| TiO ₂ | 0.01 | -0.13 | 0.04 | 0.04 | 0.13 | 1.94 | 0.01 | 0.01 | 0.07 |
| Cr ₂ O ₃ | 0.03 | -0.04 | 0.01 | 0.06 | 0.01 | 0.16 | 0.07 | 0.07 | 0.07 |
| FeO | 27.18 | 26.86 | 27.26 | 27.75 | 27.3 | 3.83 | 27.69 | 28.11 | 27.72 |
| MgO | 3.13 | 3.13 | 3.09 | 2.66 | 2.35 | 1.01 | 2.67 | 2.87 | 2.91 |
| MnO | 7.95 | 7.97 | 7.71 | 8.93 | 9.64 | 0.42 | 8.94 | 8.47 | 8.11 |
| CaO | 3.7 | 3.7 | 3.61 | 2.88 | 2.82 | 0.31 | 2.75 | 2.88 | 3.2 |
| Na ₂ O | 0.04 | 0.04 | 0.03 | -0.01 | 0 | 0.35 | 0.04 | 0.01 | 0.02 |
| K ₂ O | 0 | 0.02 | -0.01 | 0.02 | 0.02 | 10.80 | 0.01 | 0.04 | 0.01 |

| | | | | | | | | | |
|-------|--------|--------|--------|--------|--------|------------------|--------|--------|--------|
| Total | 100.87 | 100.29 | 100.44 | 101.08 | 101.40 | 95.56 | 101.07 | 101.27 | 100.94 |
|-------|--------|--------|--------|--------|--------|------------------|--------|--------|--------|

**Garnet
Analyses**

| | 137-1II | 137-1II | 137-1II | 137- 1II | 137-1II | 137-1II | 137-1II | 137-1II | 137-1II |
|--------------------------------|---------|---------|---------|-------------|---------|------------------|---------|---------|---------|
| Sample | rim | rim | rim | rim | rim | rim | rim | rim | rim |
| SiO ₂ | 37.48 | 37.23 | 37.47 | 36.52 | 36.78 | 34.92 | 37.25 | 37.34 | 37.08 |
| Al ₂ O ₃ | 21.76 | 21.55 | 21.44 | 21.56 | 21.53 | 0.04 | 21.5 | 21.73 | 21.28 |
| TiO ₂ | 0.13 | -0.01 | 0.06 | 0.11 | 0.21 | 0.02 | 0.01 | 0.07 | -0.01 |
| Cr ₂ O ₃ | 0.16 | 0.08 | 0.11 | 0.11 | 0.14 | 0.03 | 0.07 | 0.06 | 0.06 |
| FeO | 26.65 | 26.45 | 26.55 | 25.82 | 26.58 | 0.30 | 25.77 | 27.73 | 27.30 |
| MgO | 2.88 | 2.76 | 2.82 | 2.55 | 2.76 | 0 | 2.74 | 2.93 | 2.45 |
| MnO | 8.86 | 8.75 | 8.56 | 8.7 | 8.83 | 0.05 | 8.69 | 8.58 | 9.46 |
| CaO | 3.85 | 4.20 | 4.23 | 3.85 | 3.67 | 0.04 | 4.70 | 2.8 | 2.65 |
| Na ₂ O | 0.02 | 0.03 | 0.03 | 0 | 0.02 | 0 | 0.05 | 0.03 | 0.02 |
| K ₂ O | 0.03 | 0 | 0.01 | 0.25 | 0.02 | 0.03 | 0.03 | 0.02 | 0.02 |
| Total | 101.81 | 101.05 | 101.27 | 99.46 | 100.54 | 95.36 | 100.80 | 101.27 | 100.30 |

**Garnet
Analyses**

| | 137-1II |
|--------------------------------|---------|---------|---------|---------|---------|---------|---------|---------|---------|
| Sample | rim | rim | rim | rim | rim | core | core | core | core |
| SiO ₂ | 37.12 | 36.97 | 37.29 | 37.04 | 37.04 | 37.53 | 37.23 | 37.45 | 37.29 |
| Al ₂ O ₃ | 21.71 | 21.54 | 21.61 | 21.72 | 21.68 | 21.74 | 21.55 | 21.58 | 21.56 |
| TiO ₂ | 0.13 | 0.12 | -0.06 | -0.06 | 0.06 | 0.06 | 0.06 | 0.08 | 0.04 |
| Cr ₂ O ₃ | 0 | 0.01 | 0.01 | 0.04 | -0.02 | 0.04 | -0.02 | 0.09 | 0.09 |
| FeO | 27.54 | 27.69 | 27.69 | 27.75 | 27.00 | 27.25 | 26.86 | 26.72 | 26.98 |
| MgO | 2.66 | 2.6 | 2.82 | 2.68 | 2.97 | 3.15 | 3.09 | 2.98 | 3.09 |
| MnO | 9.22 | 9.46 | 9.16 | 9.12 | 8.19 | 8.34 | 8.09 | 8.36 | 8.17 |
| CaO | 2.6 | 2.68 | 2.58 | 2.60 | 3.7 | 3.72 | 3.90 | 3.75 | 3.59 |
| Na ₂ O | 0.02 | 0.01 | 0.02 | 0.01 | 0.04 | 0.02 | 0.04 | 0.06 | 0.03 |
| K ₂ O | 0.03 | 0.01 | 0.03 | 0.04 | 0.01 | 0.01 | 0.03 | 0 | 0 |
| Total | 101.03 | 101.08 | 101.16 | 100.94 | 100.68 | 101.85 | 100.82 | 101.08 | 100.82 |

**Garnet
Analyses**

| | 137-1II | sect |
|--------------------------------|---------|---------|---------|---------|---------|---------|---------|---------|---------|
| Sample | core | 137-1II |
| SiO ₂ | 37.45 | 37.17 | 37.60 | 37.25 | 36.13 | 34.47 | 36.17 | 37.55 | 36.73 |
| Al ₂ O ₃ | 21.47 | 21.76 | 21.77 | 21.72 | 21.52 | 19.57 | 21.31 | 21.34 | 21.53 |
| TiO ₂ | 0.05 | 0.01 | 0.02 | 0.11 | 0.06 | 0.06 | 0.07 | -0.01 | -0.01 |
| Cr ₂ O ₃ | -0.02 | 0.04 | 0.05 | 0.12 | 0.05 | 0.04 | 0.08 | 0.12 | -0.01 |
| FeO | 27.27 | 26.58 | 26.81 | 26.92 | 27.04 | 25.76 | 27.26 | 26.50 | 26.74 |
| MgO | 2.95 | 2.67 | 2.85 | 2.85 | 3.04 | 2.37 | 3.2 | 2.63 | 2.87 |
| MnO | 8.08 | 8.72 | 8.66 | 8.94 | 8.90 | 8.57 | 8.23 | 9.25 | 8.72 |
| CaO | 3.63 | 4.11 | 3.63 | 3.68 | 3.46 | 2.67 | 3.18 | 3.63 | 3.83 |

| | | | | | | | | | |
|-------------------|--------|--------|--------|--------|--------|-------|-------|--------|--------|
| Na ₂ O | 0 | 0.03 | -0.01 | 0.02 | 0.02 | 0.03 | 0.01 | 0.05 | 0.05 |
| K ₂ O | 0.01 | 0.02 | 0.05 | 0.02 | 0.02 | 1.24 | 0.22 | 0 | 0.02 |
| Total | 100.88 | 101.09 | 101.44 | 101.63 | 100.22 | 94.78 | 99.71 | 101.04 | 100.47 |

Garnet Analyses

| Sample | sect 137-1II | sect 137-1II | sect 137-1II | sect 137-1II | sect 137-1II | sect 137-1II | sect 137-1II |
|--------------------------------|--------------|--------------|--------------|------------------|-------------------------|--------------|--------------|
| SiO ₂ | 36.56 | 37.30 | 37.7 | 95.87 | 94.47 | 37.56 | 37.14 |
| Al ₂ O ₃ | 21.07 | 21.69 | 21.86 | 0.08 | 0.5 | 21.73 | 21.57 |
| TiO ₂ | 0.01 | 0.17 | 0.01 | 0.04 | 0.03 | 0.08 | 0.04 |
| Cr ₂ O ₃ | 0.16 | 0.01 | 0.01 | 0.02 | 0.02 | 0.09 | 0.06 |
| FeO | 26.48 | 27.28 | 26.84 | 0.54 | 0.86 | 27.04 | 27.12 |
| MgO | 3.18 | 2.83 | 2.85 | 0.03 | 0.18 | 2.85 | 2.98 |
| MnO | 8.07 | 8.5 | 8.59 | 0.14 | 0.15 | 8.27 | 7.99 |
| CaO | 3.81 | 4.05 | 4.00 | 0.02 | 0.04 | 4.07 | 3.75 |
| Na ₂ O | 0.05 | 0.01 | 0.02 | 0 | 0.01 | 0.02 | 0.04 |
| K ₂ O | 0.04 | 0.03 | 0.02 | 0.01 | 0.05 | 0 | 0.03 |
| Total | 99.42 | 101.88 | 101.9 | 96.75 | 96.30 | 101.71 | 100.70 |

Garnet Analyses

| Sample | sect 137-1II | sect 137-1II | sect 137-1II | sect 137-1II | sect 137-1II | sect 137-1II | sect 137-1II | sect 137-1II | sect 137-1II |
|--------------------------------|--------------|--------------|--------------|------------------|--------------|--------------|--------------|------------------|--------------|
| SiO ₂ | 37.07 | 37.37 | 37.27 | 94.27 | 37.29 | 37.38 | 37.40 | 91.27 | 37.59 |
| Al ₂ O ₃ | 21.63 | 21.77 | 21.78 | 0.05 | 21.98 | 21.64 | 21.48 | 2.26 | 15.62 |
| TiO ₂ | 0.01 | 0.01 | 0.03 | 0.03 | 0.03 | 0.03 | 0.06 | 0.04 | 0.62 |
| Cr ₂ O ₃ | 0.02 | -0.02 | -0.05 | 0.03 | 0.01 | 0.07 | 0.05 | 0.08 | -0.01 |
| FeO | 27.16 | 27.38 | 27.27 | 0.62 | 27.72 | 27.81 | 27.86 | 1.96 | 11.08 |
| MgO | 3.07 | 3.13 | 3.14 | 0.02 | 3.12 | 2.99 | 2.82 | 0.11 | 0.08 |
| MnO | 7.76 | 7.61 | 7.72 | 0.16 | 7.77 | 7.95 | 8.53 | 0.69 | 0.18 |
| CaO | 3.89 | 4.03 | 3.72 | 0.03 | 3.71 | 3.62 | 2.84 | 0.39 | 34.28 |
| Na ₂ O | 0.01 | 0.04 | 0.01 | 0.01 | -0.01 | 0.02 | 0.03 | 0.01 | 0 |
| K ₂ O | 0.02 | 0.05 | 0.02 | 0.01 | 0.01 | 0.03 | 0.05 | 0.03 | 0.02 |
| Total | 100.65 | 101.36 | 100.92 | 95.1 | 101.64 | 101.53 | 101.12 | 96.81 | 99.46 |

Garnet Analyses

| Sample | 59-1II Rim | 59-1II Rim | 59-1II rim | 59-1II rim | 59-1II rim | 59-1II rim | 59-1II core | 59-1II core |
|--------------------------------|------------|------------|------------------|------------------|------------------|------------------|-------------|-------------|
| SiO ₂ | 37.12 | 37.17 | 31.36 | 35.00 | 28.22 | 28.24 | 37.17 | 37.27 |
| Al ₂ O ₃ | 21.65 | 21.79 | 18.04 | 17.27 | 18.52 | 18.33 | 21.84 | 21.75 |
| TiO ₂ | -0.02 | -0.07 | 1.05 | 2.00 | 1.06 | 0.11 | 0.08 | 0.06 |
| Cr ₂ O ₃ | 0.03 | 0.01 | 0.05 | 0.05 | 0.04 | 0.03 | -0.01 | 0.04 |
| FeO | 29.32 | 29.3 | 23.48 | 19.89 | 23.27 | 25.22 | 30.33 | 30.54 |
| MgO | 2.84 | 2.87 | 11.46 | 9.34 | 12.93 | 13.81 | 3.12 | 3.12 |
| MnO | 6.55 | 6.74 | 0.38 | 0.29 | 0.39 | 0.43 | 6.04 | 5.91 |

| | | | | | | | | |
|-------------------|--------|--------|------------------|------------------|------------------|-----------------|-------|--------|
| CaO | 2.91 | 2.93 | 0.06 | 0.01 | 0.51 | 0.08 | 2.49 | 2.6 |
| Na ₂ O | 0 | 0.01 | 0.02 | 0.14 | 0 | 0.01 | 0.01 | 0 |
| K ₂ O | 0.01 | 0.02 | 4.75 | 9.58 | 1.08 | 0.26 | 0.04 | 0.01 |
| Total | 100.41 | 100.77 | 90.65 | 93.58 | 86.03 | 86.5 | 101.1 | 101.29 |

Garnet Analyses

| Sample | 59-11l core | 59-11l core | 59-11l core | Line 1 | Line 2 | Line 3 | Line 4 | Line 5 | Line 6 | Line 7 |
|--------------------------------|-------------|-------------|-------------|------------------|------------------|--------|--------|--------|------------|--------|
| SiO ₂ | 36.98 | 37.51 | 37.27 | 97.62 | 61.83 | 37.13 | 36.87 | 37.28 | 37.42 | 37.11 |
| Al ₂ O ₃ | 21.7 | 21.93 | 21.62 | 0.02 | 9.33 | 21.67 | 21.66 | 21.62 | 21.61 | 21.74 |
| TiO ₂ | 0.08 | -0.06 | -0.09 | -0.02 | 0.07 | 0.07 | -0.01 | -0.03 | -0.05 | 0.01 |
| Cr ₂ O ₃ | 0.03 | 0.07 | 0.11 | -0.03 | -0.04 | -0.01 | -0.01 | 0.10 | -0.03 | 0.03 |
| FeO | 30.03 | 30.14 | 30.15 | 0.56 | 14.47 | 30.32 | 30.21 | 30.27 | 30.34 | 30.28 |
| MgO | 3.05 | 3.03 | 2.98 | 0 | 1.11 | 3.25 | 3.30 | 3.17 | 3.28 | 3.24 |
| MnO | 6.33 | 6.22 | 6.53 | 0.09 | 4.6 | 5.6 | 5.49 | 5.45 | 5.38 | 5.41 |
| CaO | 2.5 | 2.49 | 2.55 | 0.02 | 1.46 | 2.70 | 2.73 | 2.76 | 2.78 | 2.77 |
| Na ₂ O | 0.01 | 0.01 | 0.02 | -0.01 | 0.01 | 0.01 | -0.01 | 0.02 | 0.02 | -0.01 |
| K ₂ O | 0.03 | 0.03 | 0.01 | 0.02 | 0.05 | 0.03 | 0.02 | 0.02 | 0.03 | 0.04 |
| Total | 100.72 | 101.37 | 101.14 | 98.26 | 92.87 | 100.77 | 100.26 | 100.65 | 100.7 9 | 100.63 |

Garnet Analyses

| Sample | Line 8 | Line 9 | Line 10 | Line 11 | Line 12 | Line 13 | Line 14 | Line 15 | Line 16 | Line 17 |
|--------------------------------|------------|--------|------------|---------|---------|------------|---------|---------|---------|---------|
| SiO ₂ | 37.64 | 37.46 | 37.68 | 37.33 | 37.00 | 37.65 | 37.48 | 37.62 | 37.34 | 36.69 |
| Al ₂ O ₃ | 21.81 | 21.68 | 21.92 | 21.52 | 21.63 | 21.59 | 21.82 | 21.71 | 21.91 | 21.38 |
| TiO ₂ | 0.04 | 0.02 | 0 | 0.02 | 0.06 | 0.02 | 0.04 | 0.01 | 0.02 | 0.01 |
| Cr ₂ O ₃ | -0.01 | 0.04 | 0.04 | -0.03 | 0.03 | -0.03 | 0 | 0.04 | 0.04 | -0.03 |
| FeO | 30.57 | 30.48 | 30.51 | 30.25 | 30.39 | 29.91 | 30.54 | 30.16 | 30.13 | 29.04 |
| MgO | 3.28 | 3.30 | 3.11 | 3.24 | 3.28 | 3.14 | 3.27 | 3.19 | 3.2 | 3.12 |
| MnO | 5.34 | 5.40 | 5.53 | 5.38 | 5.46 | 5.41 | 5.31 | 5.22 | 5.32 | 5.32 |
| CaO | 2.83 | 2.93 | 2.91 | 2.94 | 3.04 | 3.14 | 3.00 | 3.07 | 3.28 | 3.56 |
| Na ₂ O | 0.01 | 0.01 | 0.04 | -0.01 | 0.03 | 0.02 | 0.01 | 0.03 | 0 | 0 |
| K ₂ O | 0.04 | 0.02 | 0.02 | 0.01 | 0.02 | 0.03 | 0.01 | 0.03 | 0 | 0.01 |
| Total | 101.5 5 | 101.33 | 101.7 6 | 100.64 | 100.92 | 100.8 7 | 101.47 | 101.06 | 101.22 | 99.1 |

Garnet Analyses

| Sample | Line 18 | Line 19 | Line 20 | Line 21 | Line 22 | Line 23 | Line 24 | Line 25 | 59-11l rim |
|--------------------------------|---------|---------|---------|---------|------------------|---------|---------|---------|------------|
| SiO ₂ | 37.79 | 37.28 | 36.73 | 37.4 | 41.46 | 37.09 | 37.37 | 37.43 | 37.49 |
| Al ₂ O ₃ | 21.87 | 21.76 | 21.17 | 21.72 | 14.80 | 21.76 | 21.75 | 22.02 | 21.84 |
| TiO ₂ | 0.04 | 0.06 | 0.04 | 0.02 | -0.09 | 0.07 | 0.05 | -0.03 | 0.02 |
| Cr ₂ O ₃ | 0 | 0.01 | -0.04 | 0.01 | 0.05 | 0.03 | 0.04 | 0.04 | 0.05 |
| FeO | 30.11 | 29.40 | 29.60 | 29.60 | 29.31 | 29.41 | 29.45 | 29.29 | 29.76 |

| | | | | | | | | | |
|-------------------|--------|--------|-------|--------|------------------|--------|--------|--------|--------|
| MgO | 3.18 | 3.14 | 3.11 | 3.14 | 2.34 | 3.04 | 2.94 | 2.90 | 2.69 |
| MnO | 5.5 | 5.57 | 5.84 | 5.96 | 6.39 | 6.28 | 6.73 | 6.93 | 7.41 |
| CaO | 3.15 | 3.22 | 3.02 | 3.1 | 1.71 | 3.1 | 2.86 | 2.74 | 2.55 |
| Na ₂ O | 0.03 | 0.02 | 0.04 | -0.01 | 0.09 | 0.01 | 0.03 | 0.01 | 0.04 |
| K ₂ O | 0.02 | 0.01 | 0.04 | 0 | 0.52 | 0.02 | 0.01 | 0.02 | 0.05 |
| Total | 101.68 | 100.47 | 99.56 | 100.95 | 96.58 | 100.79 | 101.23 | 101.35 | 101.89 |

Garnet Analyses

| Sample | 59-1ll rim | 59-1ll rim | 59-1ll rim | 59-1ll rim | 59-1ll core | 59-1ll core | 59-1ll core |
|--------------------------------|------------|------------|------------|------------|-------------|-------------|-------------|
| SiO ₂ | 37.78 | 37.22 | 37.66 | 37.06 | 37.40 | 37.75 | 37.60 |
| Al ₂ O ₃ | 21.78 | 21.44 | 21.81 | 21.59 | 21.66 | 21.91 | 21.78 |
| TiO ₂ | 0.02 | -0.07 | -0.03 | 0.01 | 0.02 | 0.05 | -0.03 |
| Cr ₂ O ₃ | 0.08 | 0.02 | 0.06 | 0.1 | 0.02 | -0.03 | 0.02 |
| FeO | 29.71 | 28.89 | 29.25 | 29.03 | 29.78 | 30.04 | 29.73 |
| MgO | 2.89 | 2.24 | 2.41 | 2.29 | 2.92 | 2.88 | 2.85 |
| MnO | 6.69 | 8.43 | 8.07 | 8.45 | 6.96 | 7.09 | 7.07 |
| CaO | 2.75 | 2.76 | 2.88 | 2.77 | 2.49 | 2.47 | 2.56 |
| Na ₂ O | 0.01 | 0.01 | 0.03 | 0.01 | 0.02 | 0.02 | 0.02 |
| K ₂ O | 0.02 | 0.02 | 0.02 | 0.02 | 0.03 | 0.01 | 0.02 |
| Total | 101.72 | 100.95 | 102.15 | 101.31 | 101.31 | 102.19 | 101.63 |

Garnet Analyses

| Sample | 59-1ll core | 59-1ll rim | 59-1ll rim | 59-1ll rim | 59-1ll rim | 59-1ll rim | 59-1ll rim | 59-1ll core |
|--------------------------------|-------------|------------------|------------|------------|------------|------------|------------|-------------|
| SiO ₂ | 37.55 | 45.17 | 37.22 | 37.38 | 31.45 | 28.95 | 33.19 | 38.52 |
| Al ₂ O ₃ | 21.81 | 9.56 | 21.66 | 21.79 | 17.56 | 17.75 | 17.39 | 22.47 |
| TiO ₂ | -0.01 | -0.01 | -0.02 | 0.04 | 0.56 | 0.15 | 1.26 | 0.06 |
| Cr ₂ O ₃ | 0.06 | -0.01 | 0.01 | 0.01 | 0.05 | 0.06 | 0.06 | 0 |
| FeO | 29.89 | 44.93 | 29.25 | 29.55 | 24.09 | 24.60 | 22.19 | 30.43 |
| MgO | 2.93 | 1.25 | 2.39 | 2.56 | 11.93 | 12.53 | 10.36 | 3.63 |
| MnO | 6.80 | 5.13 | 8.23 | 7.41 | 0.38 | 0.38 | 0.28 | 6.12 |
| CaO | 2.57 | 24.82 | 2.8 | 2.85 | 0 | 0.12 | 0.01 | 2.65 |
| Na ₂ O | 0.01 | 0.07 | 0.02 | 0 | 0.02 | -0.01 | 0.01 | 0.02 |
| K ₂ O | 0 | 0.06 | 0.05 | 0.01 | 4.88 | 2.08 | 6.89 | 0.05 |
| Total | 101.60 | 70.97 | 101.61 | 101.61 | 90.93 | 86.60 | 91.65 | 103.95 |

Garnet Analyses

| Sample | 59-1ll core | 59-1ll core | 59-1ll core | 59-1ll core |
|--------------------------------|-------------|-------------|-------------|-------------|
| SiO ₂ | 37.81 | 37.65 | 37.8 | 37.37 |
| Al ₂ O ₃ | 21.72 | 21.64 | 21.59 | 21.81 |
| TiO ₂ | 0.04 | -0.01 | 0.03 | -0.03 |
| Cr ₂ O ₃ | -0.07 | 0.02 | -0.03 | -0.03 |
| FeO | 30.12 | 30.02 | 29.98 | 29.76 |
| MgO | 3.00 | 2.98 | 3.02 | 3.04 |
| MnO | 6.22 | 6.16 | 6.09 | 5.84 |

| | | | | |
|-------------------|--------|--------|-------|--------|
| CaO | 2.85 | 2.75 | 2.80 | 3.03 |
| Na ₂ O | 0.03 | 0.001 | 0 | -0.01 |
| K ₂ O | 0.01 | 0.04 | 0.02 | 0.02 |
| Total | 101.73 | 101.26 | 101.3 | 100.82 |

Biotite Analyses

| Sample | 137-1II |
|--------------------------------|---------|---------|---------|---------|---------|---------|---------|---------|---------|---------|
| SiO ₂ | 36.11 | 35 | 35.71 | 36.16 | 35.73 | 36.41 | 36.37 | 37.23 | 36.72 | 25.06 |
| Al ₂ O ₃ | 17.39 | 17.9 | 18.95 | 17.38 | 17.3 | 18.46 | 18.85 | 18.57 | 18.56 | 20.87 |
| TiO ₂ | 1.66 | 1.77 | 1.46 | 2.68 | 2.9 | 1.88 | 2.2 | 2.11 | 2.01 | 0.16 |
| Cr ₂ O ₃ | 0.14 | 0.11 | 0.08 | 0.08 | 0.04 | 0.14 | 0.11 | 0.14 | 0.11 | 0.1 |
| FeO | 19.94 | 19.17 | 19.21 | 17.72 | 17.5 | 18.03 | 17.27 | 15.21 | 15.89 | 22.41 |
| MgO | 11.21 | 12.08 | 7.88 | 11.38 | 11.60 | 11.39 | 11.37 | 12.92 | 12.55 | 16.33 |
| MnO | 0.38 | 0.45 | 2.88 | 0.31 | 0.34 | 0.31 | 0.29 | 0.24 | 0.23 | 0.44 |
| CaO | -0.02 | 0.01 | 0.61 | 0.04 | 0.04 | -0.02 | -0.01 | -0.02 | -0.02 | 0.04 |
| Na ₂ O | 0 | 0.02 | 0.02 | 0.16 | 0.27 | 0.17 | 0.22 | 0.36 | 0.31 | 0.03 |
| K ₂ O | 9.11 | 8.32 | 7.04 | 9.55 | 9.25 | 9.53 | 9.53 | 9.11 | 9.41 | 0.16 |
| Total | 95.92 | 94.78 | 93.85 | 95.44 | 94.94 | 96.29 | 96.21 | 95.87 | 95.76 | 85.61 |

Biotite Analyses

| Sample | 137-1II | 59-1II | 59-1II | 59-1II |
|--------------------------------|---------|---------|---------|---------|---------|---------|---------|--------|--------|--------|
| SiO ₂ | 37.25 | 36.03 | 34.5 | 36.29 | 36.22 | 96.75 | 96.38 | 32.67 | 49.45 | 27.59 |
| Al ₂ O ₃ | 18.68 | 17.65 | 16.46 | 18.45 | 18.61 | 0.01 | 0.06 | 17.94 | 21.69 | 19.61 |
| TiO ₂ | 1.73 | 1.53 | 4.28 | 2.53 | 2.16 | 0.08 | 0.02 | 1.61 | 0.06 | 0.36 |
| Cr ₂ O ₃ | 0.1 | 0.09 | 0.01 | 0.08 | 0.14 | -0.02 | 0.01 | 0.10 | 0 | 0.15 |
| FeO | 15.54 | 18.62 | 16.87 | 17.2 | 17.16 | 0.56 | 0.40 | 22.86 | 23.41 | 24.92 |
| MgO | 13.24 | 11.74 | 10.89 | 11.16 | 11.40 | -0.01 | 0.02 | 10.24 | 1.35 | 14.70 |
| MnO | 0.23 | 0.33 | 0.21 | 0.24 | 0.25 | 0.08 | 0.08 | 0.34 | 11.42 | 0.32 |
| CaO | -0.02 | -0.01 | 2.87 | -0.02 | -0.02 | 0.03 | 0.11 | 0.10 | 2.6 | 0.05 |
| Na ₂ O | 0.35 | 0.21 | 0.07 | 0.14 | 0.35 | 0 | 0 | 0.02 | 0.03 | 0.01 |
| K ₂ O | 8.88 | 9.08 | 7.18 | 9.35 | 9.38 | 0.03 | 0.05 | 7.67 | 0.08 | 1.13 |
| Total | 95.98 | 95.26 | 93.34 | 95.41 | 95.64 | 97.51 | 97.11 | 93.55 | 110.08 | 88.84 |

Biotite Analyses

| Sample | 59-1II |
|--------------------------------|--------|--------|--------|--------|--------|--------|--------|--------|--------|--------|
| SiO ₂ | 29.30 | 27.83 | 60.89 | 37.01 | 35.79 | 37.73 | 37.45 | 59.20 | 35.58 | 33.17 |
| Al ₂ O ₃ | 18.84 | 19.68 | 19.63 | 22.64 | 19.66 | 22.59 | 22.34 | 25.59 | 18.06 | 17.37 |
| TiO ₂ | 0.64 | 0.14 | 0.02 | 0.01 | 0.18 | 0.02 | 0.02 | 0.01 | 1.81 | 1.25 |
| Cr ₂ O ₃ | 0.19 | 0.13 | 0.02 | 0.02 | 0.05 | 0.02 | 0.10 | -0.06 | 0.10 | 0.13 |
| FeO | 23.97 | 25.47 | 3.60 | 30.03 | 25.42 | 29.71 | 27.88 | 0.68 | 20.61 | 20.81 |
| MgO | 13.73 | 15.18 | 2.1 | 2.84 | 5.37 | 2.64 | 1.81 | 0.01 | 10.47 | 10.64 |
| MnO | 0.38 | 0.39 | 0.05 | 7.98 | 6.58 | 8.32 | 11.36 | 0.07 | 0.25 | 0.29 |
| CaO | 0.05 | 0.01 | 0.11 | 2.76 | 2.14 | 2.66 | 2.56 | 6.59 | -0.01 | 0.02 |
| Na ₂ O | 0.03 | 0.01 | 2.97 | 0.01 | 0.01 | 0.03 | 0 | 7.76 | 0.11 | 0.05 |

| | | | | | | | | | | |
|------------------|-------|-------|-------|--------|-------|--------|--------|--------|-------|-------|
| K ₂ O | 2.27 | 0.71 | 9.51 | 0.04 | 3.06 | 0.01 | 0.04 | 0.25 | 9.69 | 8.15 |
| Total | 89.40 | 89.56 | 98.89 | 103.35 | 98.25 | 103.73 | 103.57 | 100.09 | 96.67 | 91.87 |

Biotite Analyses

| | | | | | |
|--------------------------------|--------|--------|--------|--------|--------|
| Sample | 59-1II | 59-1II | 59-1II | 59-1II | 59-1II |
| SiO ₂ | 29.19 | 34.05 | 34.07 | 29.55 | 31.25 |
| Al ₂ O ₃ | 15.70 | 17.65 | 17.13 | 19.32 | 18.24 |
| TiO ₂ | 5.14 | 1.30 | 2.33 | 0.36 | 0.73 |
| Cr ₂ O ₃ | 0.15 | 0.03 | 0.06 | 0.04 | -0.02 |
| FeO | 22.02 | 22.44 | 22.72 | 24.06 | 24 |
| MgO | 11.97 | 11.26 | 10.32 | 13.65 | 13.33 |
| MnO | 0.26 | 0.29 | 0.17 | 0.35 | 0.34 |
| CaO | 4.96 | 0.01 | 0.04 | 0.10 | 0 |
| Na ₂ O | 0 | 0.02 | 0.01 | 0.01 | 0.03 |
| K ₂ O | 1.82 | 8.46 | 8.73 | 1.11 | 4.53 |
| Total | 91.21 | 95.52 | 95.57 | 88.54 | 92.42 |

Epidote Analyses

| | | | | |
|--------------------------------|---------|---------|---------|---------|
| Sample | 255-1II | 255-1II | 255-1II | 255-1II |
| SiO ₂ | 37.52 | 37.60 | 37.24 | 37.8 |
| Al ₂ O ₃ | 24.93 | 24.97 | 23.06 | 25.29 |
| TiO ₂ | 0.11 | 0.01 | 0.47 | 0.23 |
| Cr ₂ O ₃ | 0.02 | 0.06 | 0 | 0 |
| FeO | 10.19 | 10.65 | 12.06 | 10.21 |
| MgO | 0.04 | 0.02 | 0.03 | 0.03 |
| MnO | 0.09 | 0.1 | 0.07 | 0.09 |
| CaO | 23.77 | 23.89 | 23.85 | 23.93 |
| Na ₂ O | 0 | 0.01 | 0.03 | 0.01 |
| K ₂ O | 0.01 | 0.02 | 0.02 | 0.01 |
| Total | 96.69 | 97.32 | 96.83 | 97.6 |

Epidote Analyses

| | | | | | | | |
|--------------------------------|---------|------------------|------------------|------------------|------------------|-------------------|------------------|
| Sample | 160-1II | 160-1II | 160-1II | 160-1II | 160-1II | 160-1II | 160-1II |
| SiO ₂ | 37.55 | 96 | 95.03 | 34.5 | 91.23 | 65.65 | 31.03 |
| Al ₂ O ₃ | 22.93 | 0.07 | 0.08 | 0.15 | 0 | 19.23 | 16.37 |
| TiO ₂ | 0.04 | -0.07 | 0 | 0.02 | 0.07 | -0.06 | 0.01 |
| Cr ₂ O ₃ | -0.02 | -0.02 | 0.04 | 0 | -0.03 | 0.07 | 0.03 |
| FeO | 12.54 | 0.29 | 0.28 | 0.35 | 0.16 | 3.60 | 27.33 |
| MgO | 0.01 | 0.1 | 0.07 | 0.08 | 0.01 | 1.01 | 11.38 |
| MnO | 0.2 | 0.02 | 0.06 | 0.12 | 0.05 | 0.04 | 0.51 |
| CaO | 23.35 | 0.06 | 0.16 | 36.37 | 0.95 | 0.07 | 0.07 |
| Na ₂ O | -0.01 | 0 | 0.01 | 0.02 | 0.01 | 10.6 | 0.08 |
| K ₂ O | 0.02 | 0.02 | 0.02 | 0 | 0.03 | 0.42 | 0.03 |
| Total | 96.61 | 96.46 | 95.74 | 71.62 | 92.48 | 100.63 | 86.84 |

Epidote Analyses

| Sample | 159-1II core | 159-1II core | 159-1II core | 159-1II core | 159-1II core | 159-1II core |
|--------------------------------|-----------------|-----------------|-----------------|-----------------|-----------------|-----------------|
| SiO ₂ | 37.8 | 49.9 | 39.08 | 36.43 | 37.53 | 39.02 |
| Al ₂ O ₃ | 24.81 | 13.86 | 22.09 | 20.84 | 24.46 | 20.85 |
| TiO ₂ | 0.08 | -0.01 | 0.14 | -0.02 | 0.11 | 0.19 |
| Cr ₂ O ₃ | -0.03 | -0.01 | 0 | 0.05 | 0.07 | 0.05 |
| FeO | 10.79 | 23.52 | 12.42 | 14.18 | 11.16 | 11.99 |
| MgO | 0.01 | 9 | 0.51 | 0.02 | 0 | 1.28 |
| MnO | 0.06 | 0.4 | 0.16 | 0.16 | 0.29 | 0.13 |
| CaO | 23.97 | 0.19 | 22.37 | 22.9 | 23.92 | 22.48 |
| Na ₂ O | 0.01 | 0.01 | 0.1 | 0.09 | 0.03 | 0.03 |
| K ₂ O | 0.02 | 0.02 | 0.31 | 0.01 | 0.01 | 0.03 |
| Total | 97.51 | 96.86 | 97.19 | 94.66 | 97.58 | 96.04 |

Epidote Analyses

| Sample | 107-1II core | 107-1II core | 107-1II core | 107-1II core | 107-1II core | 107-1II core |
|--------------------------------|-----------------|-----------------|-----------------|------------------|-----------------|------------------|
| SiO ₂ | 37.55 | 37.61 | 37.73 | 39.62 | 35.56 | 43.29 |
| Al ₂ O ₃ | 25.17 | 25.43 | 24.93 | 22.56 | 20.63 | 20.02 |
| TiO ₂ | 0.12 | 0.04 | 0.11 | 0.11 | 0.07 | 0.05 |
| Cr ₂ O ₃ | -0.02 | 0.05 | 0.01 | 0.09 | 0.11 | -0.04 |
| FeO | 9.9 | 9.73 | 10.63 | 11.41 | 15.19 | 12.47 |
| MgO | 0.03 | 0.04 | 0.04 | 0.24 | 3.62 | -0.04 |
| MnO | 0.41 | 0.4 | 0.40 | 0.22 | 0.19 | 0.08 |
| CaO | 23.49 | 23.63 | 23.38 | 20.99 | 17.53 | 20.68 |
| Na ₂ O | 0.01 | 0 | 0 | 0.41 | 0.02 | 0.25 |
| K ₂ O | 0 | 0.04 | 0.04 | 0.32 | 0.02 | 0.08 |
| Total | 96.65 | 96.96 | 97.27 | 95.95 | 92.93 | 96.88 |

APPENDIX 3

Geothermometric data obtained from Spears GTB Program

Sample **137-III Grt core** compositions paired with Biotite
 Reaction: Garnet-Biotite Fe-Mg Exchange
 Average Compositions used

| | Garnet | Biotite |
|------------------|---------|---------|
| Si | 2.966 | 5.445 |
| Al | 2.024 | 3.193 |
| Ti | 0.003 | 0.263 |
| Cr | 0.003 | 0.012 |
| Fe ²⁺ | 1.787 | 2.269 |
| Fe ³⁺ | 0.000 | 0.258 |
| Mg | 0.349 | 2.641 |
| Mn | 0.566 | 0.035 |
| Ca | 0.319 | 0.039 |
| Na | 0.004 | 0.034 |
| K | 0.002 | 1.754 |
| Ave Wt % Oxide | | |
| Ave | 101.201 | 95.442 |

| Calibration: | Hodges and Spear (1982) | |
|------------------------|-------------------------|---------|
| Results: (21 data pts) | P (bars) | T (C) |
| | 0 | 582.7 |
| | 500 | 584.5 |
| | 1000 | 586.3 |
| | 1500 | 588.1 |
| | 2000 | 589.9 |
| | 2500 | 591.7 |
| | 3000 | 593.5 |
| | 3500 | 595.3 |
| | 4000 | 597.1 |
| | 4500 | 598.9 |
| | 5000 | 600.8 |
| | 5500 | 602.6 |
| | 6000 | 604.4 |
| | 6500 | 606.2 |
| | 7000 | 608 |
| | 7500 | 609.8 |

| | | |
|--|-------|-------|
| | 8000 | 611.6 |
| | 8500 | 613.4 |
| | 9000 | 615.2 |
| | 9500 | 617 |
| | 10000 | 618.8 |

Calibration: Ferry and Spear (1978) w/ Berman
(1990)

| Results: (11 data pts) | P (bars) | T (C) |
|------------------------|----------|---------|
| | 0 | 576.9 |
| | 1000 | 580.9 |
| | 2000 | 584.9 |
| | 3000 | 588.8 |
| | 4000 | 592.8 |
| | 5000 | 596.7 |
| | 6000 | 600.7 |
| | 7000 | 604.6 |
| | 8000 | 608.6 |
| | 9000 | 612.5 |
| | 10000 | 616.5 |

Calibration: Gessmann et al (1997)

| Results: (11 data pts) | P (bars) | T (C) |
|------------------------|----------|---------|
| | 0 | 575.4 |
| | 1000 | 579.5 |
| | 2000 | 583.6 |
| | 3000 | 587.6 |
| | 4000 | 591.7 |
| | 5000 | 595.7 |
| | 6000 | 599.8 |
| | 7000 | 603.9 |
| | 8000 | 607.9 |
| | 9000 | 612 |
| | 10000 | 616 |

APPENDIX 3 cont.

Geothermometric data obtained from Spears GTB Program,
cont.

Sample **137-111 Garnet rims** paired with biotite
Garnet-Biotite Fe-Mg

Reaction: Exchange

Average Compositions used

| | Garnet | Biotite |
|--------------------|---------|---------|
| Si | 2.958 | 5.445 |
| Al | 2.036 | 3.193 |
| Ti | 0.003 | 0.263 |
| Cr | 0.003 | 0.012 |
| Fe ²⁺ | 1.844 | 2.269 |
| Fe ³⁺ | 0.000 | 0.258 |
| Mg | 0.329 | 2.641 |
| Mn | 0.593 | 0.035 |
| Ca | 0.257 | 0.039 |
| Na | 0.002 | 0.034 |
| K | 0.003 | 1.754 |
| Ave Wt % Oxide Ave | 101.049 | 95.442 |

Calibration: Hodges and Spear (1982)

| Results: (21 data pts) | P (bars) | T (C) |
|------------------------|----------|---------|
| | 0 | 546.1 |
| | 500 | 547.9 |
| | 1000 | 549.6 |
| | 1500 | 551.4 |
| | 2000 | 553.1 |
| | 2500 | 554.9 |
| | 3000 | 556.7 |
| | 3500 | 558.4 |
| | 4000 | 560.2 |
| | 4500 | 561.9 |
| | 5000 | 563.7 |
| | 5500 | 565.4 |
| | 6000 | 567.2 |
| | 6500 | 569 |
| | 7000 | 570.7 |
| | 7500 | 572.5 |
| | 8000 | 574.2 |

APPENDIX 3, cont

Geothermometric data collected from Spears GTB Program, cont.

Sample 59-111 Garnet core compositions paired with biotite

Garnet-Biotite Fe-Mg

Reaction:

Exchange

Average Compositions used

| | Garnet | Biotite |
|--------------------|---------|---------|
| Si | 2.965 | 4.800 |
| Al | 2.038 | 3.124 |
| Ti | 0.003 | 0.271 |
| Cr | 0.002 | 0.007 |
| Fe ²⁺ | 2.015 | 2.174 |
| Fe ³⁺ | 0.000 | 0.353 |
| Mg | 0.372 | 2.381 |
| Mn | 0.399 | 0.022 |
| Ca | 0.223 | 0.006 |
| Na | 0.002 | 0.001 |
| K | 0.002 | 1.723 |
| Ave Wt % Oxide Ave | 100.942 | 88.538 |

Calibration:

Hodges and Spear (1982)

| Results: (21 data pts) | P (bars) | T (C) |
|------------------------|----------|---------|
| | 0 | 572.1 |
| | 500 | 573.9 |
| | 1000 | 575.7 |
| | 1500 | 577.5 |
| | 2000 | 579.4 |
| | 2500 | 581.2 |
| | 3000 | 583 |
| | 3500 | 584.9 |
| | 4000 | 586.7 |
| | 4500 | 588.5 |
| | 5000 | 590.3 |
| | 5500 | 592.2 |
| | 6000 | 594 |
| | 6500 | 595.8 |
| | 7000 | 597.6 |
| | 7500 | 599.5 |
| | 8000 | 601.3 |

| | | |
|--|-------|-------|
| | 8500 | 603.1 |
| | 9000 | 604.9 |
| | 9500 | 606.8 |
| | 10000 | 608.6 |

Calibration: Ferry and Spear (1978) w/ Berman
(1990)

| Results: (11 data pts) | P (bars) | T (C) |
|------------------------|----------|---------|
| | 0 | 568.1 |
| | 1000 | 572.2 |
| | 2000 | 576.2 |
| | 3000 | 580.3 |
| | 4000 | 584.3 |
| | 5000 | 588.4 |
| | 6000 | 592.4 |
| | 7000 | 596.5 |
| | 8000 | 600.5 |
| | 9000 | 604.5 |
| | 10000 | 608.6 |

Calibration: Gessmann et al (1997)

| Results: (11 data pts) | P (bars) | T (C) |
|------------------------|----------|---------|
| | 0 | 624.9 |
| | 1000 | 629.1 |
| | 2000 | 633.2 |
| | 3000 | 637.4 |
| | 4000 | 641.5 |
| | 5000 | 645.7 |
| | 6000 | 649.8 |
| | 7000 | 654 |
| | 8000 | 658.1 |
| | 9000 | 662.3 |
| | 10000 | 666.4 |

APPENDIX 3 cont.

Geothermometric data collected from Spears GTB Program

Sample **59-III Garnet rim** compositions paired with biotite

Garnet-Biotite Fe-Mg

Reaction:

Exchange

Average Compositions used

| | Garnet | Biotite |
|--------------------|---------|---------|
| Si | 2.968 | 4.800 |
| Al | 2.035 | 3.124 |
| Ti | 0.001 | 0.271 |
| Cr | 0.000 | 0.007 |
| Fe ²⁺ | 1.969 | 2.174 |
| Fe ³⁺ | 0.000 | 0.353 |
| Mg | 0.335 | 2.381 |
| Mn | 0.456 | 0.022 |
| Ca | 0.249 | 0.006 |
| Na | 0.002 | 0.001 |
| K | 0.002 | 1.723 |
| Ave Wt % Oxide Ave | 100.974 | 88.538 |

Calibration:

Hodges and Spear (1982)

| Results: (21 data pts) | P (bars) | T (C) |
|------------------------|----------|---------|
| | 0 | 550 |
| | 500 | 551.7 |
| | 1000 | 553.5 |
| | 1500 | 555.3 |
| | 2000 | 557 |
| | 2500 | 558.8 |
| | 3000 | 560.6 |
| | 3500 | 562.3 |
| | 4000 | 564.1 |
| | 4500 | 565.9 |
| | 5000 | 567.6 |
| | 5500 | 569.4 |
| | 6000 | 571.2 |
| | 6500 | 572.9 |
| | 7000 | 574.7 |
| | 7500 | 576.5 |
| | 8000 | 578.2 |

| | | |
|--|-------|-------|
| | 8500 | 580 |
| | 9000 | 581.8 |
| | 9500 | 583.5 |
| | 10000 | 585.3 |

Calibration: Ferry and Spear (1978) w/ Berman
(1990)

| Results: (11 data pts) | P (bars) | T (C) |
|------------------------|----------|---------|
| | 0 | 546.5 |
| | 1000 | 550.5 |
| | 2000 | 554.4 |
| | 3000 | 558.3 |
| | 4000 | 562.2 |
| | 5000 | 566.1 |
| | 6000 | 570.1 |
| | 7000 | 574 |
| | 8000 | 577.9 |
| | 9000 | 581.8 |
| | 10000 | 585.7 |

Calibration: Gessmann et al (1997)

| Results: (11 data pts) | P (bars) | T (C) |
|------------------------|----------|---------|
| | 0 | 600.6 |
| | 1000 | 604.7 |
| | 2000 | 608.7 |
| | 3000 | 612.7 |
| | 4000 | 616.7 |
| | 5000 | 620.7 |
| | 6000 | 624.8 |
| | 7000 | 628.8 |
| | 8000 | 632.8 |
| | 9000 | 636.8 |
| | 10000 | 640.8 |

APPENDIX 3, cont.

Geothermometric data collected from Spears GTB Program, cont.

Sample 139-11l Hornblende-plagioclase pairs

Average Compositions used

| | Hornblende | Plagioclase |
|--------------------|------------|-------------|
| Si | 6.483 | 2.747 |
| Al | 1.858 | 1.253 |
| Ti | 0.056 | 0.000 |
| Fe ²⁺ | 1.451 | 0.005 |
| Fe ³⁺ | 0.726 | 0.000 |
| Mg | 2.356 | 0.001 |
| Mn | 0.062 | 0.000 |
| Ca | 1.892 | 0.257 |
| Na | 0.356 | 0.716 |
| K | 0.192 | 0.011 |
| Cr | 0.008 | 0.000 |
| Ave Wt % Oxide Ave | 97.366 | 100.382 |

Calibration: Holland and Blundy (1994)

| Results: (21 data pts) | P (bars) | T (C) |
|------------------------|----------|---------|
| | 0 | 663.8 |
| | 500 | 666.1 |
| | 1000 | 668.4 |
| | 1500 | 670.8 |
| | 2000 | 673.1 |
| | 2500 | 675.4 |
| | 3000 | 677.7 |
| | 3500 | 680.1 |
| | 4000 | 682.4 |
| | 4500 | 684.7 |
| | 5000 | 687.1 |
| | 5500 | 689.4 |
| | 6000 | 691.7 |
| | 6500 | 694 |
| | 7000 | 696.4 |
| | 7500 | 698.7 |

| | | |
|--|-------|-------|
| | 8000 | 701 |
| | 8500 | 703.3 |
| | 9000 | 705.7 |
| | 9500 | 708 |
| | 10000 | 710.3 |